School of Medicine and Health

Fredrik Bajers Vej 7

9220 Aalborg Ø

http://www.smh.aau.dk/

Theme: Master's Thesis

Sports Technology: 10th Semester

Researchgroup: 10201

Authors:

Erik Føge Jensen

Jan Lund Nørgaard

Joakim Raunsbæk

Supervisor:

John Rasmussen

Miguel Nobre Castro

Pages: 47

Appendix: 33

Release date: 07-06-2017

Those who are born with amyoplasia are typically not able to perform activities of daily living (ADL) due to decreased muscle mass, joint contractures, and unnatural limb positioning. It is possible to use an orthosis to aid in ADL and increase their independency. A passive orthosis can support the weight of their arm against gravity, allowing them to perform movements with less muscle force. This study presents a prototype design that uses musculoskeletal modeling to optimise spring stiffnesses to gravitationally balance the arm while compensating for the excessive internal rotation of the glenohumeral joint. A subject-specific musculoskeletal was developed to simulate the effects of the orthosis during ADL. The simulations showed that a biarticular spring with a stiffness of 233.33 Nm^{-1} was able to lower the maximal muscle activity to a level in which tasks of ADL can potentially be performed.

Development of a Passive Upper Extremity Orthosis for Amyoplasia

Erik Føge Jensen[1*], Joakim Raunsbæk[1*], Jan Nørgaard Lund[1*]
John Rasmussen[2], Miguel Nobre Castro[2]

[1] Department of Health Science and Technology, Aalborg University
[2] Department of Mechanical and Manufacturing Engineering, Aalborg University
*MSc student

Abstract

Those who are born with amyoplasia are typically not able to perform activities of daily living (ADL) due to decreased muscle mass, joint contractures, and unnatural limb positioning. It is possible to use an orthosis to aid in ADL and increase their independency. A passive orthosis can support the weight of their arm against gravity, allowing them to perform movements with less muscle force. This study presents a prototype design that uses musculoskeletal modeling to optimise spring stiffnesses to gravitationally balance the arm while compensating for the excessive internal rotation of the glenohumeral joint. A subject-specific musculoskeletal was developed to simulate the effects of the orthosis during ADL. The simulations showed that a biarticular spring with a stiffness of 233.33 Nm^{-1} was able to lower the maximal muscle activity to a level in which tasks of ADL can potentially be performed.

Keywords: Passive orthosis, exoskeleton, arthrogryposis, amyoplasia, musculoskeletal modeling

1 Introduction

Sports technology has been used in different ways to optimise and improve performance of athletes (Haake, 2009). However, in the case of disabled people the ability to perform activities of daily life (ADL) can be a similarly challenging physical accomplishment that can be enabled with development of appropriate equipment (Dunning and Herder, 2013). The movement capabilities of the upper extremities are essential for independence (Maciejasz et al., 2014). Arthrogryposis Multiplex Congenita (AMC) is a disorder in which people often lack these movement capabilities. This is classified as a heterogeneous group of diseases with more than 300 different conditions, with the main characteristic involving multiple congenital joint contractures (Hall et al., 2014, Kowalczyk and Feluś, 2016). The prevalence of AMC is one in 3000 live births (Bamshad et al., 2009). The most common type of AMC is amyoplasia, which is a combination of decreased muscle mass and joint contractures with some distinct characteristics; typically the shoulders are adducted and internally rotated, the elbows are extended, and the wrists are flexed and ulnarly deviated. (Bernstein, 2002, Bamshad et al., 2009, Kimber, 2015, Kowalczyk and Feluś, 2016). However, these anatomical characteristics might differ between subjects (Bernstein, 2002). Decreased muscle mass is usually found in the deltoids, the biceps brachii, and the brachialis muscles (Kowalczyk and Feluś, 2016). The combination of contractures and muscular weakness makes activities such as self-feeding, reaching the face, and handling objects difficult or impossible (Rahman et al., 2006). The occurrence of amyoplasia is sporadic and the genetic cause is still unknown (Ezaki, 2010, Van Heest, 2015). According to Kimber (2015) the exact pathogenesis is also unknown but is hypothesized to be due to poor blood circulation to the fetus and thereby causing hypotension and hypoxia. As a consequence, the anterior horn cells are damaged leading to underdevelopment of muscle tissue which is replaced by adipose and fibrous tissue.

Treatment of subjects with amyoplasia is performed in different ways, primarily to improve the quality of life and enable ADL (Kowalczyk and Feluś, 2016, Van Heest, 2015). Physical therapy, stretching, and splinting are used to mobilize the joints and stimulate muscle growth (Hall, 2014, Kimber, 2015). Surgery is another treatment method and is primarily used in order to treat the lack of elbow flexion (Bamshad et al., 2009). However, according to Haumont et al. (2011) the different surgical procedures attempting to improve the elbow function have not resulted in any significant improvement.

As an alternative to the therapeutic and surgical methods, there has been extensive research in assistive devices, such as orthoses, that are able to compensate for

the muscular weakness of the upper extremities and assist the subject in performing ADL (Dunning and Herder, 2013). These assistive devices can be sorted into three different groups: (i) robotic manipulators, (ii) active and (iii) passive orthoses (Dunning and Herder, 2013). The robotic manipulators are intended for subjects with no muscle activity and there is a number of commercially available robotic manipulators on the market, such as the Jaco (Focal Meditech) and the iARM (Exact Dynamics). Robotic manipulators tend to be heavy and bulky, which according to Brackbill et al. (2009) makes them usable for rehabilitation purpose, but not suitable for ADL. An active orthosis transfers torque to the joints using actuators and a power source. This way an active orthosis works as a man-machine intelligence system where not only the intelligence of the machine is enhanced, but the power of the user is enhanced as well (Gopura et al., 2011). A beneficial attribute of active orthoses is that they are mounted to the trunk of the user, meaning that the users do not need to be bound to a wheelchair or an immovable object. Due to active orthoses' reliance on power sources and actuators, they have increased weight and a large volume, which affects the wearability and comfort of the user (Dunning and Herder, 2013).

The passive devices are based on the principle of gravity balancing by resorting to potential elastic energy stored in mechanical components such as zero free length springs, which are springs where the force generated is proportional to its full length (Dunning and Herder, 2013). These are advantageous compared to the active devices since no power supply is required. According to Lin et al. (2013) the passive devices are preferable since no sensors or actuators are needed, making the passive devices safer, less expensive, and lighter. There are different commercially available passive orthoses that are able to balance the arm in a wide range of configurations, which helps the subjects performing ADL. According to Van der Heide et al. (2014)'s review, the vast majority of passive devices are designed to be fixed on an object, such as a wheelchair. An example of a wearable orthosis is the Wilmington Robotic Exoskeleton (WREX) (Rahman et al., 2006). The WREX is a four degrees of freedom (DOF) passive device using parallelograms to gravity balance the upper limb. The WREX consists of a shoulder joint allowing for abduction/adduction, flexion/extension, and an elbow joint allowing flexion/extension but only partial humeral rotation at the shoulder (Gunn et al., 2016). Another wearable orthosis is the A-gear (Kooren et al., 2015). The A-gear is a four DOF passive orthosis that uses a serial linkage approach to gravity balance the upper limbs. The A-gear allows for the same shoulder and elbow motions as the WREX. In regards to amyoplasia, the internally rotated position of the shoulder affects the elbow, and consequently affects the hand, thus making the plane of movement and the function of the hand position problematic (Ferguson and Wainwright, 2013). Mechanisms such as these, supporting external rotation of the glenohumeral joint, would therefore improve the ability of subjects with amyoplasia to grab objects. Kroksmark et al. (2006) emphasizes the importance of muscle development over treatment of contractures since the muscular strength is more important regarding motor function. This further encourages development of orthoses that allows subjects to move their upper extremities.

this work, a passive orthosis prototype is proposed to bring the internally rotated glenohumeral joint into neutral position while providing assistance through an increased range of motion (ROM) for subjects with amyoplasia. The orthosis uses zero free length springs to counterbalance gravity in different upper extremity configurations while maintaining low friction. Musculoskeletal modelling is used for designing and selection of spring stiffnesses by simulation of a reduction in muscle strength. Furthermore, the orthosis is tested on one healthy subject to observe the functionality.

2 Methods and Materials

2.1 Design Specifications of the Orthosis

The main objective of the orthosis is to assist the performance of ADL. The majority of these tasks usually involves the hand reaching a point in space, grasping an object and then controlling and orienting the object until the task is completed (Nef et al., 2009). Examples of important ADL include feeding and personal hygiene which includes touching of the face and head (Herder et al., 2006). Being able to perform these tasks can provide more independence to the user as well as improve their quality of life. Therefore, the orthosis must able to support and follow the movements of the shoulder and elbow. If the device is not kinematically compatible, or if there are misalignments, the reachable workspace will be reduced, and

pain and discomfort will be experienced by the user (Koo et al., 2011). The movements will be aided by mechanical springs capable of counterbalancing gravity. In addition, an extra spring will aid the external rotation of the user's glenohumeral joint, thus bringing the humerus into a more neutral position. Considering that the orthosis is meant to be wearable, it is mounted onto the thorax of the user rather than on a wheelchair. There is further aspiration that the motion enabled by the orthosis can aid in the promotion of muscle development (Rahman et al., 2007, Kimber, 2015). The orthosis is designed using SolidWorks software v.2015x64 Edition SP5.0 (Dassault Systèmes, SolidWorks Corp., Massachusetts, USA). The orthosis is made up of three main components: the thorax shell, the upper arm shell, and the forearm shell – all of which account for attachment points of the device onto the body. The orthosis, without the thorax shell, is illustrated in figure 1.

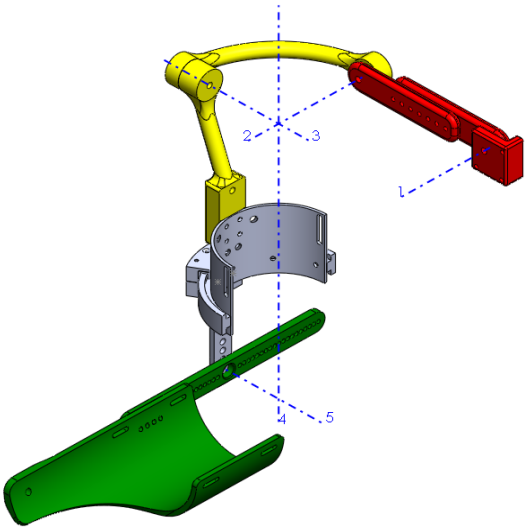

Figure 1: Full orthosis: 1. shoulder elevation-depression 2. shoulder abduction-adduction 3. shoulder flexion-extension 4. shoulder internal-external rotation 5. elbow flexion-external. Red - Back Parts, Yellow - Shoulder Parts, Grey - Upper Arm, Green - Forearm

2.1.1 Thorax Shell

A shell made of Aquaplast™(Homecraft Roylan, Sutton-in-Ashfield, UK), a thermoplastic material normally used for orthotic and splinting products was molded onto the thorax of one subject. This helps create a subject-specific shell that comfortably fits the user's torso. The thorax shell allows for a large surface area, in which the orthosis and spring attachments can be mounted in various positions. The mold is reinforced with fiberglass in order to strengthen the material.

2.1.2 Shoulder Mechanism

The shoulder is a complex joint and the importance of the orthosis producing similar movements to the joint brings added difficulty to the design. The glenohumeral joint is a synovial ball and socket joint, which allows the humerus to rotate about the glenoid cavity of the scapula in three DOFs. These three movements are classified as flexion/extension, abduction/adduction, and internal/external rotation. The sternoclavicular joint is the joint between the clavicle and the manubrium of the sternum, which has two DOF classified as shoulder elevation/depression and retraction/protraction (Lo and Xie, 2012). The complexity of the device escalates as the number of DOF increases (Maciejasz et al., 2014). Therefore, the majority of the orthoses and robotic upper arm devices only account for the common three DOF in the shoulder complex. However, several researchers have considered the movements produced by the sternoclavicular joint when developing their robotic exoskeletons. The MGA, ARMin III, and IntelliArm devices account for the elevation/depression of the shoulder, while the MEDARM includes both shoulder elevation/depression and retraction/protraction (Lo and Xie, 2012). Because of the additional complexities extra DOF present, the importance of the amount of DOFs that the device can allow is dependent on the amount of movement of the user's limb, as well as the purpose of the device. An example of this would be a rehabilitation device which focuses specifically on the muscles in the shoulder girdle would likely need more DOF than a device only focusing on shoulder flexion/extension.

The primary design objective of the shoulder was to investigate possible designs which would allow for the needed movement of the target user. Based on previous literature, two different methods, a three revolute (3R) serial joints and a four revolute (4R) serial joints, were investigated. These early concepts are illustrated in figure 2 and figure 3. The 3R with 90° links have been used in the past for exoskeletons to replicate the movement of the body without colliding with it (Lo and Xie, 2013). This design allows for the three movements of the shoulder but contains singular configurations. These occur when the joints align, resulting in a loss of one DOF (Perry et al.,

2007). The 3R mechanism possesses two distinct singular configurations. One singular configuration arises when the distal joint in the same direction as the base joint, while the second occurs when the axis of the distal joint is 180° opposite to that of the first configuration (Lo and Xie, 2013).

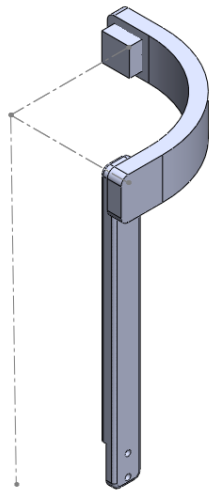

Figure 2: 3R mechanism

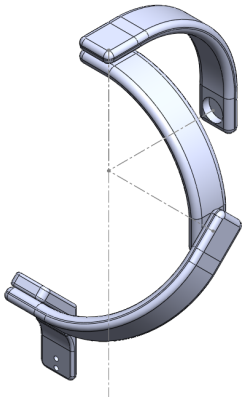

Figure 3: 4R mechanism

The purpose of the 4R mechanism is to prevent the system from reaching a singular configuration by adding a redundant joint (Lo and Xie, 2013). Singularities should be avoided because they inhibit the user's shoulder movement, as well as cause injuries or discomfort (Lo and Xie, 2013). Nevertheless, the 4R mechanism would contribute to a larger ROM, thus allowing for more reachable workspace. Since the mechanism should be able to limit internal/external rotation of the upper extremity, the addition of a fourth revolute joint does not bring an advantage, as one of the three revolute joints has to be stabilized by a spring-loaded system. This can be achieved through a revolute joint coincident to the longitudinal axis of the humerus. It is then expected that the fourth redundant joint would still allow the mechanism functioning as a spherical joint even if that internal/external rotation axis was spring-loaded. While the redundancy problem with the 4R cannot be adjusted, the singularity issue with the 3R can be avoided. Because shoulder elevation required for everyday tasks is usually less than 90° in all axes (Buckley et al., 1996), it can be assumed that this singularity will normally be located outside of the desired workspace. It has further been suggested that a future design strategy could be to neglect the full vertical ROM, focusing on only the support of the most essential ADL (Dunning and Herder, 2013). It is important for the mechanism to be designed in a way in which the revolute joints have the same center of rotation, but are sufficiently distanced from the body to avoid collision. To mimic the shoulder's movements, its center of rotation needs to be well aligned with the shoulder. As previously mentioned, the shoulder complex includes more than the three DOF accounted for in previous exoskeleton designs. Carignan and Liszka (2005) accounted for the elevation of the shoulder in their design due to it being the largest scapulothoracic motion, occurring deliberately e.g. shoulder shrug, or incidentally during the abduction of the glenohumeral joint. The latter is due to the phenomenon in which shoulder elevation occurs as the upper arm abducts over the horizontal plane (Lo and Xie, 2012). Considering this factor, the orthosis must be designed to avoid this potential misalignment between the mechanism's rotational axis and the shoulder's rotational axis in order to avoid impingement of the rotator cuff muscles between the humerus and the acromion (Nef et al., 2007). To allow for this DOF, a revolute joint is added at the adjustable connection point of the thorax shell and the shoulder mechanism.

The final axis of rotation of the 3R is located on the humeral axis. To keep this axis aligned with the humerus, as well as the center of the rotation of the glenohumeral joint, it needs to be concentrically aligned with the upper arm at all positions while allowing for rotation about the humerus. The design allows for the part originating from the shoulder to be attached onto the upper limb and for the axial rotation to be provided by a curved sliding rail mechanism, shown in figure 4. The rail is attached to the anchored upper arm shell, while the slider is attached by an adjustable link to the elbow joint. As the humerus internally and externally rotates, the slider follows accordingly. Considering that the most common pattern of deformity in the upper extremity due to amyoplasia is the internal rotation of the shoulder, along with weak or absent shoulder girdle muscles (Van Heest, 2015), the purpose of this mechanism is to aid the alignment of the shoulder into a neutral position. Using two parallel attachment points, located on the upper arm shell and the slider, a zero free length spring is attached. On the shell, anteriorly and posteriorly located between the attachments there are two bolts that act as pulleys. As the user internally or exter-

nally rotates the humerus, the pulleys act on the spring increasing the force and tension as the slider moves further.

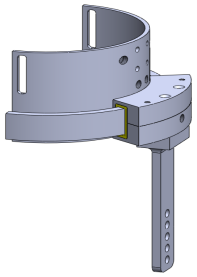

Figure 4: Slider mechanism that limits humeral rotation.

2.1.3 Elbow Mechanism

The elbow joint provides one simple DOF. The elbow joint connects the slider mechanism with the forearm by allowing for flexion and extension. Adjustable links on the connections between the upper arm and forearm allow for the device's joint to be accurately aligned with the user's anatomical elbow joint as well as allow for attachment points for the springs that will gravitationally compensate the entire upper limb. The inferior component of the orthosis' elbow joint is attached to the half-cylindrical forearm shell which is proximally constrained to the forearm – not restricting the pronation/supination axis.

2.2 Computational Modelling

In order to simulate the effects of the orthosis, a musculoskeletal model of the right arm is created in AnyBody Modeling System 6.1 (AMS) (AnyBody Technology, Aalborg, Denmark) from the built-in repository v1.6.3. The musculoskeletal model comprises eight DOF: three DOF at sternoclavicular joint, three DOF at the glenohumeral joint, and two DOF at the elbow joint. The model is scaled to a subject by experimentally obtained motion capture data by the method of Andersen et al. (2010) which minimises the least-square difference between the recorded markers and the virtual markers defined on the musculoskeletal model. For the inverse dynamics analysis, the min/max muscle recruitment criterion is used, developed by Rasmussen et al. (2001).

In order to have realistic posture inputs for the musculoskeletal model, motion capture data of ten different ADL was obtained resorting to Andersen et al. (2009) which deals with over-determinate systems as the result of driving the model with the reflective markers. The last frame of the motions is used as posture input. The ten different postures are illustrated in figure 5 and these were used to solve the inverse dynamics.

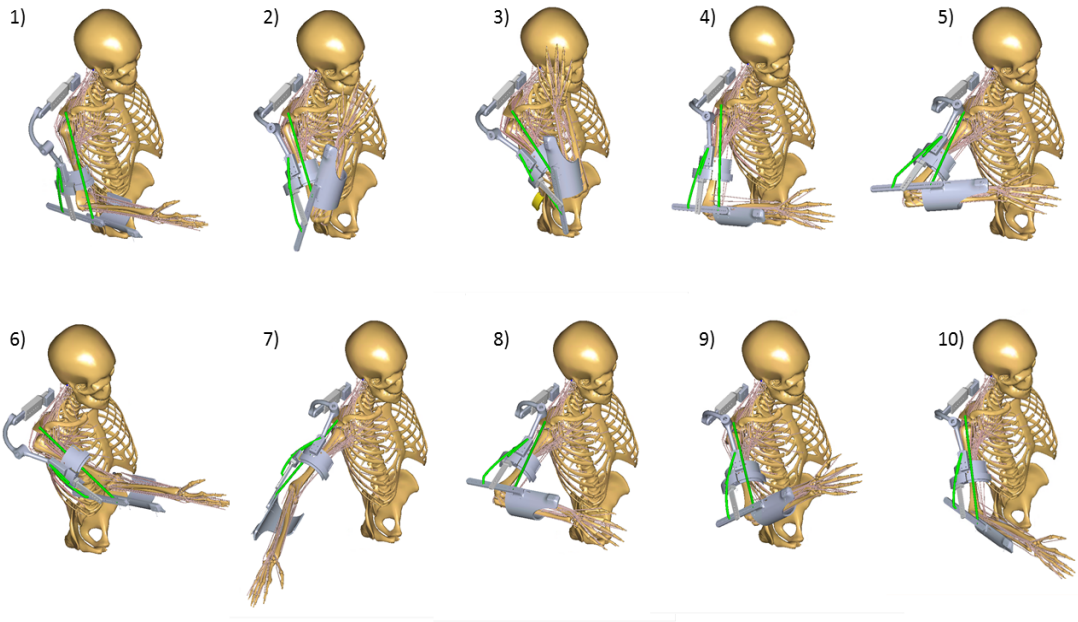

Figure 5: The ten different postures of the inverse dynamics analyses

2.2.1 Human-Orthosis Biomechanical System

The human body and the orthosis create a biomechanical system in which the orthosis must work in cohesion with functions of the human arm. To determine if the orthosis is capable of fulfilling its intended function, the interaction between the orthosis and the human body has to be examined. In this study, the essential aspect of the musculoskeletal modeling is the simulation of how the human body is affected by the external forces produced by the orthosis. The CAD model of the orthosis along with the mass properties of the individual parts of the orthosis were imported into AMS. To establish the human-orthosis biomechanical system, the orthosis is attached to the musculoskeletal model through three predefined reference nodes: the thorax, the humerus, and the ulna. The musculoskeletal model wearing the orthosis can be seen in figure 5.

The human-orthosis system combines the human arm and the orthosis, a kinematic diagram is shown in figure 6. The blue lines represent the human arm and the red lines are representing the orthosis. The orthosis supporting the glenohumeral joint is represented as three revolute joints θ_{a1}, θ_{a2}, θ_{a3}, and flexion at the elbow θ_{a4}. The orthosis itself is composed of five revolute joints. The θ_{o1} allows for elevation/depression of the shoulder. The three revolute joints θ_{o2}, θ_{o3}, and θ_{o4} represents the three DOFs of the shoulder. The connection between the upper arm shell and the forearm shell is created by a revolute joint θ_{o5}. As a consequence, the human-orthosis system has too few constraints and is thereby kinematically indeterminate. In order to resolve this issue, the joints between the human arm and the orthosis have to be defined. The upper arm attachment is modelled as a spherical joint θ_{c1}, θ_{c2}, θ_{c3} and the forearm attachment as a trans-spherical joint θ_{c5}, θ_{c6}, θ_{c7}, and p_{c4} which are illustrated by the purple geometries on figure 6.

In figure 7 the springs working in human-orthosis biomechanical are illustrated by the dashed lines. The S_1 is a biarticular spring located above the glenohumeral joint and along the ulna of the forearm assisting the glenohumeral and elbow flexion. The S_2 is monoarticular spring located along the humerus and posterior to the elbow assisting the extension. The S_3 is located on the humerus which brings the humerus to neutral position.

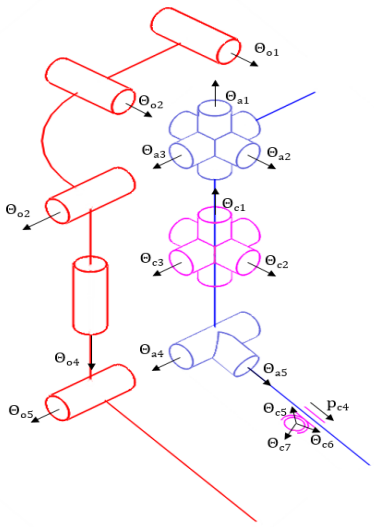

Figure 6: Kinematic diagram of the human-orthosis biomechanical system

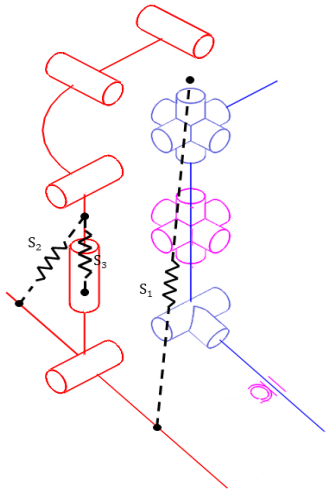

Figure 7: Kinematic diagram of the human-orthosis biomechanical system with springs

2.2.2 Modeling Amyoplasia

The advantage of musculoskeletal modeling is the possibility of adjusting it towards subject-specific modeling. In the current study, musculoskeletal modeling assumptions were made to best resemble a subject with amyoplasia:

1. All muscles with a positive contribution to elbow flexion are disabled and substituted by a weak elbow flexion torque provider – a "diagnostic" muscle. The anterior deltoid is also disabled.

2. The joint and muscle contractures are neglected.

3. The inverse dynamics analyses are performed for static postures.

The output measure in the current study is based on the maximal muscle activity (MMACT), which determines whether the model is able to produce the muscle force needed for the given posture. The muscle activity is the ratio between force and strength. If the MMACT is higher than 1 for any given muscle there is insufficient muscle strength to perform the required muscle work. However, this is solved by the addition of the artificial muscles to the model allowing simulation of cases which otherwise would be impossible.

2.2.3 Parameter Study

In order to investigate a suitable and favorable spring configuration that yields the lowest MMACT, ten different parameter studies were conducted. Three different springs are defined on the orthosis. Based on calculations by the method of Lustig et al. (2015) the ranges of the parameter studies were defined. The range of the biarticular spring stiffness was 0 to 700 Nm^{-1}, and the monoarticular was 0 to 800 Nm^{-1} . The stiffness of internal/external rotation spring was 84 Nm^{-1} and remained unchanged. The ranges of the two springs were covered in ten steps in the parameter study, resulting in 100 different combinations of spring configurations for all ten postures. Initial spring locations were also estimated using the stiffness matrix approach presented by Lustig et al. (2015). The forearm attachment points for the monoarticular and biarticular spring were calculated to be 10.25 cm anterior of the elbow joint and 7.7 cm posterior to the elbow joint, respectively. However, in order to make the orthosis more compact, the spring attachments sites were relocated. The biarticular spring was attached 5 cm anterior of the elbow and the monoarticular spring was attached 7.2 cm posterior to elbow. For every step of each parameter study, an inverse dynamics analysis was performed.

3 Results

To assess the required stiffness for the monoarticular and biarticular springs, the average of the MMACT for each of the 100 spring configuration over all motions was calculated. In figure 8 the results for MMACT (A), muscle activity in the diagnostic elbow flexors (B), and muscle activ-

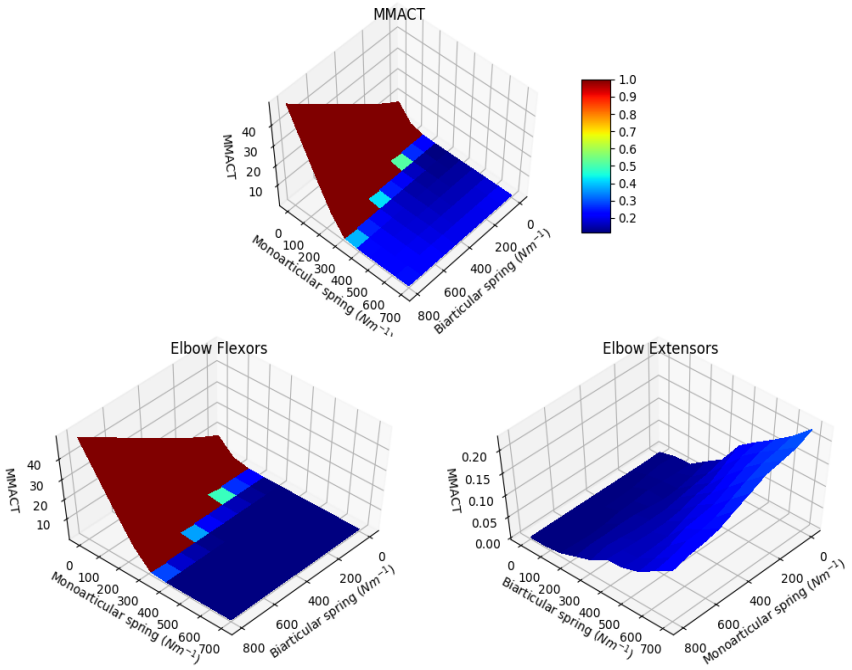

Figure 8: Graphs of the MMACT, diagnostic elbow flexor, and the elbow extensors

ity in the elbow extensors (C) can be seen. An increment of stiffness in the monoarticular spring results in higher MMACT – especially resulting from the over-recruitment of the elbow flexion torque provider – while increments to the biarticular spring lowered MMACT the elbow flexion torque provider and created increased muscle activity in the elbow extensors. The lowest average MMACT was found when the biarticular spring had a stiffness of 233.33 Nm^{-1} and the monoarticular spring had a stiffness of 0 Nm^{-1}.

The MMACT was simulated with and without the orthosis for the previously mentioned spring configurations resulting in the lowest average MMACT. A table of the results with the spring stiffness found in the parameter studies is shown in table 1. The table shows that the MMACT was above one in seven of the ten postures, when the model was not wearing an orthosis, which means that model would not be able to attain the posture. While wearing the orthosis the model could achieve all postures.

Table 1: MMACT with and without orthosis

Posture	No Orthosis	Orthosis
1	26.81	0.06
2	0.10	0.09
3	0.14	0.13
4	17.15	0.07
5	2.85	0.08
6	5.53	0.30
7	1.09	0.08
8	0.10	0.09
9	10.76	0.12
10	21.21	0.09

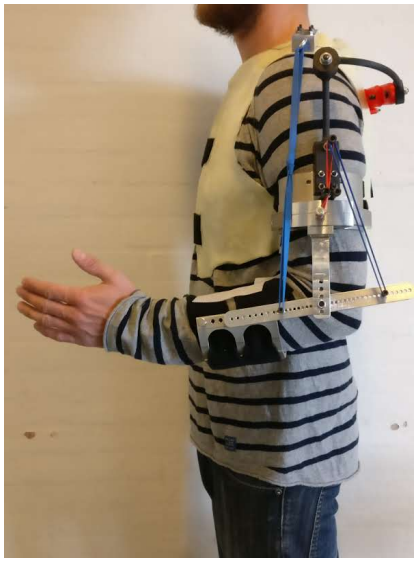

Figure 9: Subject wearing the orthosis

4 Discussion

In the present study, a musculoskeletal model imitating the disorder amyoplasia with and without an orthosis was used to simulate ten distinct postures from ADL. From the results in figure 8 it can be seen that as the work performed by the elbow flexors decrease, the work of the elbow extensors increase. This increment in muscle activity of the elbow extensors are due to the increased stiffness of the biarticular spring and shows that the musculoskeletal model represents real life situations well, as a force pulling the forearm up in a vertical direction would increase the need for muscle work in the extensor muscles. Furthermore, the results showed that a biarticular spring with a stiffness of 233.33 Nm^{-1} and a monoarticular spring stiffness of 0.0 Nm^{-1}, i.e. this spring is absent, would yield the lowest MMACT on average across all postures. These findings differ from the findings of Lustig et al. (2015), who found that both the monoarticular and biarticular spring are important to attain full gravity balancing. A possible reason for these differences compared to the method of Lustig et al. (2015), the musculoskeletal model may be overestimating the strength of the elbow extensors, making the monoarticular spring unnecessary.

The model was unable to maintain the arm in seven out of the ten positions without the orthosis due to muscle overactivation caused by the lack of strength from the idealized amyoplasia condition. On the contrary, it was successfully able to perform all ten postures while wearing the orthosis. This means that a subject resembling similar muscular characteristics as the model is able to perform all ten postures since the spring configuration is capable of providing the needed assistance.

In order to imitate amyoplasia, several assumptions were made regarding the musculoskeletal model. The specific muscles that were disabled in the musculoskeletal model may differ between different users because the exact residual muscle strength, as well as which muscles are affected, vary widely for those diagnosed with amyoplasia. The model can, however, be optimized to better resemble a specific subject. The joint contractures were not implemented in the model, which may have also produced differ-

ent results. These contractures could have been modeled as passive stiffness in the joints, which could hypothetically cause the parameter study to indicate higher spring stiffnesses required to achieve the postures of ADL defined in the study. The results of posture 2, 3 and 8 did not cause any overactivation of the muscles in the model without the orthosis. This might be due to the chosen static postures. The positions of the arm in the given postures may require a minimal amount of muscle force from the disabled muscles. If the analysis, on the other hand, had been conducted on a dynamic motion, overactivation would have been likely to occur.

The prototype developed in the current study, shown in figure 9, was tested on one healthy male to observe the physical behavior, kinematically and kinetically, of the orthosis. All shells were able to fit the user and due to the adjustability of the different links, the rotation axes could be accurately aligned to the subject's body. Before the application of springs, the orthosis was kinematically compatible with arm of the subject when performing simple and coupled motions. The expected singularity of the system did not cause any issue. This could be explained by low torsional stiffness of 3R mechanism, which aided in the misalignment of the rotation axes of the glenohumeral joint. The misalignment occasionally caused the second revolute joint of the mechanism to collide with the biarticular spring attachment of the thorax shell. Over time upper arm shell translated distally, away from the shoulder, which also caused a misalignment. Both problems can be improved by increasing the rigidity of the shoulder mechanism and improving the method of strapping the upper arm shell to the body, thus reducing the translation between the skin and shell.

Applying the biarticular spring to the prototype aided in the balancing of the gravitational forces, thus assisting the movement of the arm. When a biarticular spring with less force than simulated was applied, small movement using the triceps was able to control the system. However, when the spring force found in the parameter study was applied, the amount of required triceps force was high compared to the low activation results obtained from the simulations. Addition of the monoarticular spring was able to counterbalance the system and thereby enable movements. Due to the resulting forces in the system, the thorax shell was pulled out of position. These forces also caused discomfort in the shoulder region from the thorax shell. This is caused by the poor fixation of the thorax shell to the body and can be corrected by increasing the rigidity of the entire system, as well as enhancing the mounting of the orthosis to the trunk. This stiffness of the biarticular spring might be overestimated in the parameter studies due an overestimation of the strength of elbow extensors of the musculoskeletal model compared to reality. Consequently, the monoarticular spring should be introduced to assist in elbow extension due to the fact that the strength of the triceps muscle would be lower. The slider mechanism, limiting internal/external humeral rotation, functioned as intended. The mechanism was able to slide smoothly along the rail of the upper arm shell, however, if the orthosis and the human arm were not aligned this would cause wedging to the tolerance of the slider.

In order to optimise the results of the musculoskeletal modeling, the parameter studies should also include positioning of the springs. The musculoskeletal model should also be based on a pool of genuine data of subjects with amyoplasia. Therefore, further studies should include individuals with amyoplasia to evaluate the counterbalancing of gravity and the effects on performance of activities of daily living. It is also important to observe the sliding mechanism's effect on shoulder orientation and contractures. This would increase the validity of results. Furthermore, a full reachable space simulation as conducted by Castro et al. (2015) would be able to validate a change in ROM when using the orthosis and enable another type of appreciation on the performance of the device.

5 Conclusion

The orthosis prototype developed in the current study has shown the potential to lower the MMACT through musculoskeletal modeling. Therefore, it is feasible that an optimized version of the orthosis could be a useful device for subjects with amyoplasia to increase their ROM and ability to perform ADL. Further investigation is needed regarding the internal/external rotation mechanism to prove the actual effect on the contractures of subjects with amyoplasia.

References

Andersen, M., Damsgaard, M., MacWilliams, B. and Rasmussen, J. (2010), 'A computationally efficient optimisation-based method for parameter identification of kinematically determinate and over-determinate biomechanical systems', *Computer Methods in Biomechanics and Biomedical Engineering* **13**(2), 171–183.

Andersen, M., Damsgaard, M. and Rasmussen, J. (2009), 'Kinematic analysis of over-determinate biomechanical systems', *Computer Methods in Biomechanics and Biomedical Engineering* **12**(4), 371–384.

Bamshad, M., Van Heest, A. E. and Pleasure, D. (2009), 'Arthrogryposis: A Review and Update:', *The Journal of Bone and Joint Surgery-American Volume* **91**(Suppl 4), 40–46.

Bernstein, R. M. (2002), 'Arthrogryposis and amyoplasia', *Journal of the American Academy of Orthopaedic Surgeons* **10**(6), 417–424.

Brackbill, E. A., Mao, Y., Agrawal, S. K., Annapragada, M. and Dubey, V. N. (2009), Dynamics and control of a 4-dof wearable cable-driven upper arm exoskeleton, *in* 'Robotics and Automation, 2009. ICRA'09. IEEE International Conference on', IEEE, pp. 2300–2305.

Buckley, M. A., Yardley, A., Johnson, G. R. and Cams, D. A. (1996), 'Dynamics of the upper limb during performance of the tasks of everyday living—a review of the current knowledge base', *Proceedings of the Institution of Mechanical Engineers, Part H: Journal of Engineering in Medicine* **210**(4), 241–247. PMID: 9046184.

Carignan, C. and Liszka, M. (2005), Design of an arm exoskeleton with scapula motion for shoulder rehabilitation, *in* 'Advanced Robotics, 2005. ICAR'05. Proceedings., 12th International Conference on', IEEE, pp. 524–531.

Dunning, A. G. and Herder, J. L. (2013), A review of assistive devices for arm balancing, *in* 'Rehabilitation Robotics (ICORR), 2013 IEEE International Conference on', IEEE, pp. 1–6.

Exact Dynamics iARM.
[Online] URL: *http://www.exactdynamics.nl/site/* [Accessed on 2017-06-06]

Ezaki, M. (2010), 'An approach to the upper limb in arthrogryposis', *Journal of Pediatric Orthopaedics* **30**, 57–62.

Ferguson, J. and Wainwright, A. (2013), 'Arthrogryposis', *Orthopaedics and Trauma* **27**(3), 171–180.

Focal Meditech Jaco.
[Online] URL: *http://www.focalmeditech.nl/nl/content/jaco* [Accessed on 2017-06-06]

Gopura, R., Kiguchi, K. and Bandara, D. S. V. (2011), A brief review on upper extremity robotic exoskeleton systems, *in* 'Industrial and Information Systems (ICIIS), 2011 6th IEEE International Conference on', IEEE, pp. 346–351.

Gunn, M., Shank, T. M., Eppes, M., Hossain, J. and Rahman, T. (2016), 'User Evaluation of a Dynamic Arm Orthosis for People With Neuromuscular Disorders', *IEEE Transactions on Neural Systems and Rehabilitation Engineering* **24**(12), 1277–1283.

Haake, S. J. (2009), 'The impact of technology on sporting performance in olympic sports', *Journal of Sports Sciences* **27**(13), 1421–1431. PMID: 19764001.

Hall, J. G. (2014), 'Arthrogryposis (multiple congenital contractures): Diagnostic approach to etiology, classification, genetics, and general principles', *European Journal of Medical Genetics* **57**(8), 464–472.

Hall, J. G., Aldinger, K. A. and Tanaka, K. I. (2014), 'Amyoplasia revisited', *American Journal of Medical Genetics Part A* **164**(3), 700–730.

Haumont, T., Rahman, T., Sample, W., King, M. M., Church, C., Henley, J. and Jayakumar, S. (2011), 'Wilmington robotic exoskeleton: a novel device to maintain arm improvement in muscular disease', *Journal of Pediatric Orthopaedics* **31**(5), 44–49.

Herder, J. L., Vrijlandt, N., Antonides, T., Cloosterman, M. and Mastenbroek, P. L. (2006), 'Principle and design of a mobile arm support for people with muscular weakness', *The Journal of Rehabilitation Research and Development* **43**(5), 591.

Kimber, E. (2015), 'AMC: amyoplasia and distal arthrogryposis', *Journal of Children's Orthopaedics* **9**(6), 427–432.

Koo, D., Chang, P. H., Sohn, M. K. and Shin, J.-h. (2011), Shoulder mechanism design of an exoskeleton robot for stroke patient rehabilitation, *in* 'Rehabilitation Robotics (ICORR), 2011 IEEE International Conference on', IEEE, pp. 1–6.

Kooren, P. N., Dunning, A. G., Janssen, M. M. H. P., Lobo-Prat, J., Koopman, B. F. J. M., Paalman, M. I., de Groot, I. J. M. and Herder, J. L. (2015), 'Design and pilot validation of A-gear: a novel wearable dynamic arm support', *Journal of NeuroEngineering and Rehabilitation* **12**(1).

Kowalczyk, B. and Feluś, J. (2016), 'Arthrogryposis: an update on clinical aspects, etiology, and treatment strategies', *Archives of Medical Science* **1**, 10–24.

Kroksmark, A.-K., Kimber, E., Jerre, R., Beckung, E. and Tulinius, M. (2006), 'Muscle involvement and motor function in amyoplasia', *American Journal of Medical Genetics Part A* **140A**(16), 1757–1767.

Lin, P.-Y., Shieh, W.-B. and Chen, D.-Z. (2013), 'A theoretical study of weight-balanced mechanisms for design of spring assistive mobile arm support (MAS)', *Mechanism and Machine Theory* **61**, 156–167.

Lo, H. S. and Xie, S. Q. (2012), 'Exoskeleton robots for upper-limb rehabilitation: State of the art and future prospects', *Medical Engineering & Physics* **34**(3), 261–268.

Lo, H. S. and Xie, S. S. (2013), Optimization of a redundant 4r robot for a shoulder exoskeleton, *in* 'Advanced Intelligent Mechatronics (AIM), 2013 IEEE/ASME International Conference on', IEEE, pp. 798–803.

Lustig, M., Dunning, A. G. and Herder, J. L. (2015), Parameter analysis for the design of statically balanced seral linkages using a stiffness matrix approach with Cartesian coordinates, Vol. 2015, Research gate, Taipei, Taiwan, pp. 1–9.

Maciejasz, P., Eschweiler, J., Gerlach-Hahn, K., Jansen-Troy, A. and Leonhardt, S. (2014), 'A survey on robotic devices for upper limb rehabilitation', **11**(3), 1–29.

Nef, T., Guidali, M. and Riener, R. (2009), 'ARMin III – arm therapy exoskeleton with an ergonomic shoulder actuation', *Applied Bionics and Biomechanics* **6**(2), 127–142.

Nef, T., Mihelj, M., Kiefer, G., Perndl, C., Muller, R. and Riener, R. (2007), ARMin - Exoskeleton for Arm Therapy in Stroke Patients, IEEE, pp. 68–74.

Perry, J. C., Rosen, J. and Burns, S. (2007), 'Upper-Limb Powered Exoskeleton Design', *IEEE/ASME Transactions on Mechatronics* **12**(4), 408–417.

Rahman, T., Sample, W., Jayakumar, S., King, M. M., Wee, J. Y., Seliktar, R., Alexander, M., Scavina, M. and Clark, A. (2006), 'Passive exoskeletons for assisting limb movement', *Journal of rehabilitation research and development* **43**(5).

Rahman, T., Sample, W., Seliktar, R., Scavina, M., Clark, A., Moran, K. and Alexander, M. (2007), 'Design and Testing of a Functional Arm Orthosis in Patients With Neuromuscular Diseases', *IEEE Transactions on Neural Systems and Rehabilitation Engineering* **15**(2), 244–251.

Rasmussen, J., Damsgaard, M. and Voigt, M. (2001), 'Muscle recruitment by the min/max criterion—a comparative numerical study', *Journal of biomechanics* **34**(3), 409–415.

Van Heest, A. E. (2015), Arthrogryposis, *in* D. R. Laub, ed., 'Congenital Anomalies of the Upper Extremity', Springer US, Boston, MA, pp. 305–315. DOI: 10.1007/978-1-4899-7504-1_23.

Worksheet:

Development of a Passive Upper Extremity Orthosis for Amyoplasia

Erik Føge Jensen, Jan Nørgaard Lund & Joakim Raunsbæk

07-06-2017

Contents

Theory 1

1.1 Arthrogryposis Multiplex Congenita

Arthrogryposis Multiplex Congenita (AMC) is a term used to describe multiple congenital contractures. The diagnosis is not specific since there is more than 300 different types of AMC. The prevalence of AMC is 1 in 3000 live births (Bamshad et al., 2009). Congenital contractures are usually associated with a state of permanent contraction of muscle fibers limiting the passive and active flexion or extension of the respective joint (Kalampokas et al., 2012). The contractures are present in multiple areas of the body and usually only affecting the limbs. The contractures are not progressive and might improve over time with proper physical therapy and orthopedic care (Hall, 2014).

AMC is very heterogeneous disorder and is usually classified as classic AMC (amyoplasia), distal AMC, and syndromic AMC (Van Heest, 2015). Due to heterogeneity of AMC the etiology is naturally equally varied (Gordon, 1998), however, there is a general agreement in the literature that fetal akinesia is the main cause and common for all types of arthrogryposis (Hall, 2014, Kimber, 2015). According to Hall (2014) there is a direct relationship between the onset of the fetal akinesia and the severity of the contractures. The decreased movement of the fetus is associated with formation of connective tissue around the joints, disuse muscle atrophy, and abnormal joint surfaces (Hall, 2014). The exact etiology of fetal akinesia remains unclear but is thought to be multifactorial which includes neuropathic abnormalities, myopathic abnormalities, connective tissue abnormalities, neuromuscular end-plate abnormalities, space limitation in utero, maternal illness, compromised blood supply to fetus, and metabolic disturbances (Hall, 2014).

1.1.1 Amyoplasia

The most common type of AMC is amyoplasia, which means “no muscle growth”. Approximately one-third of all cases of arthrogryposis is of the amyoplasia type and the occurrence is sporadic. The pathogenesis is unknown but is hypothesized to be due to poor blood circulation to the fetus resulting in hypotension and hypoxia and thereby damaging the anterior horn cells. This leads to underdevelopment of muscle tissue, which is replaced with fatty or connective tissue (Kimber, 2015). However, subjects with amyoplasia are expected to have normal intelligence and life expectancy (Ezaki, 2010).

Amyoplasia is typically associated with quadrimelic involvement and some distinct anatomically char-

acteristics: internally rotated and adducted shoulders, extended elbows, flexed and ulnarly deviated wrists (Bernstein, 2002, Bamshad et al., 2009, Van Heest, 2015). For the lower extremities, the hips can be abducted and internally rotated with flexed knees or the hips can be flexed with either flexed or extended knees. Hips and knees might be dislocated. The feet are usually in equinovarus adductus position. The underdeveloped muscles are weak or in some cases absent and usually found in the shoulder girdle musculature: deltoids, rotator cuff, pectoralis, latissimus dorsi, peri-scapular (Zlotolow and Kozin, 2015) and the elbow flexors: biceps brachii and brachialis (Kowalczyk and Feluś, 2016). These characteristics hinder the subject's ability to perform activities of daily life (ADL) and thereby their independence (Ferguson and Wainwright, 2013).

The main goal of treatment for these subjects is to gain functional independence especially of the upper extremities. The contractures are most severe at birth and are usually treated by stretching and splinting to increase the range of motion (ROM) and acquire functional joint positions. Later on, orthopedic surgery can be necessary if functional independence still is not achieved (Van Heest, 2015). In terms of motor function, Kroksmark et al. (2006) stated that development of muscle strength is more important than treatment of the contractures, which makes early physical therapy important in order to mobilize the affected joints and promote muscle growth (Kimber, 2015). A variety of surgical procedures exist to treat the contractures of subjects with amyoplasia. The elbow function is essential due to the importance of hand-to-mouth function. If the passive elbow flexion of the subject is less than 90°, surgical treatment is usually proposed (Van Heest, 2015). Regarding the shoulder, surgery is rarely necessary because the internal rotation does not cause a problem but actually might be a helpful mechanism to compensate for the lack of active elbow flexion (Van Heest, 2015). Surgical procedures might be helpful for some subjects but the individual assessment of each subject is important since the subjects often are able to adapt to the situation. The surgical procedures should only be used to enhance movement capabilities without compromising already existing functionality (Zlotolow and Kozin, 2015).

1.2 Musculoskeletal modeling

Computer models and simulations have become an essential method in most fields of engineering. In most cases, it would be inconceivable to do engineering without the help of models or simulations. Biomechanics is no exception since simulations and models of the musculoskeletal system are able to provide information about internal loads that otherwise would be complicated or infeasible to obtain (Lund et al., 2012).

Simulations of the musculoskeletal system are a complicated matter. The human body is hard to describe mathematically due to complex geometries, material properties, and an autonomous control system. In order to achieve a reasonable level of efficiency, models of the musculoskeletal system have to be simplified. The models are often simplified by assuming that the body consists of rigid bodies, which allows for application of the standard rules of multibody dynamics. The muscles of the models are also a complicated issue since a reasonably accurate representation of the muscle geometry, insertion, and origin is required to achieve realistic results. Furthermore, the human body has more muscles than degrees of freedom (DOF). The mechanism of muscle activation is controlled by the central nervous system but is still largely unknown. Therefore, the muscle recruitment in musculoskeletal modelling is typically based on an optimality condition where the central nervous system (CNS) is trying to minimize the load on the muscles. This is known as the redundancy problem of the muscle recruitment (Damsgaard et al., 2006).

There are two different analytical approaches for musculoskeletal modelling: forward dynamics and inverse dynamics. The forward approach uses muscle activations as input to compute the motion of a system. It is attractive in terms of detailed modeling but is on the other hand computationally demanding. The inverse approach uses the motion and inertial properties of the bodies as input to compute the forces of the system. While the inverse approach introduces more restrictions to the model, it is on the other hand computationally efficient compared to the forward approach. This efficiency of the inverse approach can be utilized to build more complex musculoskeletal models (Damsgaard et al., 2006).

1.2.1 Kinematics

As previously mentioned, inverse dynamics analysis computes the forces based on the kinematics of the system. The most common method for obtaining kinematic data is by motion capture, which can be used to drive the musculoskeletal model. However, the use of motion capture for obtaining kinematic data often entails complications.

- *Noise*: Almost all measurements are influenced by noise and, in this case, the recorded marker positions are affected. The goal of motion capture for musculoskeletal modelling is to describe the movement of the skeleton. The main complication in the case of noise is the markers moving relative the bone, which is also known as soft tissue artifacts.

- *Kinematic over-determinacy*: A segment usually has at least three markers attached which result in nine DOF. This introduces over-determinacy because a body segment only has six DOF. Furthermore, the constraints of the human body further increases the over-determinacy.
- *Kinematic under-determinacy*: It is not always possible to measure the position of underlying bones by the use of motion capture. This leaves some bones under-determinate.
- *Missing marker visibility*: A common problem for passive motion capture is occlusion. The passive markers of a motion capture system should always be visible to at least two cameras in order to reconstruct 3D positions of the recorded markers (Andersen et al., 2009).

To overcome the aforementioned problems related to motion capture and kinematics of an over-determinate system, a local optimisation method was developed by Andersen et al. (2009) to find the best possible fit between the recorded marker trajectories and the virtual markers defined on the musculoskeletal model. In case of an over-determinate system, the kinematics has to be solved by splitting the equations into two sets of equations and solving as an optimisation problem. The first set has to be solved 'as well as possible' and the second set has to be solved correctly (Andersen et al., 2009).

Scaling and parameter identification of musculoskeletal models are also of great importance in order to solve the kinematics correctly. This has been an issue in musculoskeletal modeling (Andersen et al., 2010, Lund et al., 2012). Traditionally, scaling of musculoskeletal models is based on cadaver data and scaling laws to determine parameters such as segment lengths and joint orientations. This can however lead to incorrect estimation of body segment parameters (Lund et al., 2015). As an alternative, Andersen et al. (2010) proposed an optimisation method to overcome the issues related to traditional scaling by the use of experimental obtained kinematic data. The purpose of this method is to scale the size of subject to the model, find the local coordinates of the model markers, and alter the joint rotation axes. This is done by minimising the least squares differences between the recorded marker trajectories and the virtual markers (Andersen et al., 2010).

1.2.2 Muscle recruitment

When an inverse dynamics analysis is conducted and the musculoskeletal system is of interest, dynamic equilibrium is not easily obtained. The fundamental problem is the indeterminacy of muscle forces, which is due to the fact that the human body is statically indeterminate. In other words, there are more muscles to produce a given motion than DOF and therefore there are infinite muscle recruitment patterns able to balance a given load. As previously mentioned, this is referred to as the redundancy problem of muscle recruitment, which is solved by the CNS. The CNS is able to balance the system regarding position, movement, and the external loading situation by activating a specific set of muscles. The human body is able to reproduce

movements with fairly high precision, which leads to the reasoning that muscle activation pattern must be based on a rational criterion (Rasmussen et al., 2001).

In order to solve the muscle redundancy for an inverse dynamics analysis, an optimization problem is usually formulated based on the assumption that the CNS is trying to minimize the load on the muscles and the body. The muscle recruitment criterion, which is the objective function that has to be minimized, can have different forms such as the linear criterion, the polynomial criteria, or the min/max criterion (Rasmussen et al., 2001). The most important factor when choosing the muscle recruitment criterion is for it to be physiologically reasonable.

- *Linear*: The linear recruitment criterion is the simplest version of the objective function. This criterion is based on the assumption that strong muscles do more work and will therefore only recruit a minimum number of muscles in order to balance the forces of the system. Furthermore, the criterion does not lead to muscle synergism and is therefore not physiologically reasonable.

- *Quadratic and polynomial*: The quadratic criterion will lead to synergism and share the load between muscles. If the order of the objective function is increased, the load-sharing between muscles is increased as well. The polynomial criteria can only be considered physiologically reasonable if constraints are included that prevent muscles from exceeding their physiological maximum.

- *Min/max criterion*: The min/max criterion is similar to increasing the order of the polynomial criteria infinitely. In this criterion, the muscle forces will be distributed in such a way that the maximum relative muscle force will minimized. However, this criterion might produce too much muscle synergism (Damsgaard et al., 2006, Rasmussen et al., 2001).

1.2.3 Inverse dynamics

In order to estimate internal forces and moments of forces an inverse dynamics analysis can be conducted. An inverse dynamics analysis is a method to bridge kinematic and kinetic data and is normally used on dynamic movements, but can also be applied to static bodies (Robertson, 2004). In order to conduct an inverse dynamics analysis, an array of different input is needed: 1) body segment parameters, 2) segment kinematics and 3) the external forces acting on the system (Vaughan et al., 1999).

In AnyBody Modeling System (AnyBody Technology, Aalborg, Denmark), the muscle and joint forces are found by formulating a complete set of equations for dynamic equilibrium. These equations consist of segment masses, inertial properties, accelerations, muscle forces, reaction forces and moments, and applied/external loads for each n segment within the model (Damsgaard et al., 2006). The inverse dynamics analysis solves those equations from prior results obtained in the kinematic analysis in which the state of the system obtained for each time instant of the recorded motion.

1.3 Orthoses

An exoskeleton worn by users who have lost the ability to move their limbs in a voluntary manner is called an orthosis. These devices can be used as either rehabilitation devices combined with surgery and physiotherapy or to assist users with ADL. The users who benefit from such devices are people who have do not have the necessary strength to move their limbs (Rink, 2011).

1.3.1 Design Considerations

When designing an orthosis it is important to take a number of considerations into account, such as the cosmetics, comfort, and control of the device. It is important to take the cosmetics of the orthosis into account as this can ensure continued use as well as limiting the stigmatisation. To avoid stigmatisation of the users, an orthosis should be designed to be as small, flat, and close to the skin as possible. Furthermore, the orthosis should be light as possible, as a heavy orthosis can affect the users' posture and make movements awkward. To further increase the cosmetic value of an orthosis, it should be designed to reduce the wear and tear on clothing. This means that the orthosis should not consist of nipples or other sharp metal edges and it should not use any oil or grease that would stain the clothes (Plettenburg, 1998). The comfort of an orthosis is also an important design factor and is significantly influenced by the fitting of the orthosis to the user. It is important to have a small contact area between the orthosis and the skin, as larger skin contact can obstruct the skin's perspiration. Therefore, the orthosis should consist of multiple small fitting areas where each area is reduced to the minimum size dictated by acceptable pressure and limb stability (Plettenburg, 1998). It is important that the pressure from the orthosis to the skin is directed perpendicular. This is due to an increased risk of skin damage when the orthosis is moving in the same plane as the skin. Furthermore, users prefer devices that can be donned and doffed easily (Plettenburg, 1998, Dunning and Herder, 2013). The control of the orthosis has to be assessed so that the possible usage of the orthosis live up to the expectations of the users. According to Rahman et al. (2000) , the most important tasks for orthotic users was the ability to self-feed, groom, and manipulate objects placed on a table.

1.3.2 Gravity Balancing

An orthotic device is considered to be passively balanced when the potential energy of the system remains constant during every configuration. In order to achieve this, several different techniques are feasible. One way is by using a simple counterweight (Wang and Gosselin, 1999, Laliberté et al., 1999) where a counter mass is added to each link of the orthosis. The downside of using this method is an increase in mass, bulkiness, and high inertia at the joints (Kobayashi, 2001). Another way to achieve constant potential energy is to add springs between the joints of the orthosis. In order for this to work, it is necessary to use

zero free length springs, which means springs where the exerted spring force is proportional to the length of the spring. Other methods have included non-circular cam mechanisms or compliant flexure elements, but both these techniques have only been designed to balance one DOF (Lustig et al., 2015), whereas the other two methods can be used for balancing a serial linkage system with multiple DOF. Early work in serial linkage systems using the zero free length springs used a parallel beam structure and used mono-articular springs in order to gravity balance the limbs (Rahman et al., 1995). However, this method increases the mass and inertia of the arm and limits the range of motion (Dunning and Herder, 2015).

In recent literature two methods for gravity balancing orthotic devices, using zero free length springs, have been presented. Both methods can use multiarticular springs and do not require the use of parallel beams. The first method is the stiffness matrix approach which was proposed by Lin et al. (2010). This method uses a general expression to articulate the potential energy, U, of a mechanical system: $U = \frac{1}{2}\mathbf{Q}^T\mathbf{K}\mathbf{Q}$, where $\mathbf{K}$ represents the stiffness matrix and $\mathbf{Q}$ represents the configurations of the orthoses. In order to find a statically balanced system, the off-diagonal elements of the matrix $\mathbf{K}$ should be constrained to zero. The second method was proposed by Deepak and Ananthasuresh (2012) and is an iterative method where balancing is ensured link by link. The balancing is performed by adding two zero free length springs between a link and the fixed body, starting from the most distal link. This way the the constraint equations for each link is only affected by the current and the previous link.

Both these methods use zero free length springs and are based on an energy approach in order to gravity balance a system. Nonetheless, there are many differences between their approaches. The stiffness matrix approach suggested by Lin et al. (2010) solves all constraints for a chosen spring configuration in one go, whereas the method suggested by Deepak and Ananthasuresh (2012) only evaluates a selection of the constraints. Due to this, the method by Deepak and Ananthasuresh (2012) can give a solution for which springs can be added to a system which has no straightforward solution. The method of Lin et al. (2010) does not give this solution directly, but has the possibility to acquire information on which links are unbalanced using the stiffness matrix (Lee and Chen, 2014). Another difference between the two methods is that all the springs in Deepak and Ananthasuresh (2012)'s method must be connected to the fixed body, whereas the method of Lin et al. (2010) allows springs to be attached between any two links.

While Deepak and Ananthasuresh (2012)'s method allows for planar attachment of the springs, the method of Lin et al. (2010) sets up criteria constraining the spring placement to occur on a fixed straight line. The reason for this limitation in the method of Lin et al. (2010) is the use of two different coordinates for spring attachments and joint states. The locations of springs and center of mass (CoM) are described as polar coordinates, while joint states are described as Cartesian coordinates. To overcome this limitation, Lustig et al. (2015) proposed using Cartesian coordinates to describe the locations of the springs and the CoM. They found that this alteration allowed for planar spring location and furthermore made the method

more intuitive to use and provided simpler constraint equations (Lustig et al., 2015).

In the present study, the method of Lustig et al. (2015) was used for the foundation of the original spring attachment points as well as spring stiffnesses. The derivation of the method is described in the following section. To attain gravity balancing of a serial linkage system the following assumptions must be made. All of the links are connected using revolute joints and the most proximal joint is attached to a rigid and static fixed body. The weight of all of the springs, which are zero free length, used to gravity balance the system are neglected.

1.3.3 Stiffness matrix

The stiffness matrix can be found using a general form of the energy equations $U = \frac{1}{2}\mathbf{Q}^T\mathbf{K}\mathbf{Q}$, where $\mathbf{Q}$ is the possible states of the system and $\mathbf{K}$ is the stiffness matrix. The stiffness matrix can be derived in five steps.

1. All coordinate points are described as a function of the parameter values and the states of the links.
2. Potential energy equations of the mass component and all the spring components must be written in a general form.
3. The energy equations of the mass and spring components must be summed into a total stiffness matrix.
4. The constraint equations of the system must be obtained from the total stiffness matrix.
5. The obtained constraint equations must be solved.

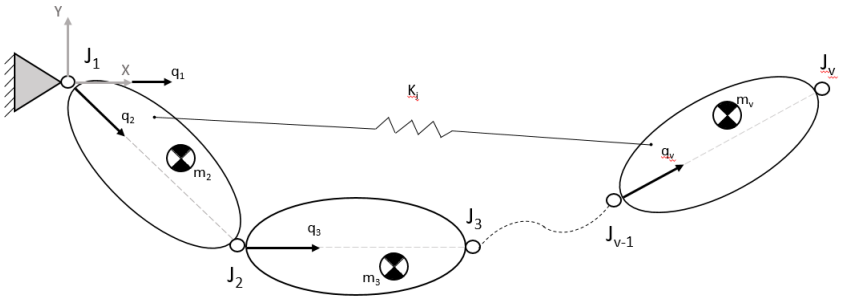

Figure 1.1: Free body diagram of a serial linkage system with v joints

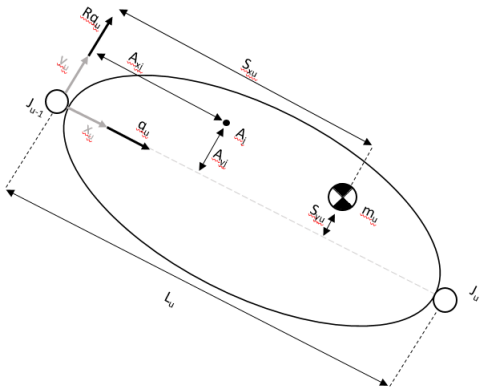

Figure 1.2: Free body diagram of a link u containing a center of mass and a spring attachment point

Step 1: Balancing a serial linkage system is to describe the coordinate points as functions of the parameter values and the states of the system's links. A representation of a serial linkage system can be seen in figure 1.1. The fixed body vector $\mathbf{q}_1$ is a constant which is aligned with the x-axis of the global coordinate system.

$$\mathbf{q}_1 = \begin{bmatrix} 1 \\ 0 \end{bmatrix} \tag{1.1a}$$

For all the moving links (u = 2 . . . n) the vector $\mathbf{q}_u$ is aligned with the local coordinate system of the link, which is located at the proximal joint $\mathbf{J}_{u-1}$.

$$\mathbf{q}_u = \begin{bmatrix} q_{xu} \\ q_{yu} \end{bmatrix} \tag{1.1b}$$

The state of all links can now be described by the vector $\mathbf{Q}$.

$$\mathbf{Q} = \begin{bmatrix} \mathbf{q}_1 \\ \vdots \\ \mathbf{q}_n \end{bmatrix} \tag{1.1c}$$

$$\mathbf{I} = \begin{bmatrix} 1 & 0 \\ 0 & 1 \end{bmatrix} \tag{1.1d}$$

The y axes of the local coordinate system are located perpendicular to the state vector $\mathbf{q}_u$. Therefore the y_u-axis can be found by rotating the state vector 90° using a rotation matrix $\mathbf{R}$.

$$\mathbf{R} = \begin{bmatrix} cos(90°) & -sin(90°) \\ sin(90°) & cos(90°) \end{bmatrix} = \begin{bmatrix} 0 & -1 \\ 1 & 0 \end{bmatrix} \tag{1.1e}$$

The global coordinates of the links' mass, spring attachment, and joint centers can be described as a linear combination of the state vectors and the constant parameters. First off, the joints locations are described. As the fixed body joint ($\mathbf{J}_1$) is located at the global coordinate system, the distal joint $\mathbf{J}_u$ can be described as a length L_u from the local coordinate system along the x-axis. The vector components of joint locations are found in equation 1.2.

$$\mathbf{J}_1 = \begin{bmatrix} 0 \\ 0 \end{bmatrix} \tag{1.2a}$$

$$\mathbf{J}_u = L_2\mathbf{I}\mathbf{q}_2 + L_3\mathbf{I}\mathbf{q}_3 + \cdots + L_u\mathbf{I}\mathbf{q}_u \sum_{i=2}^{n} L_i\mathbf{I}\mathbf{q}_i = \mathbf{J}_{u-1} + L_u\mathbf{I}\mathbf{q}_u \tag{1.2b}$$

Now the locations of the spring attachments can be found. The spring j between the joint u and v have two attachment points that are denoted as $\mathbf{A}_j$ and $\mathbf{B}_j$. The locations of these points can be found as a combination of the proximal joint component $\mathbf{J}_{u-1}$, the local x_u component and the local y_u component. These are found in equation 1.3.

$$\mathbf{A}_j = \mathbf{J}_{u-1} + (a_{xj}\mathbf{I} + a_{yj}\mathbf{R})\mathbf{q}_u \tag{1.3a}$$

$$\mathbf{B}_j = \mathbf{J}_{v-1} + (b_{xj}\mathbf{I} + b_{yj}\mathbf{R})\mathbf{q}_v \tag{1.3b}$$

The last part that needs to be located is the CoM, which is located in a similar way as the spring locations.

$$\mathbf{S}_u = \mathbf{J}_{u-1} + (s_{xu}\mathbf{I} + s_{yu}\mathbf{R})\mathbf{q}_u \tag{1.4}$$

Step 2: All energy equations must be written in their generalised form to separate the states from the stiffness matrix. The vector describing the length and orientation of the spring j, attached between link u and link v, can be described as $\mathbf{B}_j - \mathbf{A}_j$. As can be seen from figure 1.1, the length and orientation of spring j is dependent on the links' states. In equation 1.5 the expression the of vector describing length and orientation of the spring is derived.

$$\mathbf{B}_j - \mathbf{A}_j = \mathbf{J}_{v-1} + (b_{xj}\mathbf{I} + b_{yj}\mathbf{R})\mathbf{q}_v - \mathbf{J}_{u-1} - (a_{xj}\mathbf{I} + a_{yj}\mathbf{R})\mathbf{q}_u \tag{1.5a}$$

From this equation $\mathbf{J}_{v-1} - \mathbf{J}_{u-1}$ can be expressed as:

$$\mathbf{J}_{v-1} - \mathbf{J}_{u-1} = \mathbf{J}_u + \mathbf{J}_{u+1} + \cdots + \mathbf{J}_{v-1} = \sum_{n=u}^{v-1} L_n \mathbf{I} \mathbf{q}_n \tag{1.5b}$$

This expression can be inserted back into equation 1.5a which yields:

$$\mathbf{B}_j - \mathbf{A}_j = (b_{xj}\mathbf{I} + b_{yj}\mathbf{R})\mathbf{q}_v - (a_{xj}\mathbf{I} + a_{yj}\mathbf{R})\mathbf{q}_u + \sum_{n=u}^{v-1} L_n \mathbf{I} \mathbf{q}_n \tag{1.5c}$$

Now the constant parameters can be described as components $\mathbf{C}$.

$$\mathbf{B}_j - \mathbf{A}_j = \underbrace{(b_{xj}\mathbf{I} + b_{yj}\mathbf{R})}_{\mathbf{C}_v}\mathbf{q}_v + \underbrace{((L_u - a_{xj})\mathbf{I} - a_{yj}\mathbf{R})}_{\mathbf{C}_u}\mathbf{q}_u + \underbrace{\sum_{n=u}^{v-1} L_n \mathbf{I}}_{\mathbf{C}_{u+1}+\cdots+\mathbf{C}_{v-1}} \mathbf{q}_n \tag{1.5d}$$

The generalised form of the components can be seen in the following equation:

$$\mathbf{B}_j - \mathbf{A}_j = \sum_{n=1}^{v} \mathbf{C}_n \mathbf{q}_n \tag{1.5e}$$

In equation 1.6 the matrix form of the constant components $\mathbf{C}$ are found:

$$\mathbf{C}_u = \begin{bmatrix} L_u - a_{xj} & -a_{yj} \\ a_{yj} & L_u - a_{xj} \end{bmatrix} \tag{1.6a}$$

$$\mathbf{C}_i = \begin{bmatrix} L_i & 0 \\ 0 & L_i \end{bmatrix} \text{for,} i = u+1, \cdots, v-1 \tag{1.6b}$$

$$\mathbf{C}_v = \begin{bmatrix} b_{xj} & -b_{yj} \\ b_{yj} & b_{xj} \end{bmatrix} \tag{1.6c}$$

$$\mathbf{C}_i = \begin{bmatrix} 0 & 0 \\ 0 & 0 \end{bmatrix} \text{for:} \begin{cases} i = 0, \cdots, u-1 \\ i = v+1, \cdots, n \end{cases} \tag{1.6d}$$

The spring length as a function of the states has now been obtained and the potential energy can be calculated. As before mentioned, the springs are assumed to be zero free length springs, which have a spring stiffness of k_j. In equation 1.7 the generalised form of the stiffness is found. In this form, the states are separated from the parameters in the springs stiffness matrix ($\mathbf{K}_{s,j}$).

$$U_{s,j} = \frac{1}{2} k_j (\mathbf{B}_j - \mathbf{A}_j)^2 \tag{1.7a}$$

From equation 1.5e it is known that $\mathbf{B}_j - \mathbf{A}_j = \sum_{n=1}^{v} \mathbf{C}_n \mathbf{q}_n$, when inserting this into equation 1.7a following can be found:

$$= \frac{1}{2} k_j (\sum_{n=1}^{v} \mathbf{C}_u \mathbf{q}_u)^2 \tag{1.7b}$$

$$= \frac{1}{2} k_j \begin{bmatrix} \mathbf{q}_1 \\ \vdots \\ \mathbf{q}_n \end{bmatrix}^T \begin{bmatrix} \mathbf{C}_1^T \mathbf{C}_1 & \cdots & \mathbf{C}_1^T \mathbf{C}_n \\ \vdots & \ddots & \vdots \\ \mathbf{C}_n^T \mathbf{C}_n & \cdots & \mathbf{C}_n^T \mathbf{C}_n \end{bmatrix} \begin{bmatrix} \mathbf{q}_1 \\ \vdots \\ \mathbf{q}_n \end{bmatrix} \tag{1.7c}$$

Now the the function is rewritten into its generalised form:

$$U_{s,j} = \frac{1}{2} \mathbf{Q}^T \mathbf{K}_{s,j} \mathbf{Q} \tag{1.7d}$$

$$\mathbf{K}_{s,j} = \begin{bmatrix} \mathbf{C}_1^T \mathbf{C}_1 & \cdots & \mathbf{C}_1^T \mathbf{C}_n \\ \vdots & \ddots & \vdots \\ \mathbf{C}_n^T \mathbf{C}_n & \cdots & \mathbf{C}_n^T \mathbf{C}_n \end{bmatrix} \tag{1.7e}$$

Next the gravitational energy can be found in its generalised form. First, the height of the masses must be found. The global height of link u can be found in the second element of vector $\mathbf{S}_u$ found in equation 1.4. The second element can be extracted by a vector product: $height = \mathbf{S}_u \begin{bmatrix} 0 & 1 \end{bmatrix}$. To describe the direction of the gravitational force, a rotation matrix is used on the constant $\mathbf{q}_1$, so $\mathbf{R}\mathbf{q}_1 = \begin{bmatrix} 0 & 1 \end{bmatrix}$. Therefore, a generalised form of the gravitational energy combining the height of the CoM and the states can be found as $height = \mathbf{R}\mathbf{q}_1 \mathbf{S}_u$. In equation 1.8 the energy equation will be found for the mass of a single link and will thereafter be summed for all links in equation 1.9.

$$U_{m_u} = m_u g (\mathbf{R}\mathbf{q}_1)^T \mathbf{S}_u \tag{1.8a}$$

$$= m_u g \mathbf{R}^T \mathbf{q}_1^T \mathbf{S}_u \tag{1.8b}$$

From equation 1.4, $\mathbf{S}_u$ is derived and can be inserted into equation 1.8b.

$$= m_u g_1^T \mathbf{R}^T (\mathbf{J}_{u-1} + (s_{xu}\mathbf{I} + s_{yu}\mathbf{R})\mathbf{q}_u) \tag{1.8c}$$

$$= m_u g \mathbf{q}_1^T \mathbf{R}^T (\sum_{i=1}^{u-1} L_i \mathbf{I} \mathbf{q}_i + (s_{xu}\mathbf{I} + s_{yu}\mathbf{R})\mathbf{q}_u) \tag{1.8d}$$

$$U_{\sum m} = \sum_{u=2}^{n} U_{m_u} \tag{1.9a}$$

$$= \mathbf{q}_1^T \sum_{u=2}^{n} (\mathbf{R}^T m_u g (\sum_{i=1}^{u-1} L_i \mathbf{I} \mathbf{q}_i + (s_{xu}\mathbf{I} + s_{yu}\mathbf{R})\mathbf{q}_u)) \tag{1.9b}$$

Now all the constant components for calculating the gravitational energy can be collected into the variable $\mathbf{D}_u$

$$= \mathbf{q}_1^T \sum_{u=2}^{n} \underbrace{(\mathbf{R}^T((\sum_{i=u+1}^{n} m_i) g L_u \mathbf{I} + m_u g (s_{xu}\mathbf{I} + s_{yu}\mathbf{R}))}_{\mathbf{D}_u} \mathbf{q}_u) \tag{1.9c}$$

In following equation the matrix form of the constant $\mathbf{D}_u$ is found:

$$\mathbf{D}_u = \mathbf{R}^T((\sum_{i=u+1}^{n} m_i) g L_u \mathbf{I} + m_u g (s_{xu}\mathbf{I} + s_{yu}\mathbf{R})) \tag{1.10a}$$

$$\mathbf{D}_u = \begin{bmatrix} m_u g s_{yu} & m_u g s_{xu} + (\sum_{i=u+1}^{n} m_i) g L_u \\ -m_u g s_{xu} + (\sum_{i=u+1}^{n} m_i) g L_u & m_u g s_{yu} \end{bmatrix} \tag{1.10b}$$

Now that states and constant parameters have been separated, it is possible to set up the generalised equation for the gravitational energy:

$$U_{\sum m} = \frac{1}{2}\mathbf{Q}^T \mathbf{K}_m \mathbf{Q} \tag{1.11a}$$

$$\mathbf{K}_m = \begin{bmatrix} 0 & \mathbf{D}_2 & \cdots & \mathbf{D}_n \\ \mathbf{D}_2^T & 0 & \cdots & 0 \\ \vdots & \vdots & \ddots & \vdots \\ \mathbf{D}_n^T & 0 & \cdots & 0 \end{bmatrix} \tag{1.11b}$$

Step 3: The total stiffness matrix is found. This is done using the generalised form of the total combined energy U_t, which contains the energy contribution from the springs and the masses.

$$U_t = \frac{1}{2}\mathbf{Q}^T \mathbf{K}_t \mathbf{Q} \tag{1.12a}$$

$$\mathbf{K}_t = \mathbf{K}_m + (\sum_{i=1}^{n_{sprigs}} \mathbf{k}_{s,i}) \tag{1.12b}$$

Step 4: The constraint equations needed to balance a serial linkage system is found. For a system to be gravitationally balanced, the energy of the system must maintain constant energy levels regardless of the states of the links. This means that the energy difference between the states must be zero. For this to happen the off-diagonal elements in the stiffness matrix must be zero, as these represent the relative relations between states. This can be done by solving a number of constraint equations. The number of constraint equations depends on the number of links in the serial linkage system, which changes the size of the stiffness matrix ($\mathbf{K}_t$). As $\mathbf{K}_t$ is symmetrical, it is only necessary to solve the upper triangle of the matrix. Furthermore, all relations occur twice in this triangle, once in each even and uneven row. Therefore,

constraint equations only have to be found in the second row. A general rule for the number of constraint equations from a system is $n(n-1)$, where n is the number of links in the system.

Step 5: The constraint equations are solved to obtain gravity balancing. In general, the number of solvable variables is equal to the number of constraint equations and the rest of the values can be added to the equations as constants.

Methods 2

2.1 Product Requirements

This section aims to give a description of the processes involved in the development of a prototype of a passive orthosis for those diagnosed with amyoplasia. The process is introduced by identifying the current problems and the requirements of the orthosis.

2.1.1 Current Problems

According to Kowalczyk and Feluś (2016), the principal treatment goal in amyoplasia is to optimise the quality of life. This involves being able to perform ADL, which will consequently result in independent living. Despite amyoplasia being a very heterogenous disorder, there are prevalent traits. It has been reported from those with upper limb involvement at birth, 80% have internally rotated shoulders and 92% have elbows fixed in extension (Sells et al., 1996). The lack of elbow flexors is troublesome for ADL such as getting the hand to the mouth (Bernstein, 2002). Many manage through ADL by using the edge of table or using the position of one arm to aid the other (Ferguson and Wainwright, 2013). There are current passive orthoses which improve range of motion and the ability to perform ADL. Upon assessment of current passive orthoses and the disorder, there are conspicuous problems:

- Majority of passive devices are wheelchair bound, while many persons with amyoplasia are ambulatory.
- The shoulders remain internally rotated affecting the elbow position, and consequently affecting the hand, thus making the plane of movement and the function of the hand position problematic (Ferguson and Wainwright, 2013).
- None of the current passive devices support pronation/supination of the forearm (Dunning and Herder, 2013).

2.1.2 User Needs

Using the current knowledge of amyoplasia and existing problems of alternative methods of improving daily living the orthosis needs to:

- Be comfortable to wear and must not cause pain or discomfort to the user.

- Improve range of motion.
- Improve ability to perform ADL tasks.
- Support and follow the same movements of the upper limb.
- Gravitationally compensate the arm in all positions.
- Provide external rotation of the user's glenohumeral joint, keeping the the humerus in more a neutral position.
- Have an attachment point at thorax, allowing the user the option to be mobile.
- Be lightweight.
- Be composed of durable material. The orthosis and its mechanisms must be reliable and be able to withstand daily use.
- Be close fitting to the user's body, being compact and least cumbersome as possible.
- Allow adjustability to tailor to the variety of muscle strengths and joint ROM of persons with amyoplasia.

2.1.3 Target Specifications

Considering that the version of the orthosis developed is the first prototype, the objective is to identify essential specifications. The fundamental goals of the passive orthosis prototype are:

- To enhance range of motion and the ability to perform ADL tasks by gravitationally compensating the arm in all positions and providing external rotation to the humerus.
- Potentially aid in the promotion of muscle development.
- To attach the orthosis at the thorax.
- To avoid causing pain and discomfort to the user.

2.2 Conceptual Development

To best address the target specifications of the orthosis, as well as the functionality, the early stages of concept development involved research on the development of prototypes and available products of passive and active orthoses, as well as robotic exoskeletons. Ideas included hand drawings, which were then brought

to 3D designs using SolidWorks software v.2015x64 Edition SP5.0 (Dassault Systèmes, SolidWorks Corp., Massachusetts, USA). Different designs were produced at different stages, either fixing flaws in previous designs or simplifying the design while still meeting the desired function. Alterations were rapidly prototyped using 3D printing to aid in the observance of functions, while the final prototype included parts that were 3D printed as well as manufactured. Details of the manufacturing and 3D printing methods are discussed in section 2.2.4 and 2.2.5. Considering the design of the orthosis was complex and constantly evolving, the following iterations are organised by segment.

2.2.1 Back & Shoulder

The design of the shoulder prototype originates at the user's back, in order to meet the specification of the orthosis being wearable. To create an area to mount the orthosis, a mold was made from aquaplast™(Homecraft Roylan, Sutton-in-Ashfield, UK). Aquaplast™is a thermoplastic material that is normally used for orthotic and splinting products. The aquaplast™was heated using boiling water and was molded to form a fitted shell one subject. The mold was later reinforced with fiberglass to improve its strength. The mold provided a surface that could be used for mounting areas from the sternum, around the rib cage, to the spine as well as the surface of the trapezius.

To create a fixed point of the orthosis, a simple square mount was designed to be bolted into the mold. A medial and lateral arm were also created to establish a connection to the shoulder mechanisms. The medial arm attaches to the square mount through a bearing, creating a revolute joint. On the inferior and medial aspects of the square mount there is a support to prevent the medial arm from making a full 360° rotation. Both the medial and lateral parts consist of multiple holes which allow for adjustments in lengths, allowing for the shoulder mechanism to align with the user's shoulder joint center. This design can be seen in figure 2.1. The end of the lateral arm serves as the connection to the shoulder mechanism, using a bearing it creates the first of the shoulder mechanism's serial revolute joints. The purpose of this system is to form a grounded aspect of the orthosis, which allows for the elevation of the shoulder.

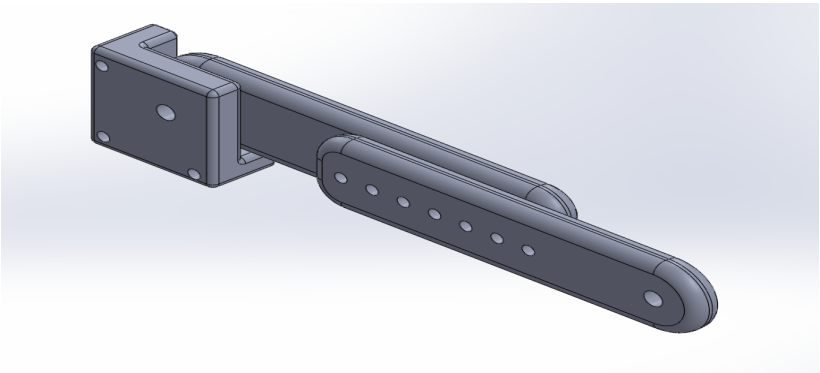

Figure 2.1: Back parts which are fixed to thorax shell

To create a mechanism that mimics the shoulder movement, prototypes of a three revolute (3R) serial joint and a four revolute (4R) serial joint mechanisms were designed, forming a connection between the back and upper arm. First designs of the 3R mechanism, seen in figure 2.2, were composed of a 90° circular arc, attaching to the a straight rectangular arm. Two of the revolute joints were located in this design. The first joint is located at the connection to the lateral back. These joints were created using bearings. The third aspect of the serial joint is located in the mechanism of the upper arm, which is discussed in section 2.2.2. The first design of the 4R, as seen in figure 2.2, was made up of three 90° circular arcs and an angled rectangular connector. The arcs in this mechanism were chosen to be larger than the 3R, to prevent it from collisions with the body. However, one of the arcs was smaller than the other two, allowing for them to have space to rotate over each other. Each arc was organised perpendicularly to the next and are connected by bearings to create revolute joints, the three revolute joints in concert provide a spherical joint. This part connects to the shoulder mechanism with the upper limb at 45°. The 45° angle is a concept taken from Carignan and Liszka (2005)'s prototype, with the aim to allow the arm to abduct further before the joints interfere with each other. The upper arm mechanism creates the final serial joint, as it does in the 3R mechanism. Both the 3R and 4R are designed to have the center of axis rotation aligned with the center of the glenohumeral joint. Considering that it is difficult to measure the center of the joint, this was estimated and also adjustable with the connection to the mounted back arm.

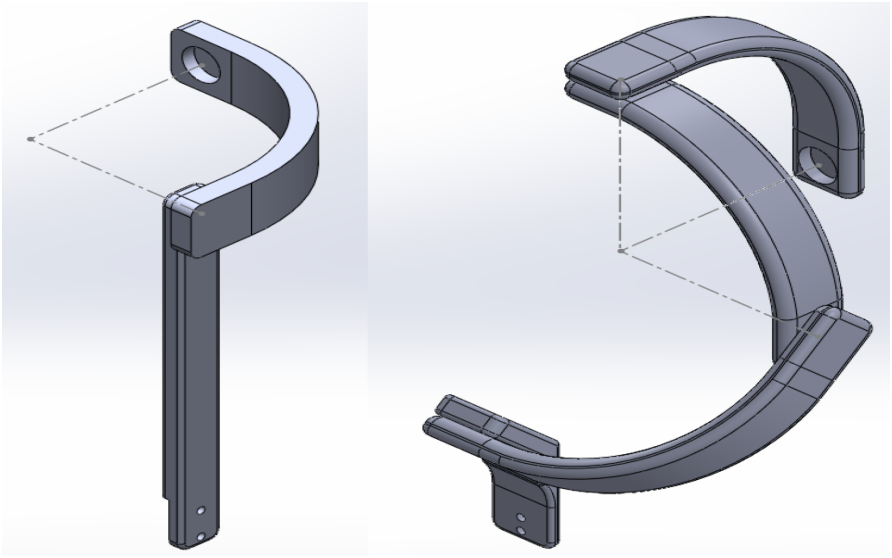

Figure 2.2: Left: 3R mechanism. Right: 4R mechanism

These early prototypes were 3D printed to observe the measurements and to test the overall reliability of the system. The 3R revealed problems with the rectangular part due to the proximal connection to the upper arm. As a consequence, the radius of the arc would need to be decreased. This created a higher risk of colliding with the body. The 3R also showed problems when forced into singularity. The redundant joint in

the 4R performed as anticipated, preventing the mechanism to reach singularity within the workable space in a healthy subject. However, the extra DOF created problems with the last serial joint on the upper arm. Considering the purpose of the last joint is to limit internal/external rotation of the humerus, discussed earlier as one of the target specifications, the redundant joint allows for the user to move in this plane. Alternative angles, lengths, and placement of the revolute joints were tested, however new singularities would arise as well as collisions with the body.

Although the 3R prototype did show an issue with singularity, a study by (Buckley et al., 1996) has found that the required shoulder elevation for ADL is usually less than 90°. Dunning and Herder (2013) have also suggested that a design strategy could be to neglect the full vertical range of motion of the shoulder in future designs, focusing only on the support of the most essential daily tasks. With regards to this information, as well as it being a less complicated design, the 3R was chosen to be further optimised and implemented into the orthosis.

Disregarding singularity, the largest complication with the 3R was the circular radius of the arc in relation to the part connecting the mechanism to the upper arm. A radius was chosen that would make the arc large enough to avoid collision with the body, yet would prevent it from being to bulky. To account for this size, either the part connecting to the upper limb would need to be angled or the upper arm attachment would need to be larger. The former was chosen to keep the overall size of the orthosis smaller and lighter. The angle was calculated in which the connection would be located at the middle of the humerus. The geometry of the two parts were changed from rectangular to tubes to account for the torsional stress that system would experience. This design can be seen in figure 2.3.

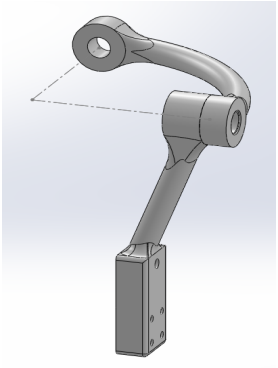

Figure 2.3: Final version of shoulder mechanism

2.2.2 Upper Limb

As mentioned in the previous section, the final axis of rotation from the 3R mechanism is located on the humeral axis. In order to allow for this rotation, the early concepts of the upper arm part involved two shells which would have the ability to slide on each other. In order to achieve this sliding mechanism, a

convex double rail system was considered. The original aim was to design a shell and to outsource a non-lubricated curved bearing and rail system. It is important that the slider must be non-lubricated, because it is important that orthoses do not possess oil, grease, and other pollutants (Plettenburg, 1998). However, it was not guaranteed that a company could provide the desired curvature to fit the arm. Therefore it was necessary for the authors to design their own non-lubricated sliding mechanism.

The first prototype consisted of a shell that covered the arm in a 180° arc. On the interior surface of the shell there would be a rectangular indent. This indent would be made of a part that would be inserted, containing circular holes which sliding rails would be fit into. This can be seen in figure 2.4. This material would be a 3D printed material made up of a tribological optimised filament, which is lubricant free, wear resistant, and has a low coefficient of friction. This material is described in more detail in section 2.2.5. The gliding rail would connect the upper arm to the elbow joint and would have springs, limiting internal and external rotation of the humerus.

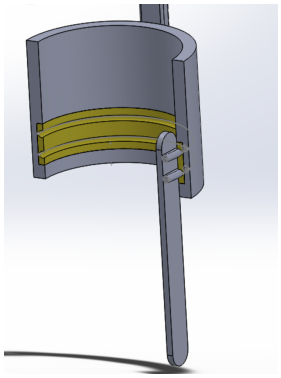

Figure 2.4: First prototype of humerus shell

This first design was filled with many limitations. The part that would need to be 3D printed would require high precision as well as a high cost for the amount of material needed. Placing the rail and bearing interaction on the inside of the shell would create a high probability of pinching between the mechanism and the skin or clothing of the user. Therefore, it was decided that the rails should be located on the outside of the shell and the bearing slider would be on the part connecting to the elbow.

The second prototype, shown in figure 2.5, was recreated to fix the previously mentioned flaws, as well as decreasing the overall size of the structure. However, new issues were exposed. Manufacturing the two rails would be difficult due to the many risks of creating an imprecise curvature. The correct curvature is very important because any imprecisions on either the rail or the slider bearing would create wedging, causing the mechanism to be locked. Although some friction is acceptable, the goal of this mechanism is to have the spring limit the user's humeral rotation. Any unwanted locking may cause discomfort or pain to the user as well as unwanted stress in the orthosis that may lead to damage of the mechanism. The design was also assumed to be quite feeble. The expected stresses in the rail have a high risk of bending the rails, which

would also change in the curvature and would result in the same locking problems as mentioned before.

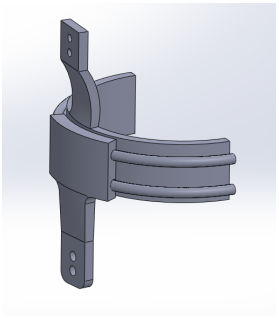

Figure 2.5: Second prototype of upper arm shell

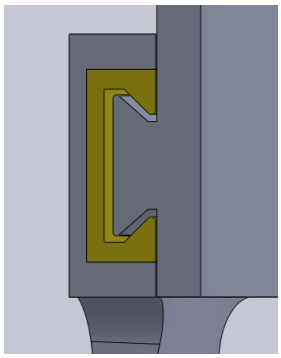

Figure 2.6: Dovetail slider mechanism

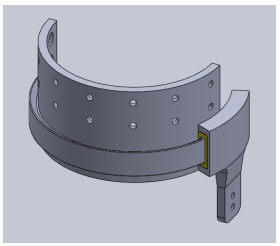

Figure 2.7: Shell and dovetail slider prototype

In the third prototype, the aim was to create a mechanism that would be able to undergo the forces, but would still be able to allow the mechanism to securely slide. The newest design would be a triangular shape, this was chosen for its geometric strength. To avoid high stresses at the sharp points of the triangle, as well as to avoid the mechanism from slipping out of the connection, a dovetail design was chosen. This part would have a small space in which the 3D printed material would fit in, a similar concept to that of the first prototype. This can be seen in figure 2.6 and figure 2.2.2. Although this design was more stable, the manufacturability was questionable. In order to undergo the forces in the springs, as well as the arm, it was planned that these parts would be made from metal. Milling a complex geometry, the dovetail design in addition to the curvature, created high risks for similar misalignment errors in the past prototypes. To simplify this complication, the design was changed into a rectangular shape. Holes are applied to the shell to allow for the strapping of the upper arm. The optimizing of manufacturability and the spring functionality are discussed in section 2.2.4 and 2.2.6, respectively.

2.2.3 Forearm

The purpose of the forearm components is to act as a support for the forearm as well as connect both the wrist and upper arm in an arrangement that allows for the orthosis to provide elbow flexion/extension. The forearm component is composed of two separate pieces: the forearm brace, which supports the forearm, and the forearm connector, which connects the forearm brace to the elbow joint. The forearm connector is a simple design, a beam with circular ends. It is composed of a hole that links to the slider, creating the elbow joint, as well as many holes which act as spring attachment points and attachment points for the forearm brace. Multiple holes allow for the adjustability of the spring locations as well as the positioning of the forearm shell.

The early designs of the forearm brace incorporate a 180° arc support. There are straps on the proximal

aspect of the circular support, allowing for strapping of the forearm. When strapped in this area of the forearm, it does not restrict forearm supination and pronation. As the part nears the wrist, there is continued support along the lateral aspect of the arm. The reasoning behind the lengthened support is that a spring attachment point can be created. This would attach to the radial aspect, near the scaphoid, of the wrist. Extra material was added to this area to account for the load from the spring. This spring is to be connected to a wrist brace to aid the forearm into supination. This was included in the design because it has been previously discussed that none of the current passive devices support pronation supination of the forearm, which is important for self-feeding, dressing, and personal hygiene (Dunning and Herder, 2013, Lee et al., 2003). The following section describes an early prototype of the wrist brace, however in the current study, the interaction of the spring mechanism between the forearm shell and the wrist were not investigated.

Taking inspiration from designs of other 3D printed wrist braces, a wrist brace was created to aid in the supination of the forearm. This design was composed of a complex design of hexagonal patterns and reinforced areas of the palmar and dorsal sides. When printed with PLA at 100% infill, one is able to take the advantage of the thermoplastic qualities of the PLA material. The print was submerged into boiling water and then can be taken out and molded onto the wrist to fit. The first version of the brace had a knob designed in the radial aspect of the wrist. This was a simple concept, in which the spring would be attached to the knob and pull the wrist into supination. This design was 3D printed to observe both the thermoplastic qualities as well as the strength and durability of the design.

Figure 2.8: Wrist brace

The molding of the wrist was successful, however both the knob and the area around it were fragile. Even if the knob was strong enough, applying the force on the middle of the brace may not be enough to pull the forearm into supination. To prevent this, 3 sets of holes were created equidistantly from each other, with the middle set being in the same location as the knob. These areas were also reinforced with extra material in the direction that would be loaded most from the forces of the spring. This design can be seen in figure 2.8.

2.2.4 Manufacturing

Before finalizing the working prototype of the orthosis, it is important to correctly select the materials and the processes that will be used to create them. With today's technological advances, it has become easy to use computer-aided model (CAD) to create, modify, analyze, and optimise a design. However, it is often difficult or expensive to physically recreate these geometries. As the availability of 3D printers have increased, so has the opportunity to easily recreate these complex geometries and rapidly produce prototypes (Bak, 2003). While there have been advancements in material sciences, thus increasing the strength and lowering the weight of materials available for 3D printing, the ability to 3D print stronger materials can be costly. While it is possible for certain parts of the final design to be made in similar processes as the early prototypes, other parts will undergo high stresses and will need to be manufactured differently. In these cases, their geometry must be altered or separated to aid in the difficulty of production. The following section will detail the materials, 3D printers, and manufacturing processes that were involved in the early prototypes as well as the final prototype.

2.2.5 3D Printing & Materials

All prototypes were printed using the MakerBot Replicator 2X (MakerBot, New York, USA) and the BCN3D Sigma (BCN3D Technologies, Barcelona, Spain). Prototypes made by the MakerBot Replicator 2X were made in acrylonitrile butadiene styrene (ABS), while prototypes made by the BCN3D Sigma were made in polylactic acid (PLA). As prototypes, there was no specific material for each part. Prototypes were used to observe functionality, size, and printing capabilities of the geometries. Later prototypes were printed in ABS with 100% infill to inspect strength. Further finite element analyses (FEA) were completed on parts that were suspected to undergo high stresses. These are parts that contain spring attachment points or which span over the joints. Parts in the final design that were deemed strong enough when made in ABS were printed by the Folger Tech FT-5 (Folger Technologies LLC, New Hampshire, USA) at 100% infill.

As previously mentioned in section 2.2.2, there is a part that would be printed in a non-lubricated material. This material is made of a tribological optimised filament named iglidur I3-PL (Igus, Cologne, Germany). This is a product that is developed for laser sintering, which allows its surfaces to be accurately made. It has a low coefficient of friction and is wear resistant. The design of the inside of the slider was sent to Igus where it was manufactured.

The first two parts of the shoulder joint, discussed in section 2.2.1, and the forearm brace were printed in Onyx (Markforged, Massachusetts, USA). Onyx is a filament that is the result of combining nylon with micro-carbon reinforcement, making it a stronger material than ABS. These parts are printed by the Mark X (Markforged, Massachusetts, USA). The Mark X is able to reinforce the design between each layer with carbon fiber.

The upper arm shell, the slider, and the forearm connector were all chosen to be manufactured in 7075-T6 aluminium using a Deckel Maho DMU60T (Deckel Maho, Seebach, Germany) milling machine. This material was chosen because its strength is comparable to many steels and is also lightweight. However, because the original designs were of high complexity and needed to fit precisely together, some of these designs needed to be simplified for manufacturing.

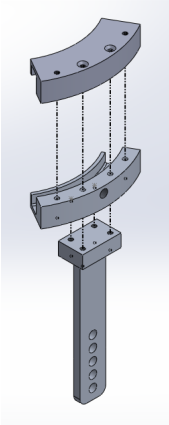

Figure 2.9: Final slider, exploded view

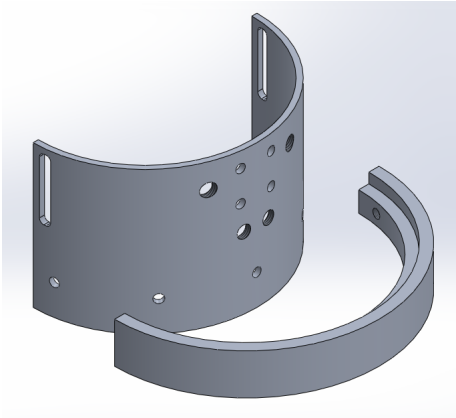

Figure 2.10: Final upper arm shell, exploded view

2.2.6 Final Design

Many of the parts discussed in the conceptual development remained similar or underwent very small changes. These are small adjustments such as the modification of measurements to fit the user better and the introduction of extra holes to allow for additional adjustments. The upper arm brace and the slider part were both split up into two and three parts, respectively. The changes can be seen in figure 2.9 and 2.10. Holes were added for spring attachments based on calculations from section 1.3.2. On the shell, anteriorly and posteriorly located between the attachment points of the springs, screws act as pulleys. As the user internally or externally rotate the humerus, the pulleys act on the spring increasing the force and tension as the slider moves further. This mechanism aids in the alignment of the shoulder into a more neutral position. The tribological slider part which is made separately are not included in figure 2.9. A rectangular cube made of 7075-T6 aluminium was also created and bolted to the thorax mold. This piece contains a screw hook where the biarticular spring will be attached to the forearm aspect of the forearm connector. There is also an attachment point to the upper arm shell which can attach to the the opposite end of the forearm connector to form monoarticular spring. The final design of the prototype can be seen in figure 2.11 and figure 2.12. Technical drawings of all parts and assemblies can be seen in Appendix A.1.

Figure 2.11: Subject wearing the orthosis, frontal view

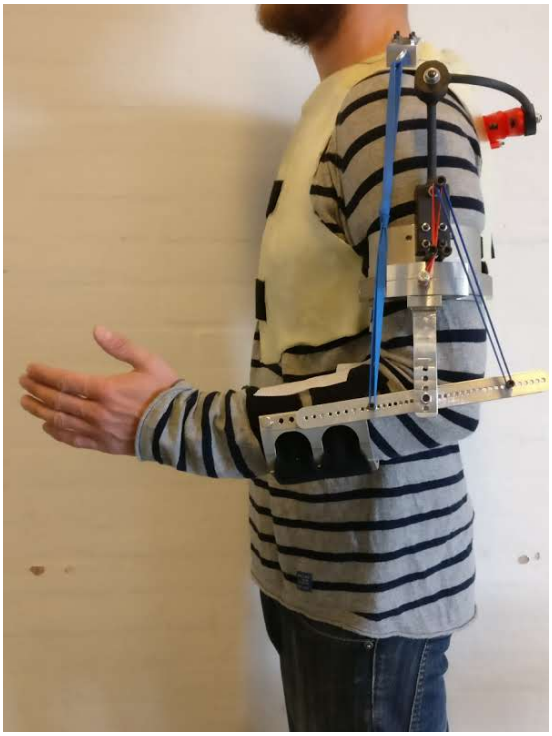

Figure 2.12: Subject wearing the orthosis, lateral view

2.3 Musculoskeletal Modeling

2.3.1 Simulations

The musculoskeletal model in the current study was scaled to experimentally obtained motion capture data by the aforementioned method of Andersen et al. (2010). The computer-aided model (CAD) was translated to AnyScript language by the use of the SolidWorks2AnyBody add-in in SolidWorks. The orthosis was then included and attached to the musculoskeletal model. In order to attach the orthosis, reference nodes were defined on the musculoskeletal model on which the orthosis could be aligned. These reference nodes were defined on the thorax, along the longitudinal axis along the humerus, and ulna. The musculoskeletal model wearing the orthosis can be seen on figure 2.13.

The springs on the orthosis were modelled as a force. In this case, the force used a *'shortest path line'* and a spring stiffness as input. The lines were attaching to reference nodes on the model. The length of *'shortest path line'* change dependently on the posture of the model and, as a consequence, act like a spring as a function of the length. The springs on the orthosis can be seen in figure 2.14 as the red, blue and green line. The green line creates a line between the glenohumeral joint and the forearm, assisting flexion of the elbow and glenohumeral joint. The blue line creates a line along the humerus, bringing the humerus to a neutral position. The red line creates a line between the humerus and the posterior side of the elbow, assisting elbow extension.

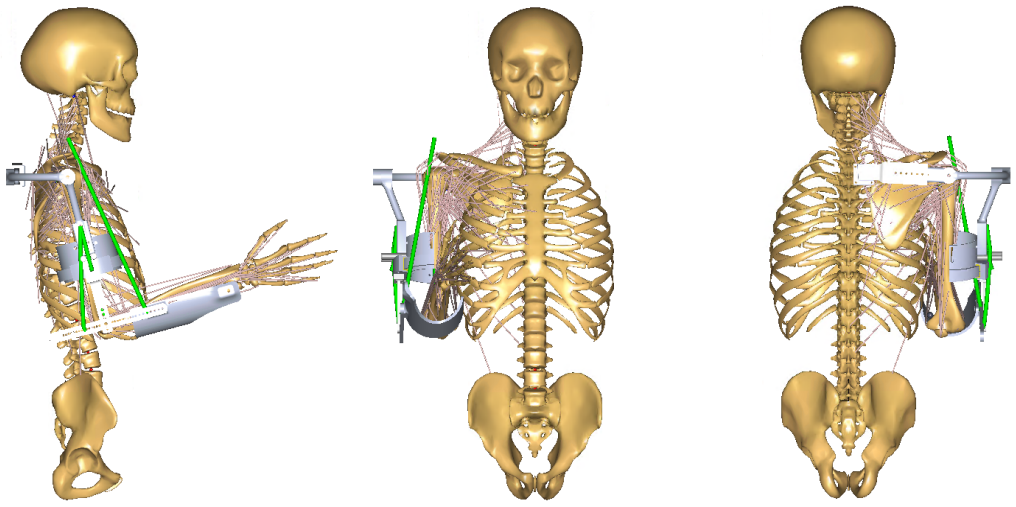

Figure 2.13: Musculoskeletal model wearing the orthosis. Lateral, frontal and posterior view

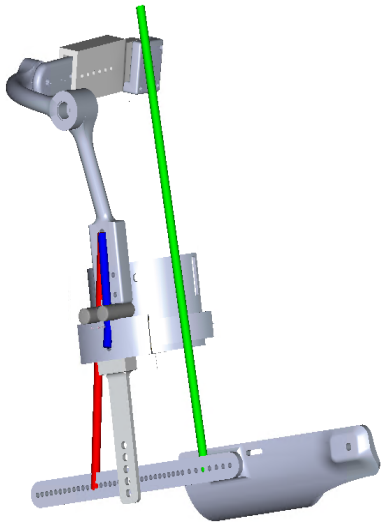

Figure 2.14: Orthosis with three different springs. Green is biarticular, red is monoarticular, blue is internal/external prevention

In order to imitate amyoplasia, modifications were made to the muscles of model. According to Bamshad et al. (2009) the elbow flexor muscles are weak or absent, and according to Kowalczyk and Feluś (2016) the deltoids are deficient. Therefore, the following muscles were disabled: biceps brachii, brachialis, pronator teres, brachioradialis, extensor carpi radialis, extensor digitorum, extensor digiti minimi, supinators, and deltoideus clavicular. Consequently, there might be situations in which the system is not able to solve the dynamics due to the muscle configuration. Therefore, artificial muscles are added to the system in order to allow simulations of muscle overactivation. Overactivation occurs when the maximal muscle activity (MMACT), which is the ratio between muscle force and muscle strength, is higher than 1. Physiologically

this means that the muscle is not able to exceed the required force (Zhou et al., 2015).

For the inverse dynamics analysis in the current study, ten different postures are used. The joint angles of these posture are shown in table 2.1. These ten postures are extracted from experimentally obtained motion capture data. To solve the kinematics of the motion capture data, the method of Andersen et al. (2010) was applied due to its ability to deal with over-determinate systems. The inverse dynamics are solved using the min/max muscle criterion due to being physiological reasonable, considering the min/max criterion uses the muscles optimally and does not exceed the upper limits of the muscles before being unavoidable.

Table 2.1: Joint angles of the ten postures

Posture	GH flexion	GH abduction	GH external rotation	Elbow flexion
1	10	0	0	90
2	50	30	0	125
3	70	10	0	125
4	20	45	0	90
5	0	80	0	120
6	90	0	0	10
7	10	90	0	90
8	10	90	0	90
9	60	50	0	70
10	45	45	0	45

2.4 Evaluation

To evaluate the orthosis, a subjective rating test of the device was performed to observe the physical behavior of the orthosis while worn on one healthy male subject. The measure of comfort and degree of difficulty on the user throughout chosen movements and tasks of daily living were observed.

Results 3

3.1 Hand calculations of gravity balancing

In order to gain an initial idea of spring stiffnesses and attachments the stiffness matrix approach described in section 1.3.2. In table 3.1 all known and calculated values for gravity balancing can be seen. The six values above the horizontal line was found by solving the equilibrium equations, while the values below know beforehand.

Table 3.1: known and calculated values of a gravity balanced system

Parameters	Values	Units
a_{x1}	0.0	[m]
b_{x1}	0.1026	[m]
b_{y1}	0.0009	[m]
b_{x2}	-0.077	[m]
b_{y2}	-0.0006	[m]
k_1	382.15	$[Nm^{-1}]$
k_2	756.0	$[Nm^{-1}]$
a_{y1}	0.070	[m]
a_{x2}	0.092	[m]
a_{y2}	0.000	[m]
m_2	2.294	[kg]
m_3	1.682	[kg]
L_2	0.28	[m]
s_{x2}	0.1275	[m]
s_{y2}	0.00	[m]
s_{x3}	0.1662	[m]
s_{y3}	-0.0011	[m]

Bibliography

Andersen, M., Damsgaard, M., MacWilliams, B. and Rasmussen, J. (2010), 'A computationally efficient optimisation-based method for parameter identification of kinematically determinate and over-determinate biomechanical systems', *Computer Methods in Biomechanics and Biomedical Engineering* **13**(2), 171–183.

Andersen, M., Damsgaard, M. and Rasmussen, J. (2009), 'Kinematic analysis of over-determinate biomechanical systems', *Computer Methods in Biomechanics and Biomedical Engineering* **12**(4), 371–384.

Bak, D. (2003), 'Rapid prototyping or rapid production? 3d printing processes move industry towards the latter', *Assembly Automation* **23**(4), 340–345.

Bamshad, M., Van Heest, A. E. and Pleasure, D. (2009), 'Arthrogryposis: A Review and Update:', *The Journal of Bone and Joint Surgery-American Volume* **91**(Suppl 4), 40–46.

Bernstein, R. M. (2002), 'Arthrogryposis and amyoplasia', *Journal of the American Academy of Orthopaedic Surgeons* **10**(6), 417–424.

Buckley, M. A., Yardley, A., Johnson, G. R. and Cams, D. A. (1996), 'Dynamics of the upper limb during performance of the tasks of everyday living—a review of the current knowledge base', *Proceedings of the Institution of Mechanical Engineers, Part H: Journal of Engineering in Medicine* **210**(4), 241–247. PMID: 9046184.

Carignan, C. and Liszka, M. (2005), Design of an arm exoskeleton with scapula motion for shoulder rehabilitation, *in* 'Advanced Robotics, 2005. ICAR'05. Proceedings., 12th International Conference on', IEEE, pp. 524–531.

Damsgaard, M., Rasmussen, J., Christensen, S. T., Surma, E. and de Zee, M. (2006), 'Analysis of musculoskeletal systems in the AnyBody Modeling System', *Simulation Modelling Practice and Theory* **14**(8), 1100–1111.

Deepak, S. R. and Ananthasuresh, G. K. (2012), 'Perfect static balance of linkages by addition of springs but not auxiliary bodies', *Journal of mechanisms and robotics* **4**(2), 021014.

Dunning, A. G. and Herder, J. L. (2013), A review of assistive devices for arm balancing, *in* 'Rehabilitation Robotics (ICORR), 2013 IEEE International Conference on', IEEE, pp. 1–6.

Dunning, A. G. and Herder, J. L. (2015), A close-to-body 3-spring configuration for gravity balancing of the arm, *in* 'Rehabilitation Robotics (ICORR), 2015 IEEE International Conference on', IEEE, pp. 464–469.

Ezaki, M. (2010), 'An approach to the upper limb in arthrogryposis', *Journal of Pediatric Orthopaedics* **30**, S57–S62.

Ferguson, J. and Wainwright, A. (2013), 'Arthrogryposis', *Orthopaedics and Trauma* **27**(3), 171–180.

Gordon, N. (1998), 'Arthrogryposis multiplex congenita', *Brain and Development* **20**(7), 507–511.

Hall, J. G. (2014), 'Arthrogryposis (multiple congenital contractures): Diagnostic approach to etiology, classification, genetics, and general principles', *European Journal of Medical Genetics* **57**(8), 464–472.

Kalampokas, E., Kalampokas, T., Sofoudis, C., Deligeoroglou, E. and Botsis, D. (2012), 'Diagnosing Arthrogryposis Multiplex Congenita: A Review', *ISRN Obstetrics and Gynecology* **2012**, 1–6.

Kimber, E. (2015), 'AMC: amyoplasia and distal arthrogryposis', *Journal of Children's Orthopaedics* **9**(6), 427–432.

Kobayashi, K. (2001), 'Comparison Between Spring Balancer and Gravity Balancer in Inertia Force and Performance', *Journal of Mechanical Design* **123**(4), 549.

Kowalczyk, B. and Feluś, J. (2016), 'Arthrogryposis: an update on clinical aspects, etiology, and treatment strategies', *Archives of Medical Science* **1**, 10–24.

Kroksmark, A.-K., Kimber, E., Jerre, R., Beckung, E. and Tulinius, M. (2006), 'Muscle involvement and motor function in amyoplasia', *American Journal of Medical Genetics Part A* **140A**(16), 1757–1767.

Laliberté, T., Gosselin, C. M. and Jean, M. (1999), 'Static balancing of 3-DOF planar parallel mechanisms', *IEEE/ASME transactions on mechatronics* **4**(4), 363–377.

Lee, M. J., LaStayo, P. C. and vonKersburg, A. E. (2003), 'A Supination Splint Worn Distal to the Elbow: A Radiographic, Electromyograohic abd Restrosoective Report', *Journal of Hand Therapy* **26**(3), 190–198.

Lee, Y.-Y. and Chen, D.-Z. (2014), 'Determination of spring installation configuration on statically balanced planar articulated manipulators', *Mechanism and Machine Theory* **74**, 319–336.

Lin, P.-Y., Shieh, W.-B. and Chen, D.-Z. (2010), 'A stiffness matrix approach for the design of statically balanced planar articulated manipulators', *Mechanism and Machine Theory* **45**(12), 1877–1891.

Lund, M. E., Andersen, M. S., de Zee, M. and Rasmussen, J. (2015), 'Scaling of musculoskeletal models from static and dynamic trials', *International Biomechanics* **2**(1), 1–11.

Lund, M. E., de Zee, M., Andersen, M. S. and Rasmussen, J. (2012), 'On validation of multibody musculoskeletal models', *Proceedings of the Institution of Mechanical Engineers, Part H: Journal of Engineering in Medicine* **226**(2), 82–94.

Lustig, M., Dunning, A. G. and Herder, J. L. (2015), Parameter analysis for the design of statically balanced seral linkages using a stiffness matrix approach with Cartesian coordinates, Vol. 2015, Research gate, Taipei, Taiwan, p. 9.

Plettenburg, D. H. (1998), Basic requirements for upper extremity prostheses: The WILMER approach, *in* 'Engineering in Medicine and Biology Society, 1998. Proceedings of the 20th Annual International Conference of the IEEE', Vol. 5, IEEE, pp. 2276–2281.

Rahman, T., Ramanathan, R., Seliktar, R. and Harwin, W. (1995), 'A simple technique to passively gravity-balance articulated mechanisms', *Transactions-American Society Of Mechanical Engineers Journal Of Mechanical Design* **117**, 655–657.

Rahman, T., Sample, W., Seliktar, R., Alexander, M. and Scavina, M. (2000), 'A body-powered functional upper limb orthosis', *Journal of rehabilitation research and development* **37**(6), 675.

Rasmussen, J., Damsgaard, M. and Voigt, M. (2001), 'Muscle recruitment by the min/max criterion—a comparative numerical study', *Journal of biomechanics* **34**(3), 409–415.

Rink, B. D. (2011), 'Arthrogryposis: a review and approach to prenatal diagnosis', *Obstetrical & gynecological survey* **66**(6), 369–377.

Robertson, D. G. E., ed. (2004), *Research methods in biomechanics*, Human Kinetics, Champaign, IL.

Sells, J. M., Jaffe, K. M. and Hall, J. G. (1996), 'Amyoplasia, the Most Common Type of Arthrogryposis: The Potential for Good Outcome', *PEDIATRICS* **97**(2), 225–231.

Van Heest, A. E. (2015), Arthrogryposis, *in* D. R. Laub, ed., 'Congenital Anomalies of the Upper Extremity', Springer US, Boston, MA, pp. 305–315. DOI: 10.1007/978-1-4899-7504-1_23.

Vaughan, C. L., Davis, B. L. and O'Connor, J. C. (1999), *Dynamics of human gait*, Kiboho Publishers, Howard Place. OCLC: 150238392.

Wang, J. and Gosselin, C. M. (1999), 'Static balancing of spatial three-degree-of-freedom parallel mechanisms', *Mechanism and Machine Theory* **34**(3), 437–452.

Zhou, L., Bai, S., Andersen, M. S. and Rasmussen, J. (2015), 'Modeling and Design of a Spring-loaded, Cable-driven, Wearable Exoskeleton for the Upper Extremity', *Modeling, Identification and Control: A Norwegian Research Bulletin* **36**(3), 167–177.

Zlotolow, D. A. and Kozin, S. H. (2015), Arthrogryposis, *in* J. M. Abzug, S. H. Kozin and D. A. Zlotolow, eds, 'The Pediatric Upper Extremity', Springer New York, New York, NY, pp. 803–837. DOI: 10.1007/978-1-4614-8515-5_35.

Appendix A

A.1 Technical drawings

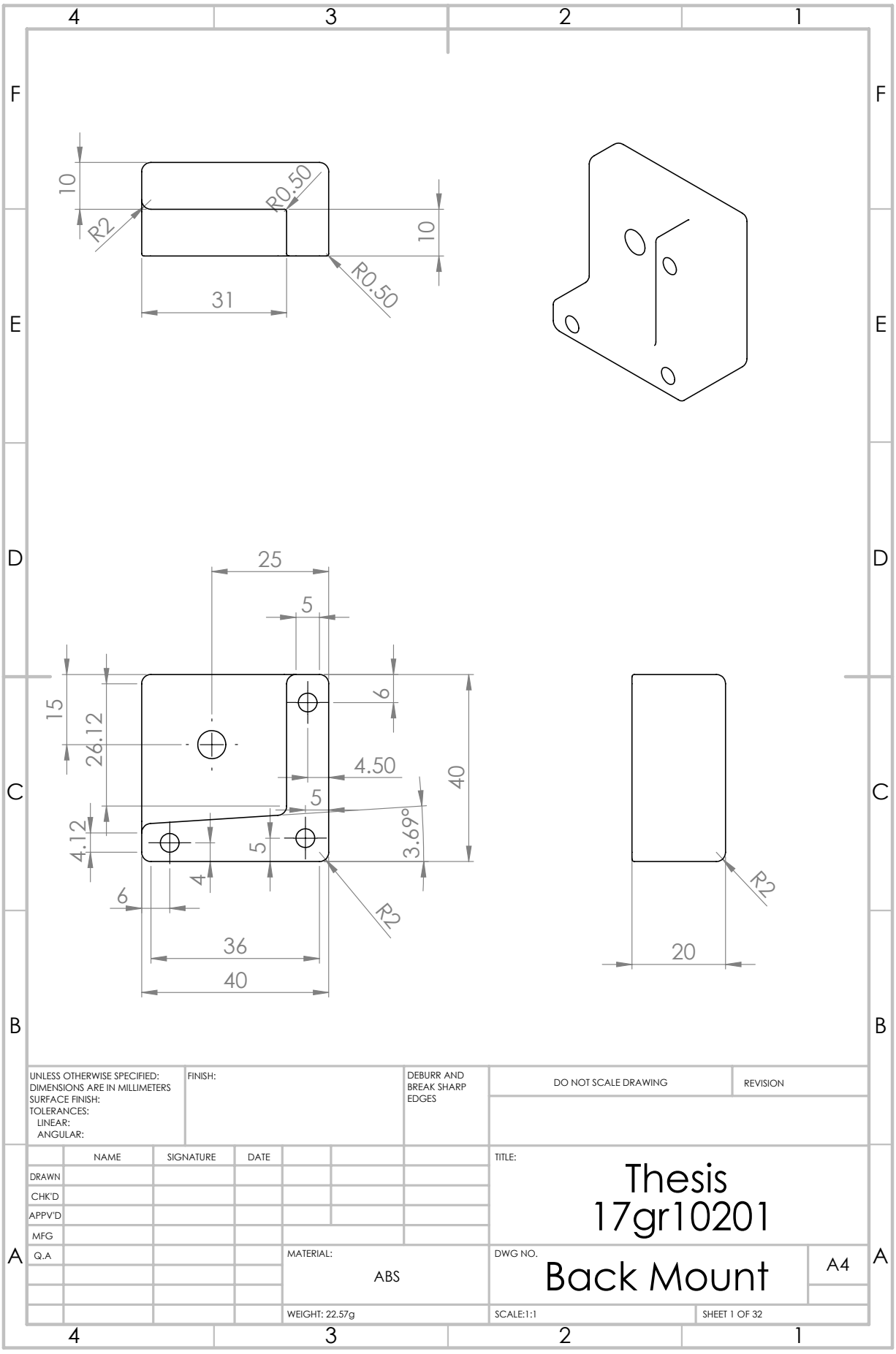
4
3
2
1
F
E
D
C
B
A
10
R2
R0.50
10
R0.50
31
25
5
15
26.12
6
4.50
40
5
4.12
5
3.69°
4
6
R2
36
40
R2
20
UNLESS OTHERWISE SPECIFIED:
DIMENSIONS ARE IN MILLIMETERS
SURFACE FINISH:
TOLERANCES:
LINEAR:
ANGULAR:
FINISH:
DEBURR AND BREAK SHARP EDGES
DO NOT SCALE DRAWING
REVISION
NAME
SIGNATURE
DATE
DRAWN
CHK'D
APPV'D
MFG
Q.A
TITLE:
Thesis
17gr10201
MATERIAL:
ABS
DWG NO.
Back Mount
A4
WEIGHT: 22.57g
SCALE:1:1
SHEET 1 OF 32

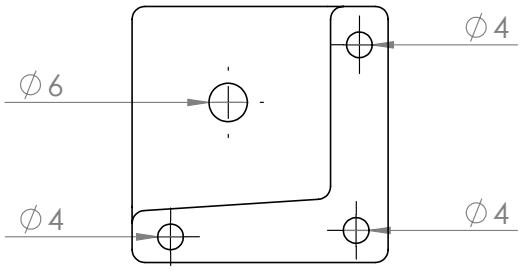

UNLESS OTHERWISE SPECIFIED: DIMENSIONS ARE IN MILLIMETERS SURFACE FINISH: TOLERANCES: LINEAR: ANGULAR:		FINISH:		DEBURR AND BREAK SHARP EDGES		DO NOT SCALE DRAWING		REVISION
	NAME	SIGNATURE	DATE				TITLE:	
DRAWN							Thesis 17gr10201	
CHK'D								
APPV'D								
MFG								
Q.A				MATERIAL: ABS			DWG NO. Back Mount	A4
				WEIGHT: 22.57g			SCALE:1:1	SHEET 2 OF 32

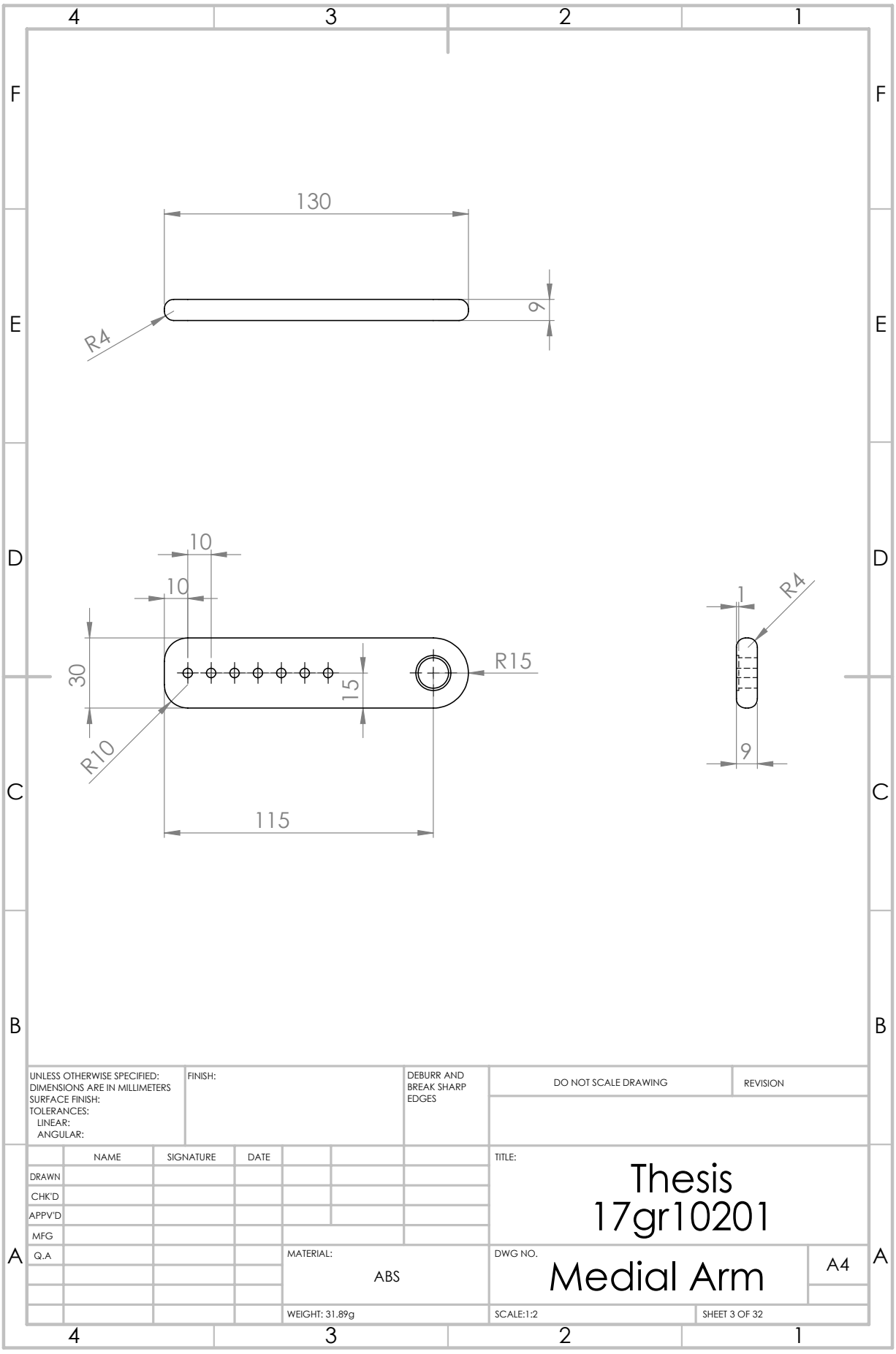
4
3
2
1
F
E
D
C
B
A
130
9
R4
10
10
30
15
R15
R10
115
1
R4
9
UNLESS OTHERWISE SPECIFIED:
DIMENSIONS ARE IN MILLIMETERS
SURFACE FINISH:
TOLERANCES:
LINEAR:
ANGULAR:
FINISH:
DEBURR AND BREAK SHARP EDGES
DO NOT SCALE DRAWING
REVISION
NAME
SIGNATURE
DATE
DRAWN
CHK'D
APPV'D
MFG
Q.A
TITLE:
Thesis
17gr10201
MATERIAL:
ABS
DWG NO.
Medial Arm
A4
WEIGHT: 31.89g
SCALE:1:2
SHEET 3 OF 32

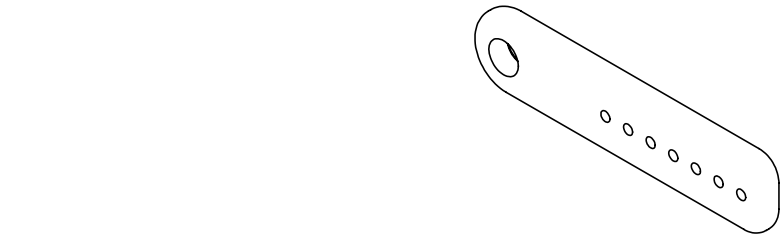

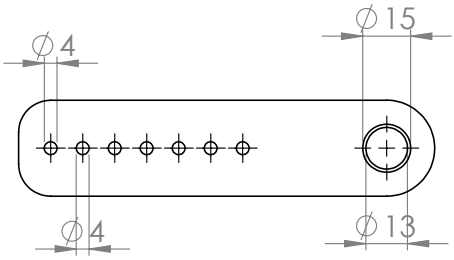

UNLESS OTHERWISE SPECIFIED: DIMENSIONS ARE IN MILLIMETERS SURFACE FINISH: TOLERANCES: LINEAR: ANGULAR:		FINISH:		DEBURR AND BREAK SHARP EDGES		DO NOT SCALE DRAWING		REVISION
	NAME	SIGNATURE	DATE				TITLE:	
DRAWN							Thesis 17gr10201	
CHK'D								
APPV'D								
MFG								
Q.A				MATERIAL:		DWG NO.		A4
				ABS		Medial Arm		
				WEIGHT: 31.89g		SCALE:1:2	SHEET 4 OF 32	

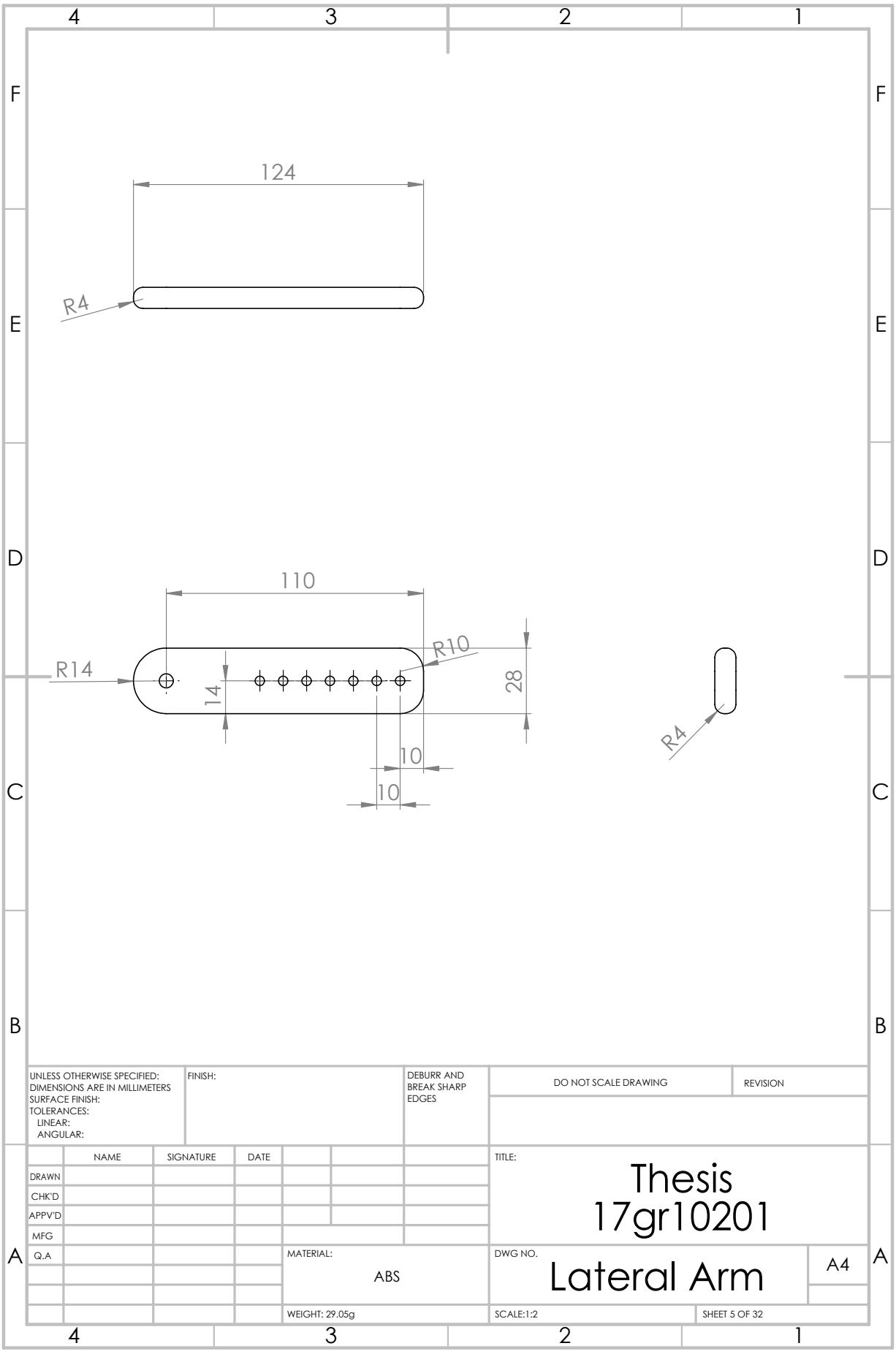
4
3
2
1
F
E
D
C
B
A
124
R4
110
R14
R10
14
28
10
10
R4
UNLESS OTHERWISE SPECIFIED:
DIMENSIONS ARE IN MILLIMETERS
SURFACE FINISH:
TOLERANCES:
LINEAR:
ANGULAR:
FINISH:
DEBURR AND BREAK SHARP EDGES
DO NOT SCALE DRAWING
REVISION
NAME
SIGNATURE
DATE
DRAWN
CHK'D
APPV'D
MFG
Q.A
TITLE:
Thesis
17gr10201
MATERIAL:
ABS
DWG NO.
Lateral Arm
A4
WEIGHT: 29.05g
SCALE:1:2
SHEET 5 OF 32

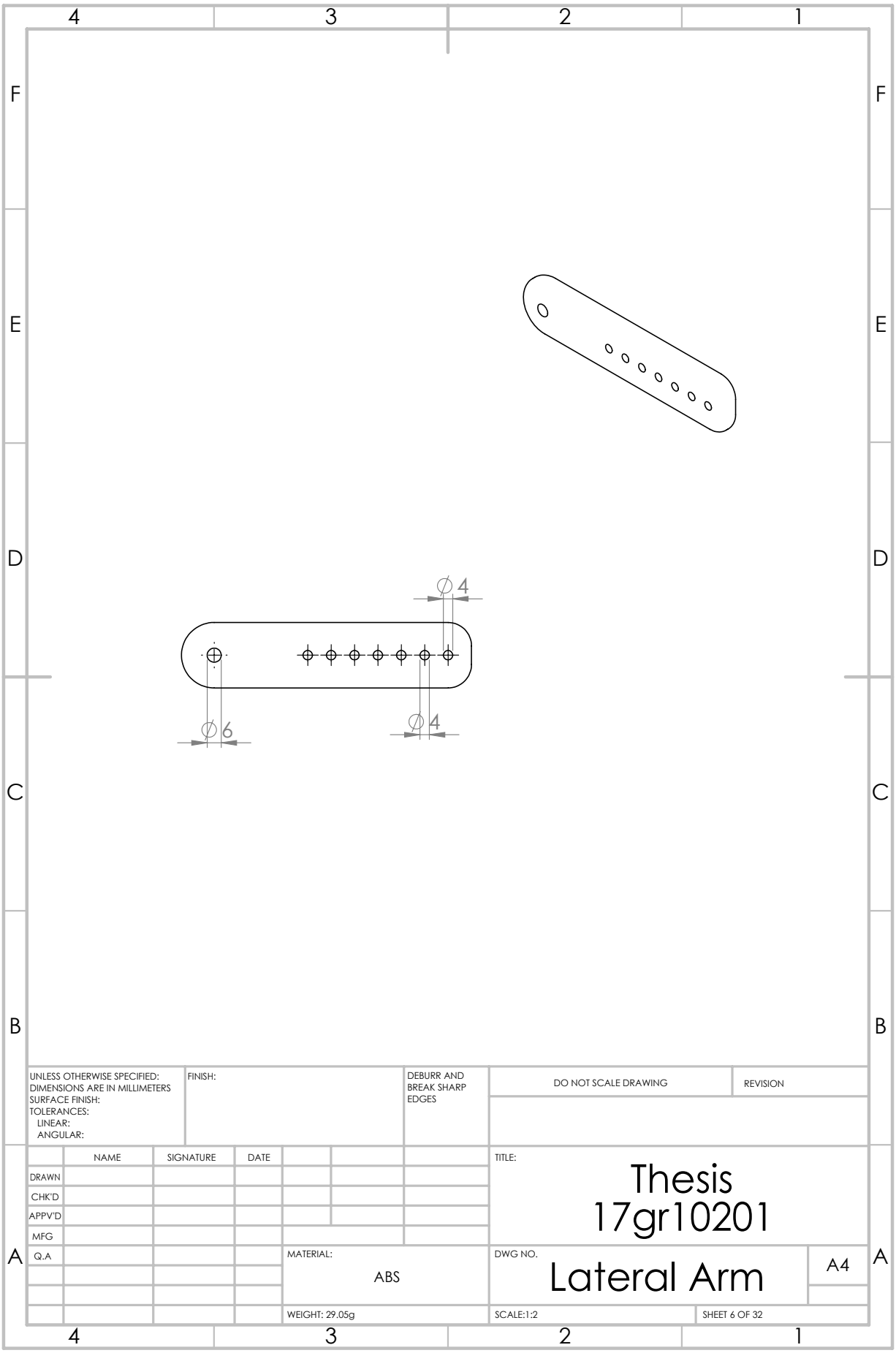
4
3
2
1
F
E
D
C
B
A
∅4
∅6
∅4
UNLESS OTHERWISE SPECIFIED:
DIMENSIONS ARE IN MILLIMETERS
SURFACE FINISH:
TOLERANCES:
LINEAR:
ANGULAR:
FINISH:
DEBURR AND BREAK SHARP EDGES
DO NOT SCALE DRAWING
REVISION
NAME
SIGNATURE
DATE
DRAWN
CHK'D
APPV'D
MFG
Q.A
TITLE:
Thesis
17gr10201
MATERIAL:
ABS
DWG NO.
Lateral Arm
A4
WEIGHT: 29.05g
SCALE:1:2
SHEET 6 OF 32

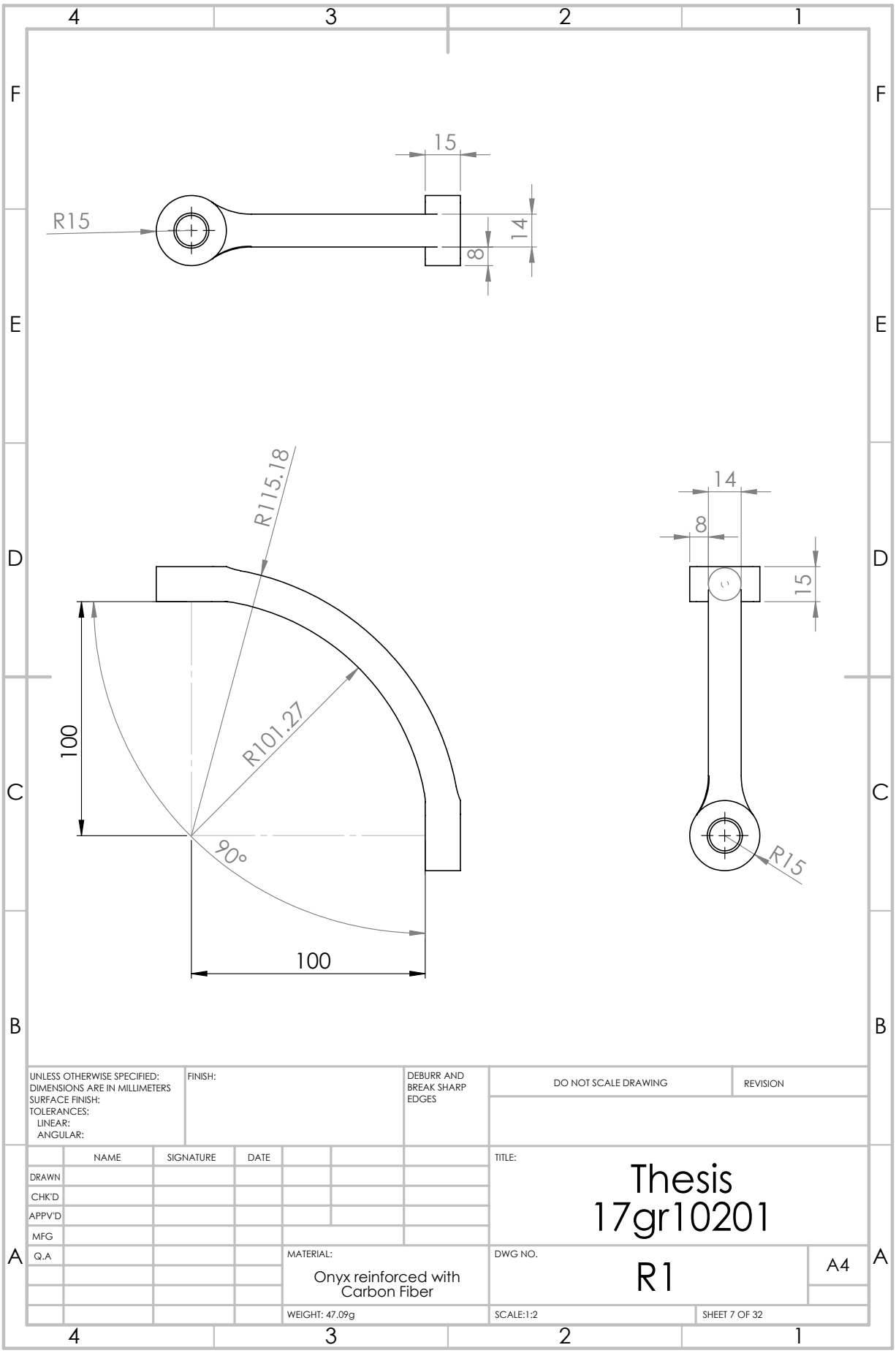
15
R15
14
8
R115.18
R101.27
100
90°
100
14
8
15
R15
UNLESS OTHERWISE SPECIFIED:
DIMENSIONS ARE IN MILLIMETERS
SURFACE FINISH:
TOLERANCES:
LINEAR:
ANGULAR:
FINISH:
DEBURR AND BREAK SHARP EDGES
DO NOT SCALE DRAWING
REVISION
NAME
SIGNATURE
DATE
DRAWN
CHK'D
APPV'D
MFG
Q.A
TITLE:
Thesis
17gr10201
MATERIAL:
Onyx reinforced with Carbon Fiber
DWG NO.
R1
A4
WEIGHT: 47.09g
SCALE:1:2
SHEET 7 OF 32

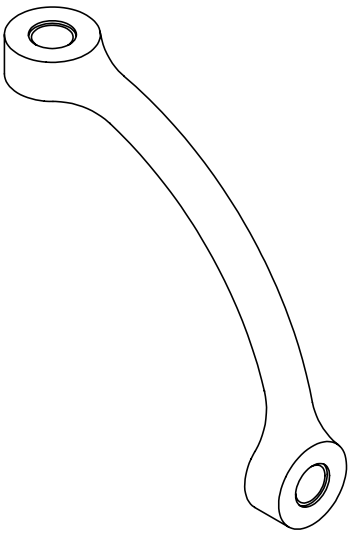

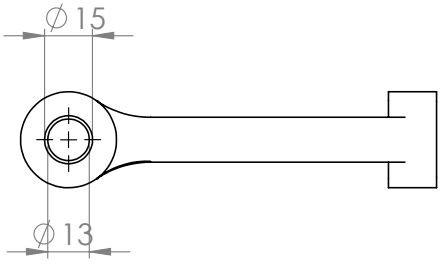

UNLESS OTHERWISE SPECIFIED: DIMENSIONS ARE IN MILLIMETERS SURFACE FINISH: TOLERANCES: LINEAR: ANGULAR:	FINISH:		DEBURR AND BREAK SHARP EDGES				DO NOT SCALE DRAWING	REVISION
	NAME	SIGNATURE	DATE				TITLE:	
DRAWN							Thesis 17gr10201	
CHK'D								
APPV'D								
MFG								
Q.A				MATERIAL:			DWG NO.	A4
				Onyx reinforced with Carbon Fiber			R1	
				WEIGHT: 47.09g			SCALE:1:2	SHEET 8 OF 32

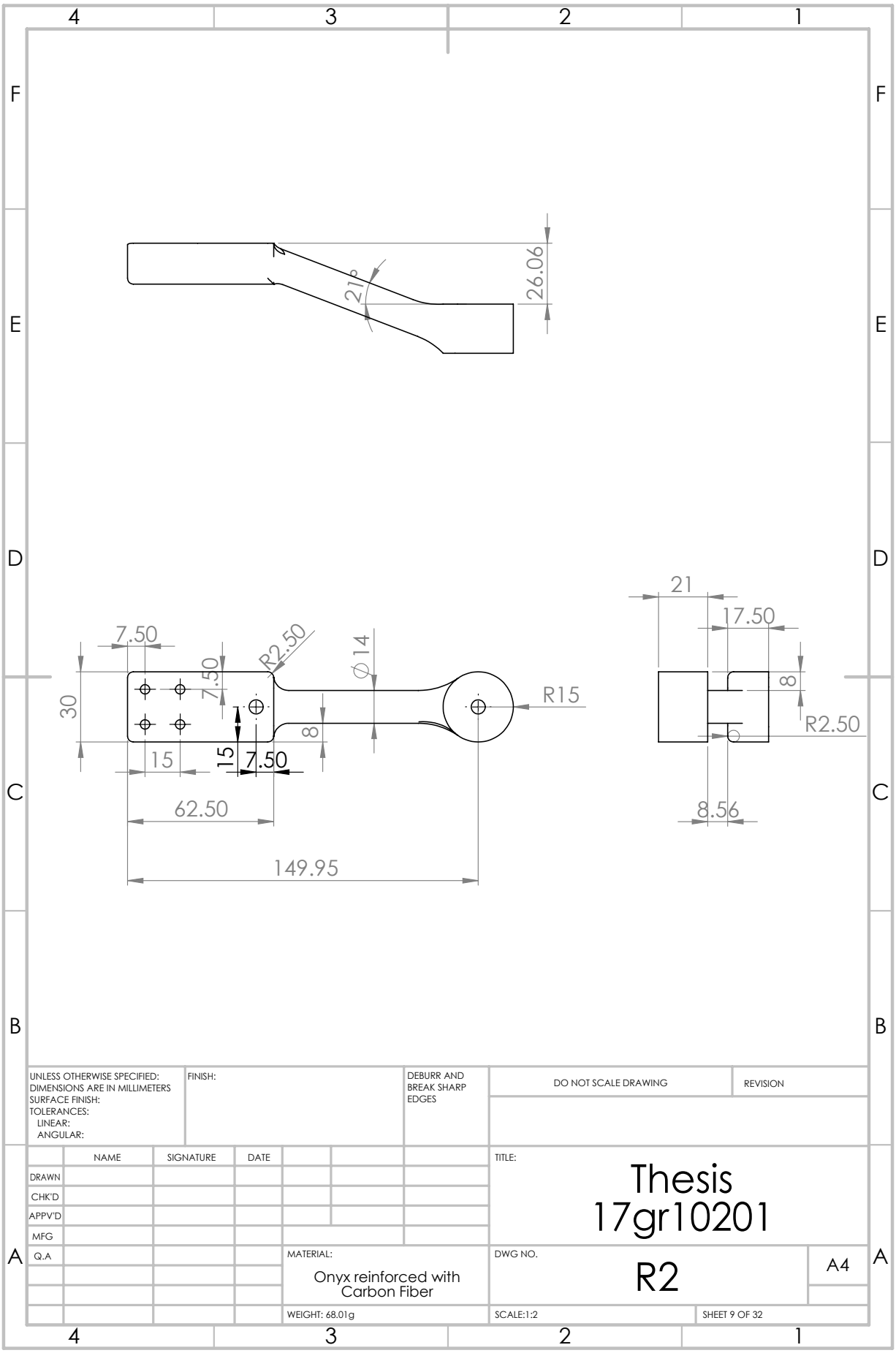
4
3
2
1
F
E
D
C
B
A
21°
26.06
7.50
7.50
R2.50
Ø14
R15
30
8
15
15
7.50
62.50
149.95
21
17.50
8
R2.50
8.56
UNLESS OTHERWISE SPECIFIED:
DIMENSIONS ARE IN MILLIMETERS
SURFACE FINISH:
TOLERANCES:
LINEAR:
ANGULAR:
FINISH:
DEBURR AND BREAK SHARP EDGES
DO NOT SCALE DRAWING
REVISION
NAME
SIGNATURE
DATE
DRAWN
CHK'D
APPV'D
MFG
Q.A
TITLE:
Thesis
17gr10201
MATERIAL:
Onyx reinforced with Carbon Fiber
DWG NO.
R2
A4
WEIGHT: 68.01g
SCALE:1:2
SHEET 9 OF 32

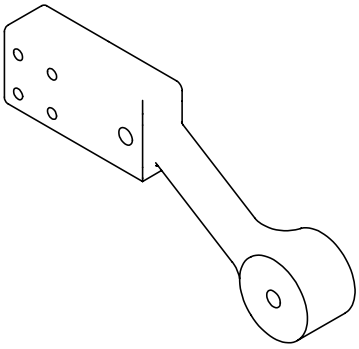

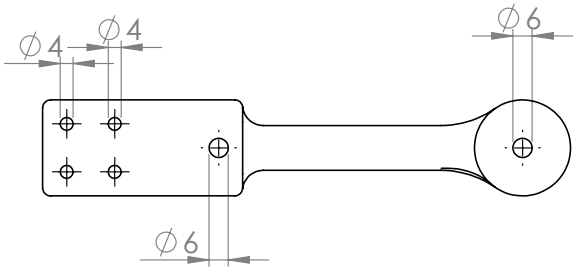

UNLESS OTHERWISE SPECIFIED: DIMENSIONS ARE IN MILLIMETERS SURFACE FINISH: TOLERANCES: LINEAR: ANGULAR:		FINISH:		DEBURR AND BREAK SHARP EDGES		DO NOT SCALE DRAWING		REVISION
	NAME	SIGNATURE	DATE				TITLE:	
DRAWN							Thesis 17gr10201	
CHK'D								
APPV'D								
MFG								
Q.A				MATERIAL:		DWG NO.		A4
				Onyx reinforced with Carbon Fiber		R2		
				WEIGHT: 68.01g		SCALE:1:2	SHEET 10 OF 32	

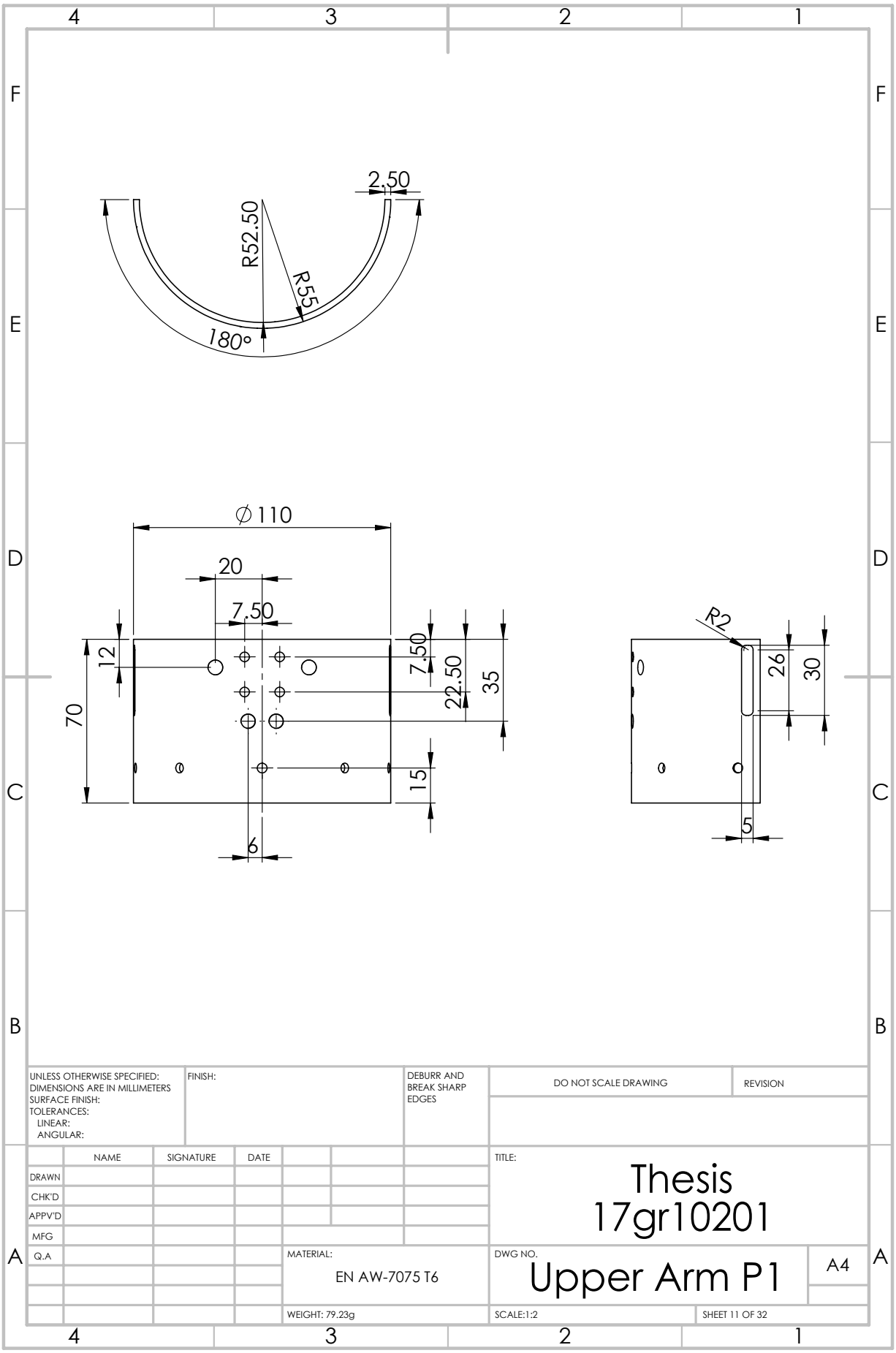
4
3
2
1
F
E
D
C
B
A
2.50
R52.50
R55
180°
∅110
20
7.50
12
70
7.50
22.50
35
15
6
R2
26
30
5
UNLESS OTHERWISE SPECIFIED:
DIMENSIONS ARE IN MILLIMETERS
SURFACE FINISH:
TOLERANCES:
LINEAR:
ANGULAR:
FINISH:
DEBURR AND BREAK SHARP EDGES
DO NOT SCALE DRAWING
REVISION
NAME
SIGNATURE
DATE
DRAWN
CHK'D
APPV'D
MFG
Q.A
TITLE:
Thesis
17gr10201
MATERIAL:
EN AW-7075 T6
DWG NO.
Upper Arm P1
A4
WEIGHT: 79.23g
SCALE:1:2
SHEET 11 OF 32

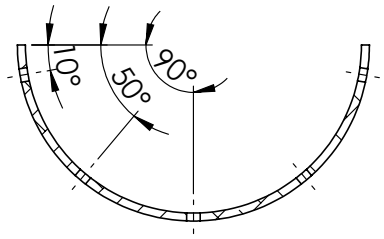

SECTION A-A

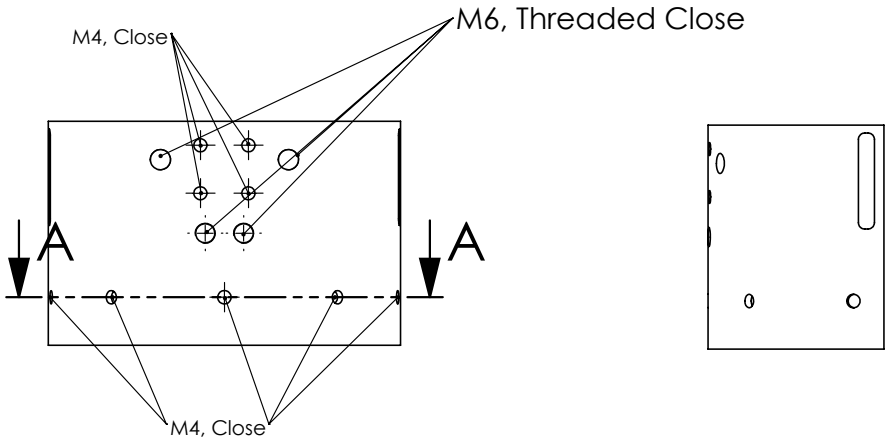

UNLESS OTHERWISE SPECIFIED: DIMENSIONS ARE IN MILLIMETERS SURFACE FINISH: TOLERANCES: LINEAR: ANGULAR:		FINISH:		DEBURR AND BREAK SHARP EDGES		DO NOT SCALE DRAWING		REVISION
	NAME	SIGNATURE	DATE				TITLE:	
DRAWN							Thesis 17gr10201	
CHK'D								
APPV'D								
MFG								
Q.A				MATERIAL:		DWG NO.		A4
				EN AW-7075 T6		Upper Arm P1		
				WEIGHT: 79.23g		SCALE:1:2	SHEET 12 OF 32	

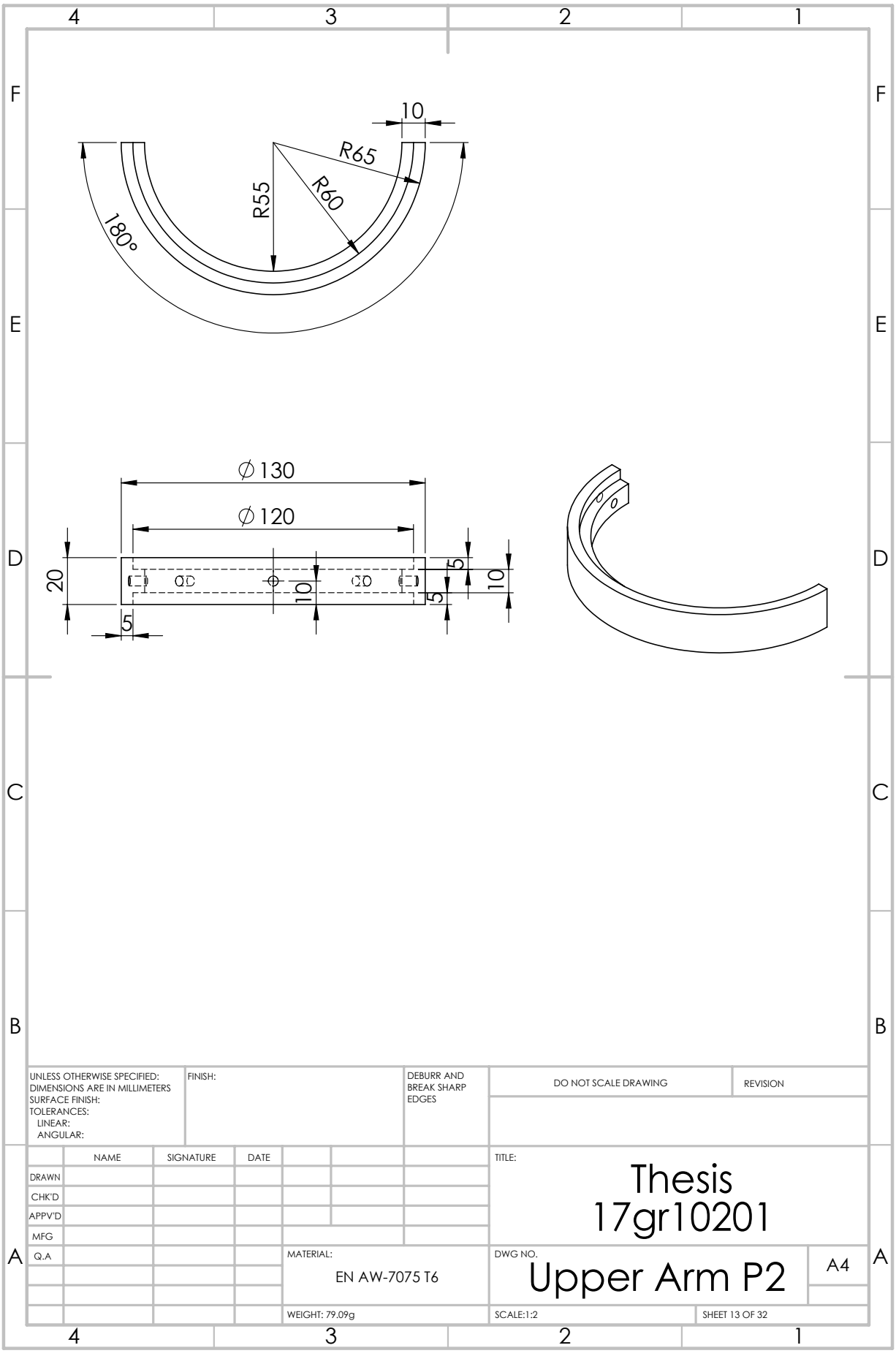
4
3
2
1
F
E
D
C
B
A
10
R65
R60
R55
180°
∅130
∅120
20
5
10
5
10
5
UNLESS OTHERWISE SPECIFIED:
DIMENSIONS ARE IN MILLIMETERS
SURFACE FINISH:
TOLERANCES:
LINEAR:
ANGULAR:
FINISH:
DEBURR AND BREAK SHARP EDGES
DO NOT SCALE DRAWING
REVISION
NAME
SIGNATURE
DATE
DRAWN
CHK'D
APPV'D
MFG
Q.A
TITLE:
Thesis
17gr10201
MATERIAL:
EN AW-7075 T6
DWG NO.
Upper Arm P2
A4
WEIGHT: 79.09g
SCALE:1:2
SHEET 13 OF 32

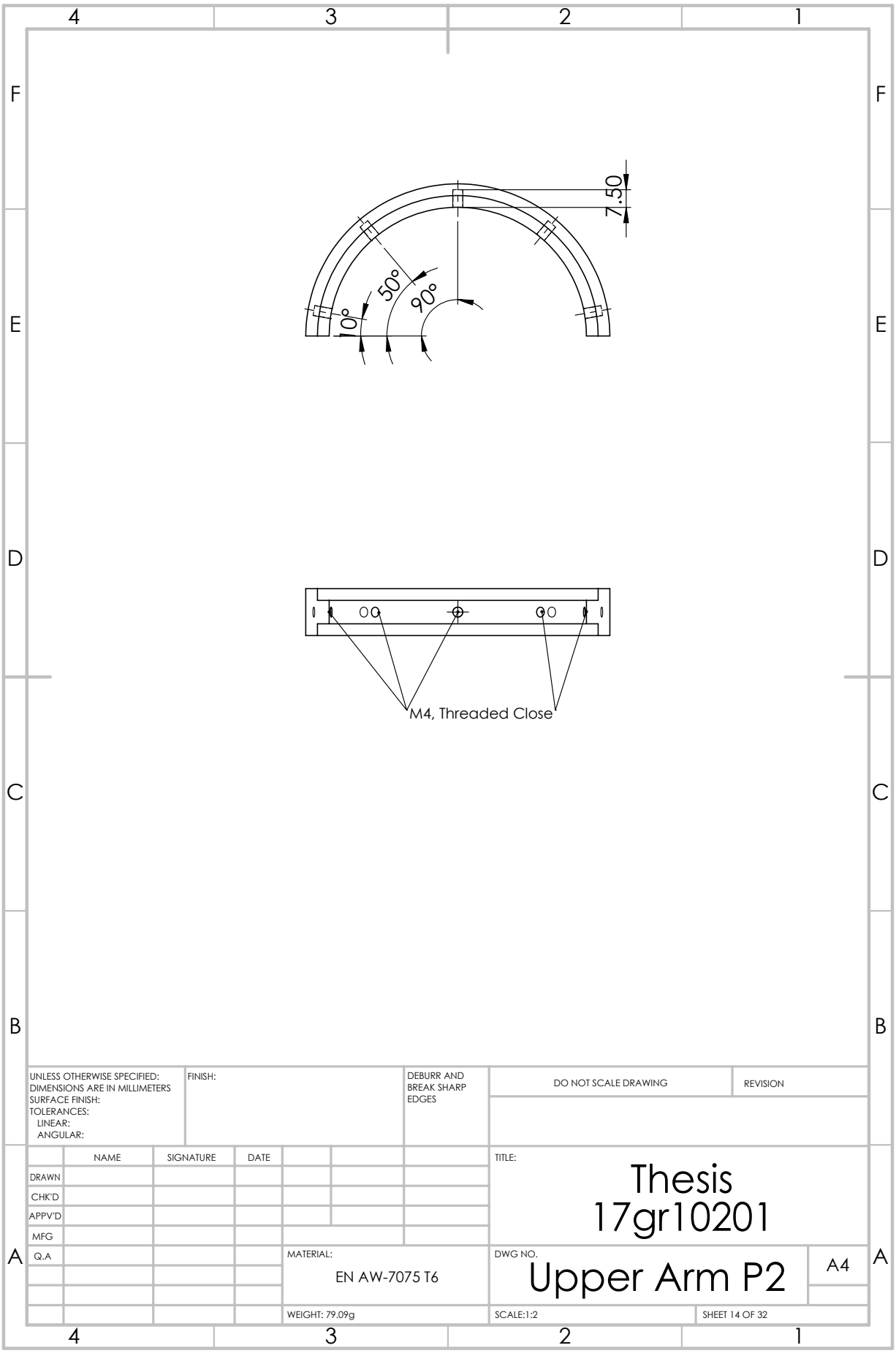
4
3
2
1
F
E
D
C
B
A
7.50
10°
50°
90°
M4, Threaded Close
UNLESS OTHERWISE SPECIFIED:
DIMENSIONS ARE IN MILLIMETERS
SURFACE FINISH:
TOLERANCES:
LINEAR:
ANGULAR:
FINISH:
DEBURR AND BREAK SHARP EDGES
DO NOT SCALE DRAWING
REVISION
NAME
SIGNATURE
DATE
DRAWN
CHK'D
APPV'D
MFG
Q.A
TITLE:
Thesis 17gr10201
MATERIAL:
EN AW-7075 T6
DWG NO.
Upper Arm P2
A4
WEIGHT: 79.09g
SCALE:1:2
SHEET 14 OF 32

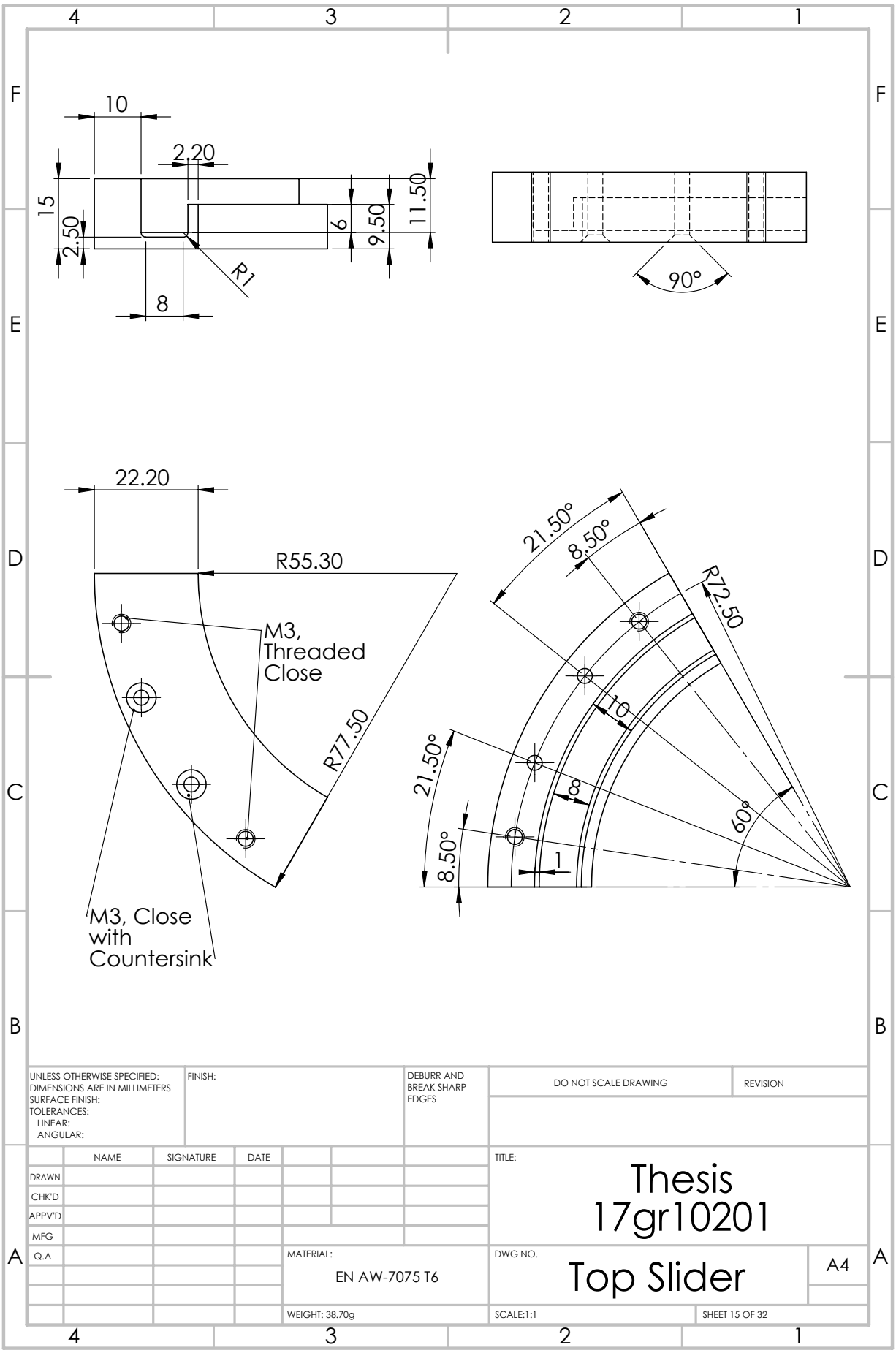
10
2.20
15
2.50
6
9.50
11.50
R1
8
90°
22.20
R55.30
M3,
Threaded
Close
R77.50
M3, Close
with
Countersink
21.50°
8.50°
R72.50
10
8
60°
1
21.50°
8.50°
UNLESS OTHERWISE SPECIFIED:
DIMENSIONS ARE IN MILLIMETERS
SURFACE FINISH:
TOLERANCES:
LINEAR:
ANGULAR:
FINISH:
DEBURR AND BREAK SHARP EDGES
DO NOT SCALE DRAWING
REVISION
NAME
SIGNATURE
DATE
DRAWN
CHK'D
APPV'D
MFG
Q.A
TITLE:
Thesis
17gr10201
MATERIAL:
EN AW-7075 T6
DWG NO.
Top Slider
A4
WEIGHT: 38.70g
SCALE:1:1
SHEET 15 OF 32

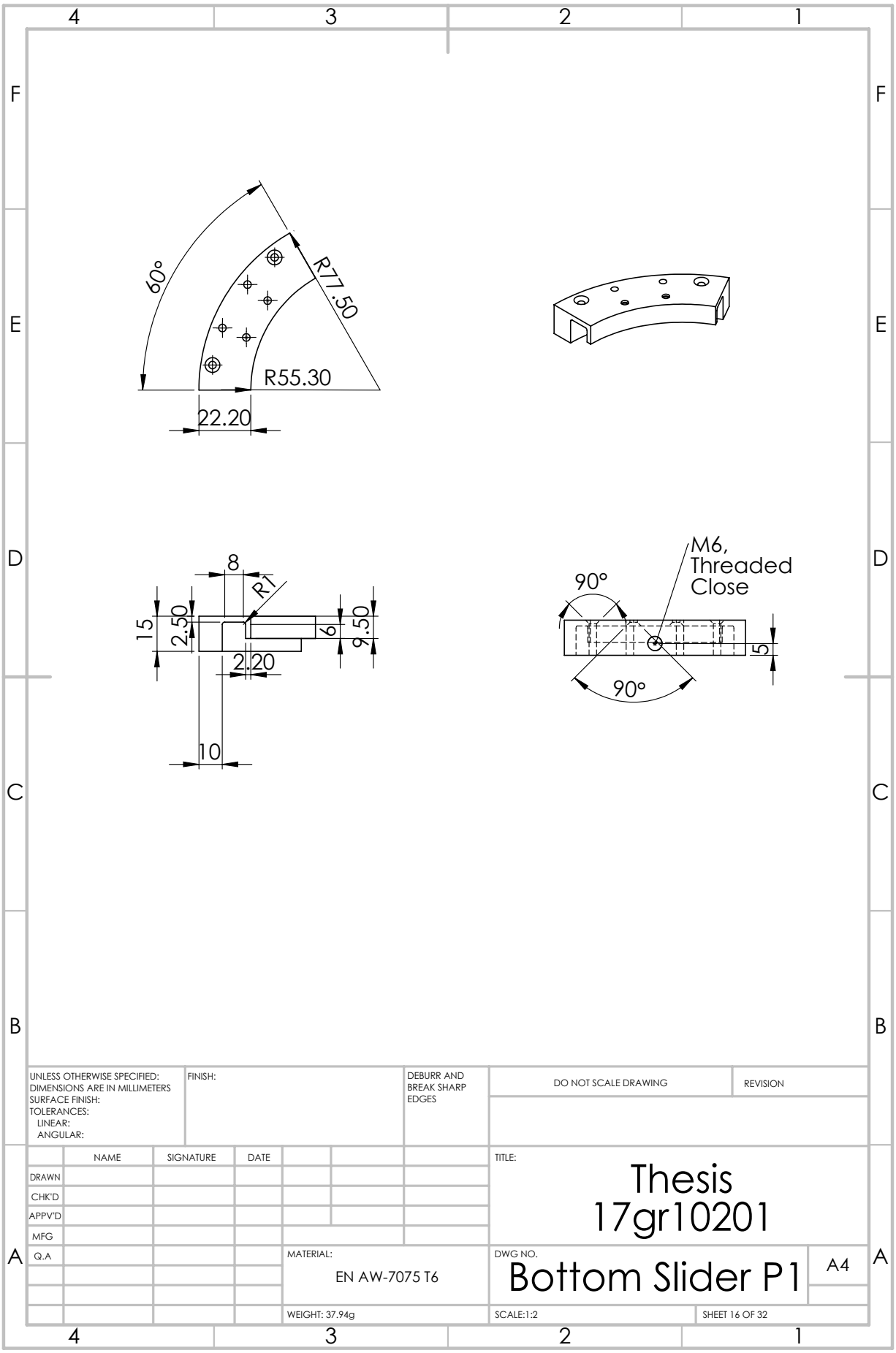
60°
R77.50
R55.30
22.20
8
R1
15
2.50
6
9.50
2.20
10
M6,
Threaded
Close
90°
90°
5
UNLESS OTHERWISE SPECIFIED:
DIMENSIONS ARE IN MILLIMETERS
SURFACE FINISH:
TOLERANCES:
LINEAR:
ANGULAR:
FINISH:
DEBURR AND BREAK SHARP EDGES
DO NOT SCALE DRAWING
REVISION
NAME
SIGNATURE
DATE
DRAWN
CHK'D
APPV'D
MFG
Q.A
TITLE:
Thesis
17gr10201
MATERIAL:
EN AW-7075 T6
DWG NO.
Bottom Slider P1
A4
WEIGHT: 37.94g
SCALE:1:2
SHEET 16 OF 32

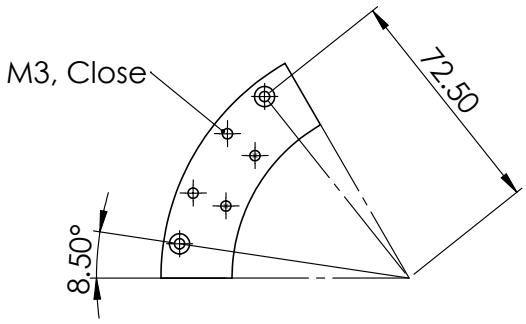

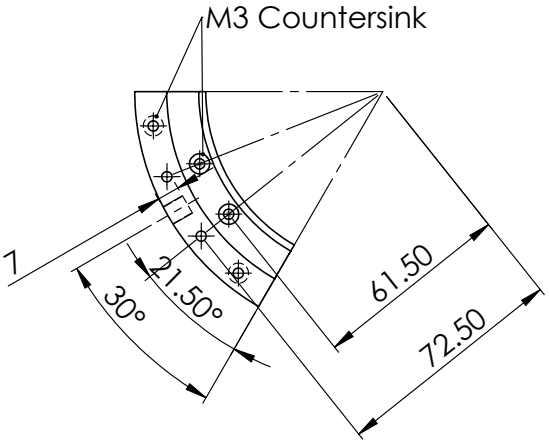

UNLESS OTHERWISE SPECIFIED: DIMENSIONS ARE IN MILLIMETERS SURFACE FINISH: TOLERANCES: LINEAR: ANGULAR:		FINISH:		DEBURR AND BREAK SHARP EDGES		DO NOT SCALE DRAWING		REVISION
	NAME	SIGNATURE	DATE				TITLE:	
DRAWN							Thesis 17gr10201	
CHK'D								
APPV'D								
MFG								
Q.A				MATERIAL:			DWG NO.	A4
				EN AW-7075 T6			Bottom Slider P1	
				WEIGHT: 37.94g			SCALE:1:2	SHEET 17 OF 32

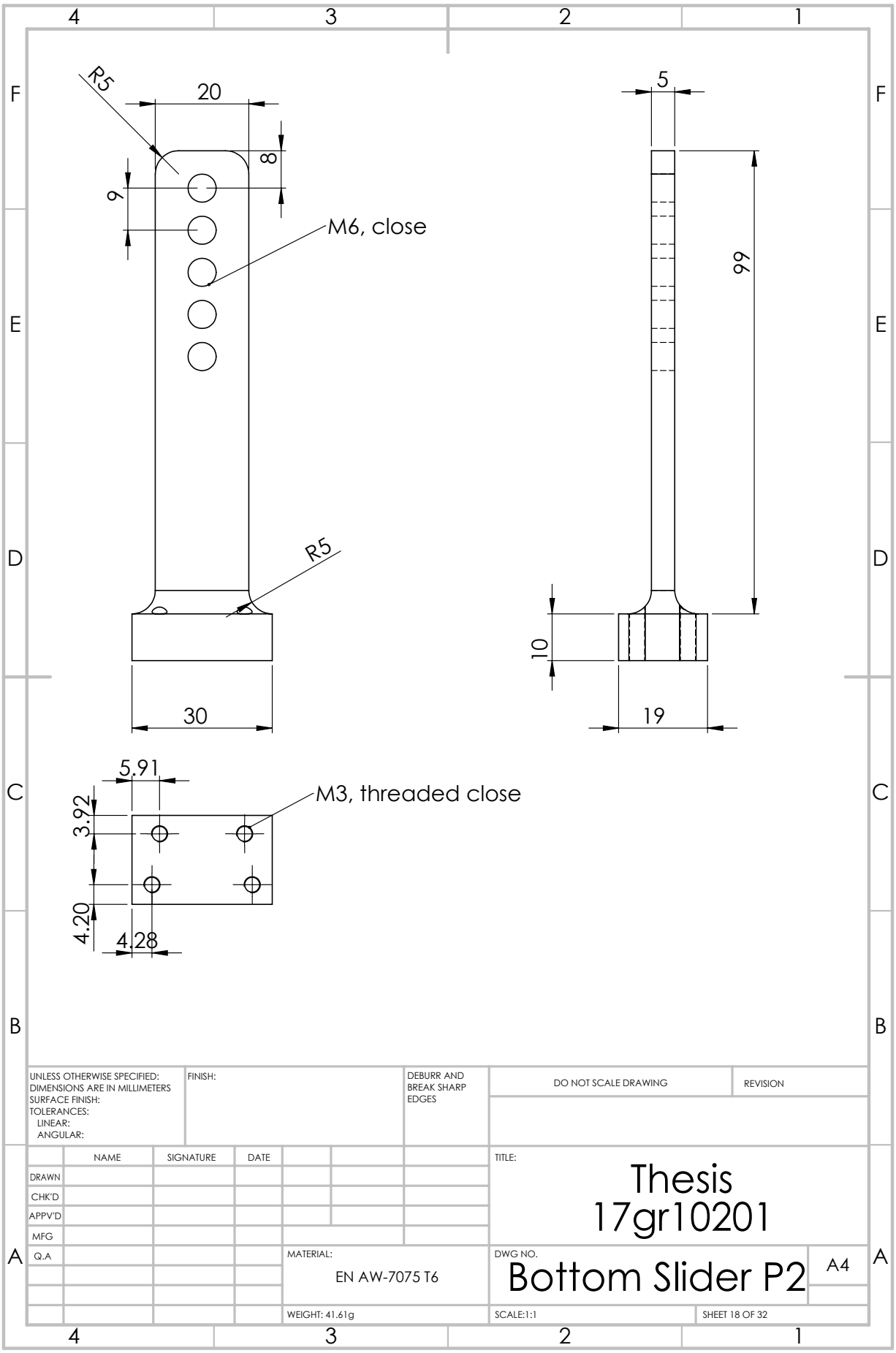
R5
20
8
9
M6, close
R5
30
5
99
10
19
5.91
3.92
M3, threaded close
4.20
4.28
UNLESS OTHERWISE SPECIFIED:
DIMENSIONS ARE IN MILLIMETERS
SURFACE FINISH:
TOLERANCES:
LINEAR:
ANGULAR:
FINISH:
DEBURR AND BREAK SHARP EDGES
DO NOT SCALE DRAWING
REVISION
NAME
SIGNATURE
DATE
DRAWN
CHK'D
APPV'D
MFG
Q.A
TITLE:
Thesis 17gr10201
MATERIAL:
EN AW-7075 T6
DWG NO.
Bottom Slider P2
A4
WEIGHT: 41.61g
SCALE:1:1
SHEET 18 OF 32

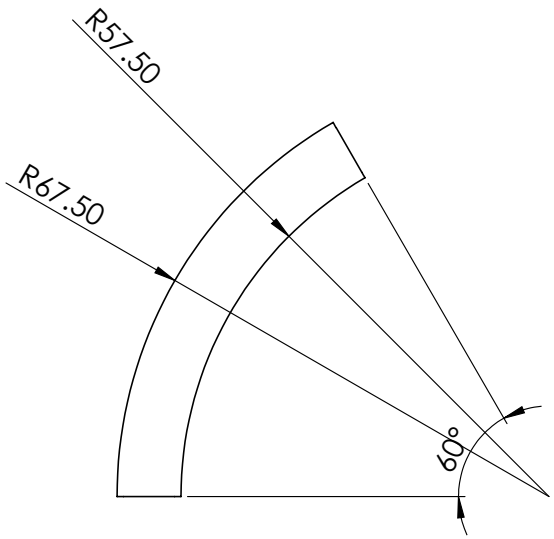

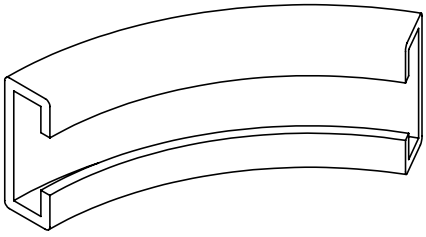

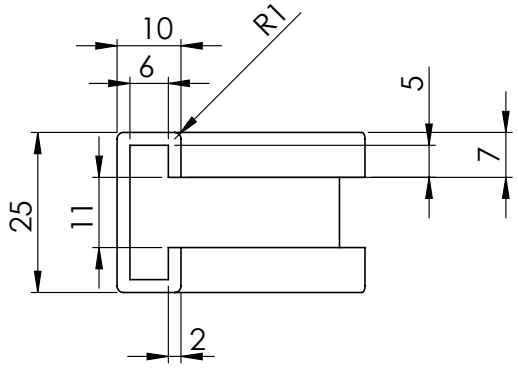

UNLESS OTHERWISE SPECIFIED: DIMENSIONS ARE IN MILLIMETERS SURFACE FINISH: TOLERANCES: LINEAR: ANGULAR:	FINISH:	DEBURR AND BREAK SHARP EDGES	DO NOT SCALE DRAWING / REVISION

	NAME	SIGNATURE	DATE
DRAWN			
CHK'D			
APPV'D			
MFG			
Q.A			

TITLE:

Thesis
17gr10201

Slider Insert

MATERIAL: iglidur I3-PL	DWG NO.	A4	
WEIGHT: 7.05g	SCALE:1:1	SHEET 19 OF 32	

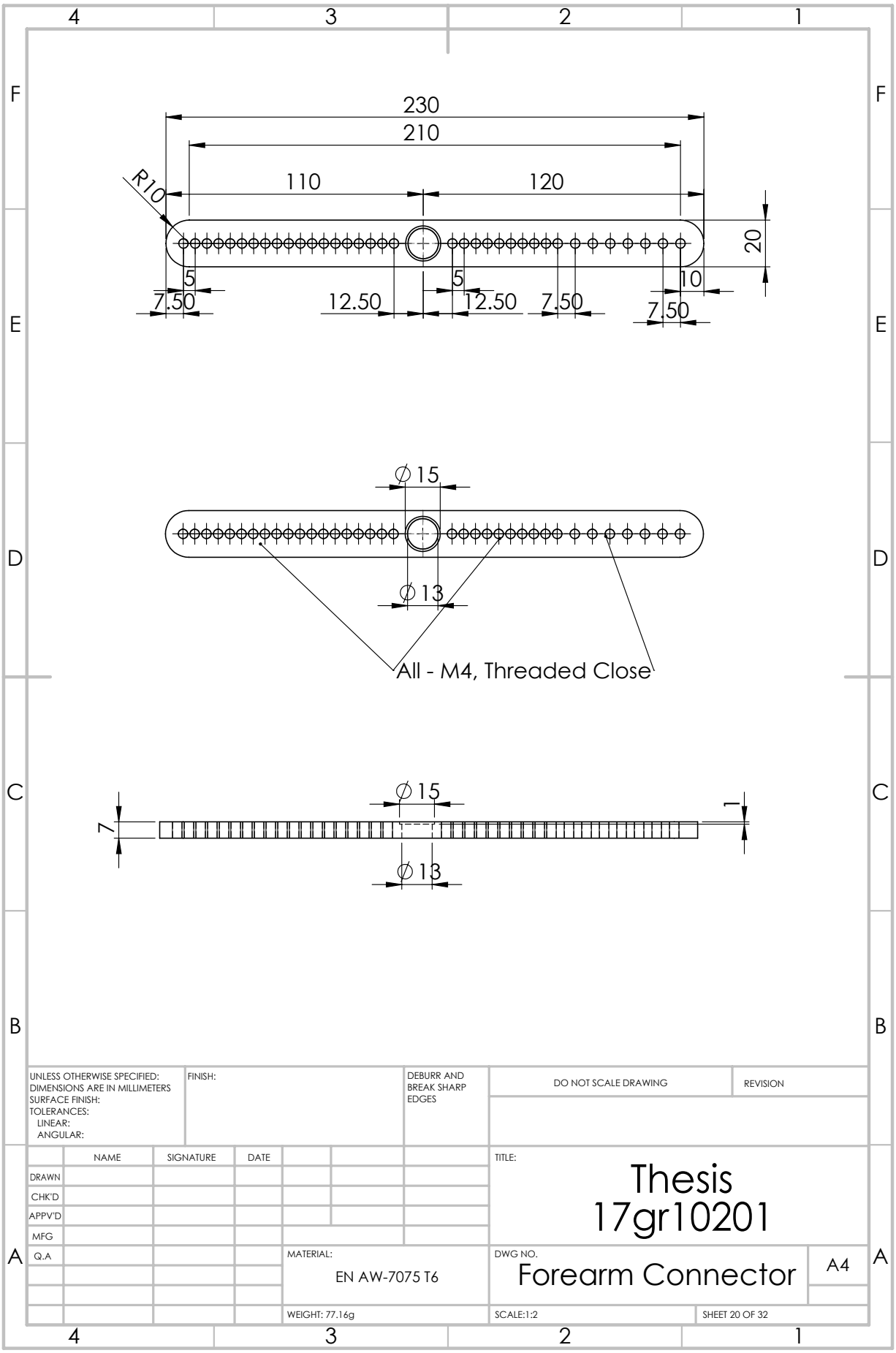
4
3
2
1
F
E
D
C
B
A
230
210
110
120
R10
20
5
5
10
7.50
12.50
12.50
7.50
7.50
∅15
∅13
All - M4, Threaded Close
∅15
∅13
7
1
UNLESS OTHERWISE SPECIFIED:
DIMENSIONS ARE IN MILLIMETERS
SURFACE FINISH:
TOLERANCES:
LINEAR:
ANGULAR:
FINISH:
DEBURR AND BREAK SHARP EDGES
DO NOT SCALE DRAWING
REVISION
NAME
SIGNATURE
DATE
DRAWN
CHK'D
APPV'D
MFG
Q.A
TITLE:
Thesis
17gr10201
MATERIAL:
EN AW-7075 T6
DWG NO.
Forearm Connector
A4
WEIGHT: 77.16g
SCALE:1:2
SHEET 20 OF 32

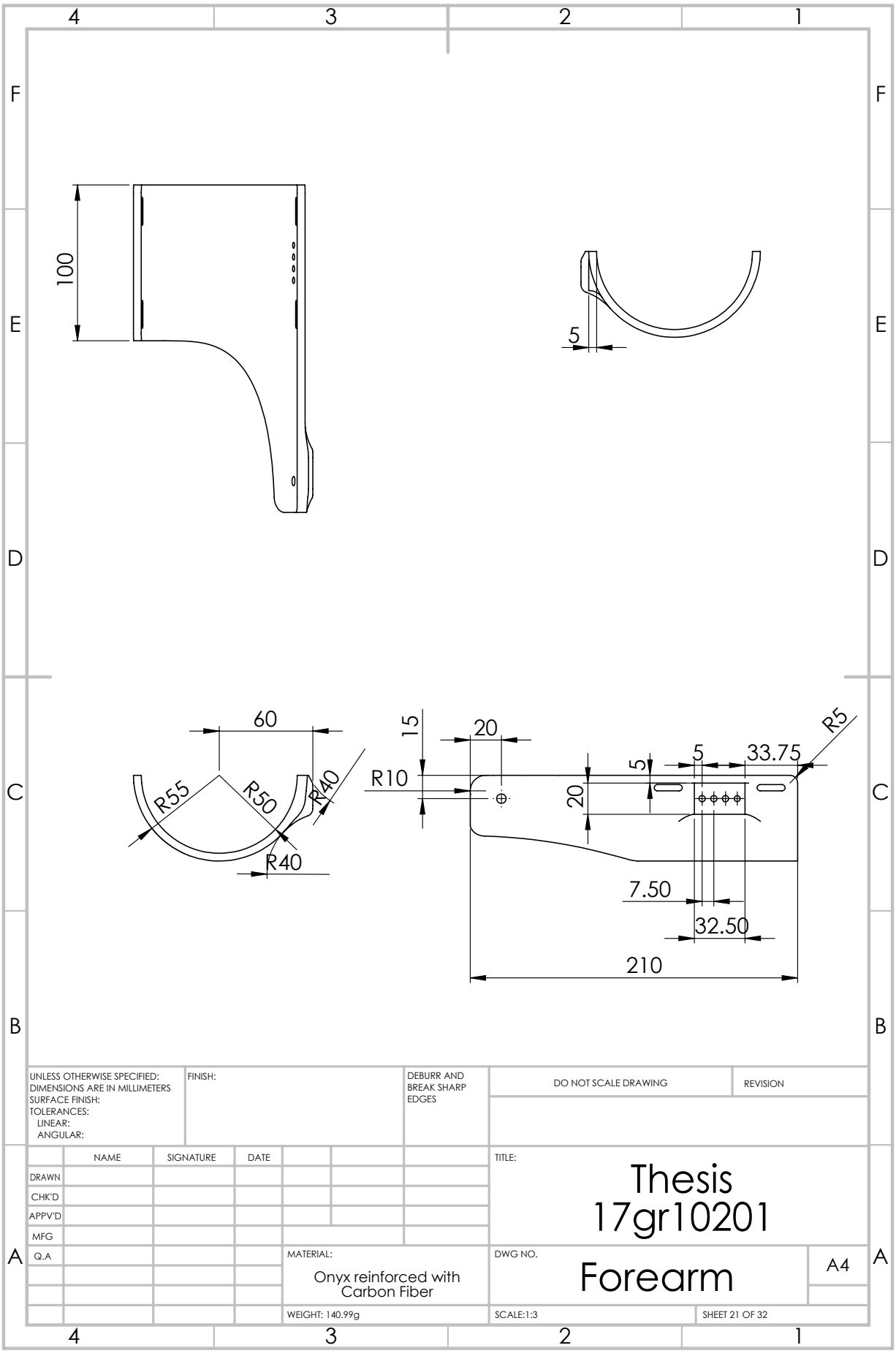
4
3
2
1
F
E
D
C
B
A
100
5
60
R55
R50
R40
R40
15
20
R10
5
5
33.75
R5
20
7.50
32.50
210
UNLESS OTHERWISE SPECIFIED:
DIMENSIONS ARE IN MILLIMETERS
SURFACE FINISH:
TOLERANCES:
LINEAR:
ANGULAR:
FINISH:
DEBURR AND BREAK SHARP EDGES
DO NOT SCALE DRAWING
REVISION
NAME
SIGNATURE
DATE
DRAWN
CHK'D
APPV'D
MFG
Q.A
TITLE:
Thesis
17gr10201
MATERIAL:
Onyx reinforced with Carbon Fiber
DWG NO.
Forearm
A4
WEIGHT: 140.99g
SCALE:1:3
SHEET 21 OF 32

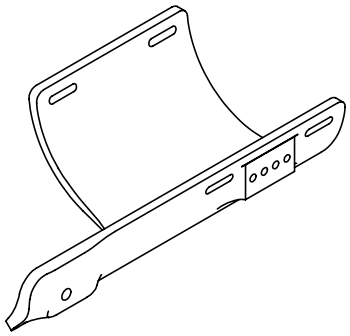

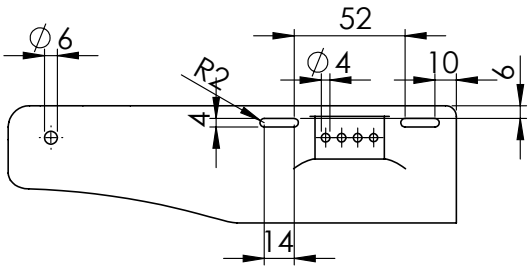

UNLESS OTHERWISE SPECIFIED: DIMENSIONS ARE IN MILLIMETERS SURFACE FINISH: TOLERANCES: LINEAR: ANGULAR:	FINISH:		DEBURR AND BREAK SHARP EDGES			DO NOT SCALE DRAWING	REVISION	
	NAME	SIGNATURE	DATE				TITLE:	
DRAWN							Thesis 17gr10201	
CHK'D								
APPV'D								
MFG								
Q.A				MATERIAL:			DWG NO.	A4
				Onyx reinforced with Carbon Fiber			Forearm	
				WEIGHT: 140.99g		SCALE:1:3	SHEET 22 OF 32	

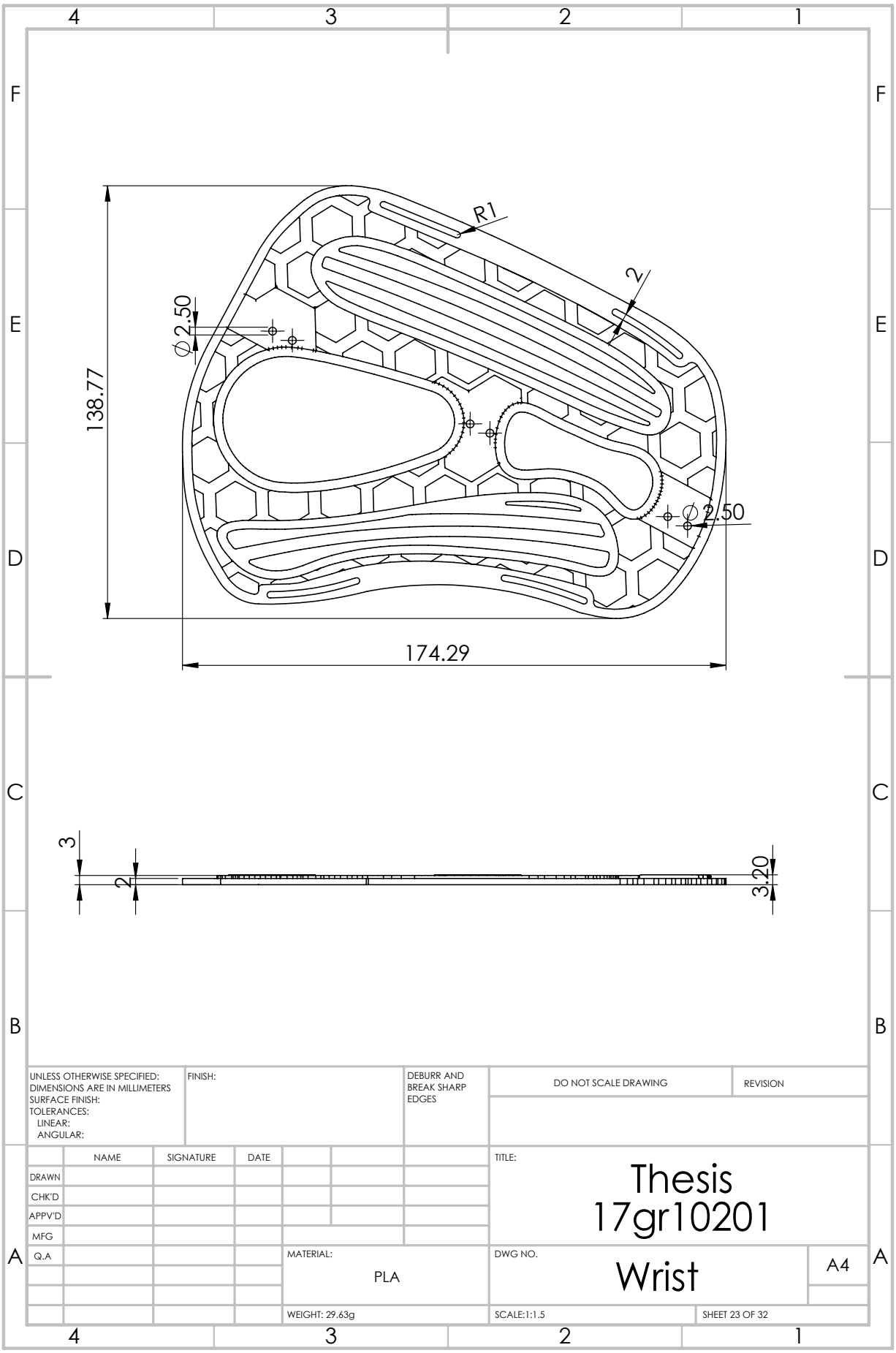
4
3
2
1
F
E
D
C
B
A
R1
2
∅2.50
138.77
∅2.50
174.29
3
2
3.20
UNLESS OTHERWISE SPECIFIED:
DIMENSIONS ARE IN MILLIMETERS
SURFACE FINISH:
TOLERANCES:
LINEAR:
ANGULAR:
FINISH:
DEBURR AND BREAK SHARP EDGES
DO NOT SCALE DRAWING
REVISION
NAME
SIGNATURE
DATE
DRAWN
CHK'D
APPV'D
MFG
Q.A
TITLE:
Thesis
17gr10201
MATERIAL:
PLA
DWG NO.
Wrist
A4
WEIGHT: 29.63g
SCALE:1:1.5
SHEET 23 OF 32

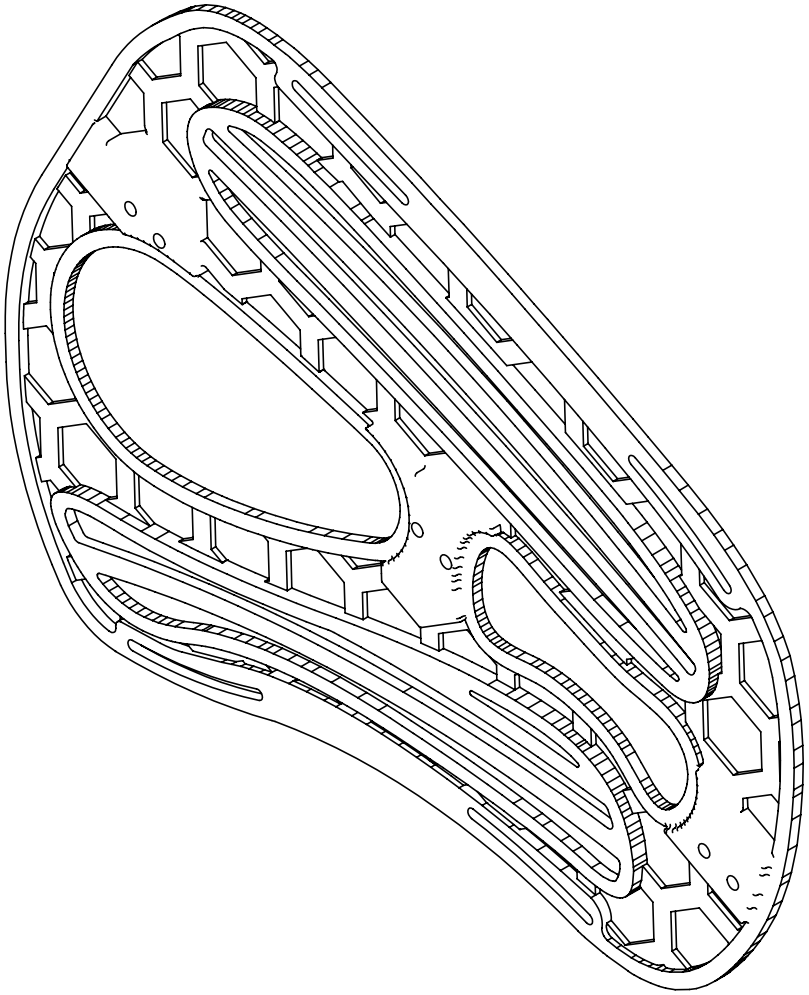

UNLESS OTHERWISE SPECIFIED: DIMENSIONS ARE IN MILLIMETERS SURFACE FINISH: TOLERANCES: LINEAR: ANGULAR:	FINISH:	DEBURR AND BREAK SHARP EDGES	DO NOT SCALE DRAWING / REVISION

	NAME	SIGNATURE	DATE
DRAWN			
CHK'D			
APPV'D			
MFG			
Q.A			

TITLE: Thesis 17gr10201

MATERIAL: PLA

DWG NO. Wrist

A4

WEIGHT: 29.63g

SCALE:1:1

SHEET 24 OF 32

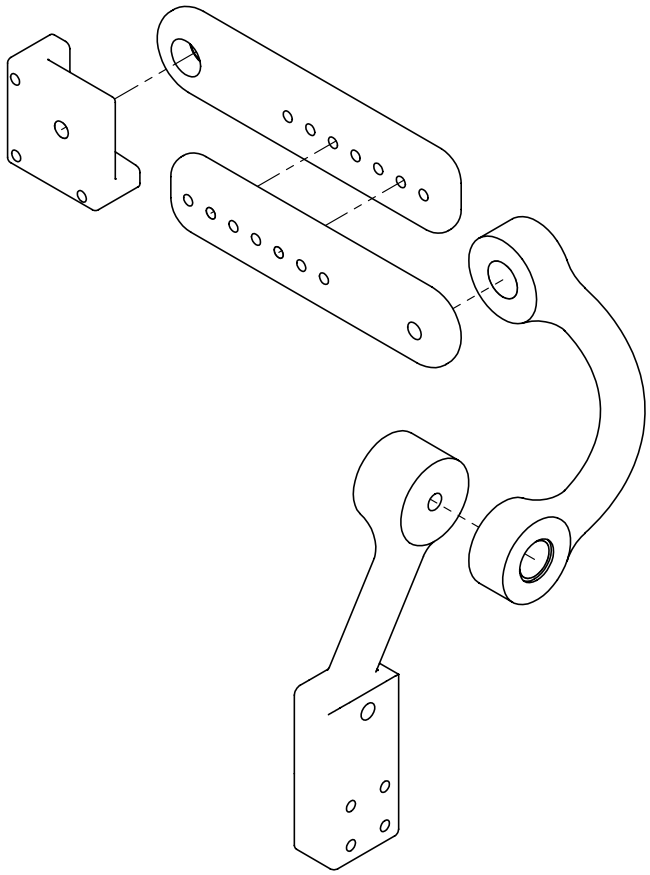

UNLESS OTHERWISE SPECIFIED: DIMENSIONS ARE IN MILLIMETERS SURFACE FINISH: TOLERANCES: LINEAR: ANGULAR:	FINISH:	DEBURR AND BREAK SHARP EDGES	DO NOT SCALE DRAWING / REVISION

	NAME	SIGNATURE	DATE
DRAWN			
CHK'D			
APPV'D			
MFG			
Q.A			

TITLE:

Thesis
17gr10201

MATERIAL:

DWG NO.
Back & Shoulder Assembly

A4

WEIGHT: 198.61g

SCALE:1:2

SHEET 25 OF 32

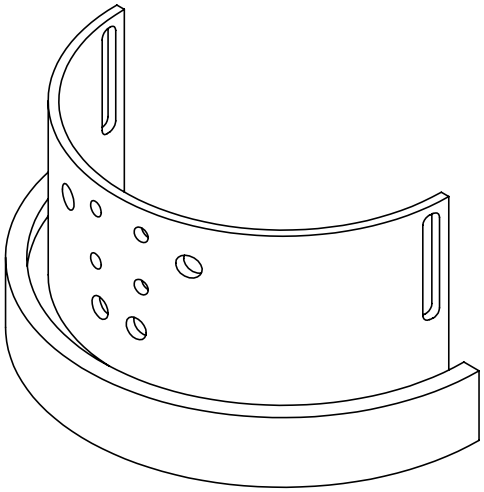

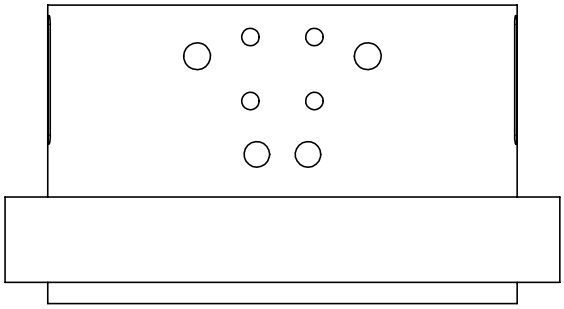

UNLESS OTHERWISE SPECIFIED: DIMENSIONS ARE IN MILLIMETERS SURFACE FINISH: TOLERANCES: LINEAR: ANGULAR:	FINISH:		DEBURR AND BREAK SHARP EDGES				DO NOT SCALE DRAWING	REVISION
	NAME	SIGNATURE	DATE				TITLE: Thesis 17gr10201	
DRAWN								
CHK'D								
APPV'D								
MFG								
Q.A				MATERIAL:			DWG NO. Upper Arm Part	A4
				WEIGHT: 158.32g			SCALE:1:1.5	SHEET 26 OF 32

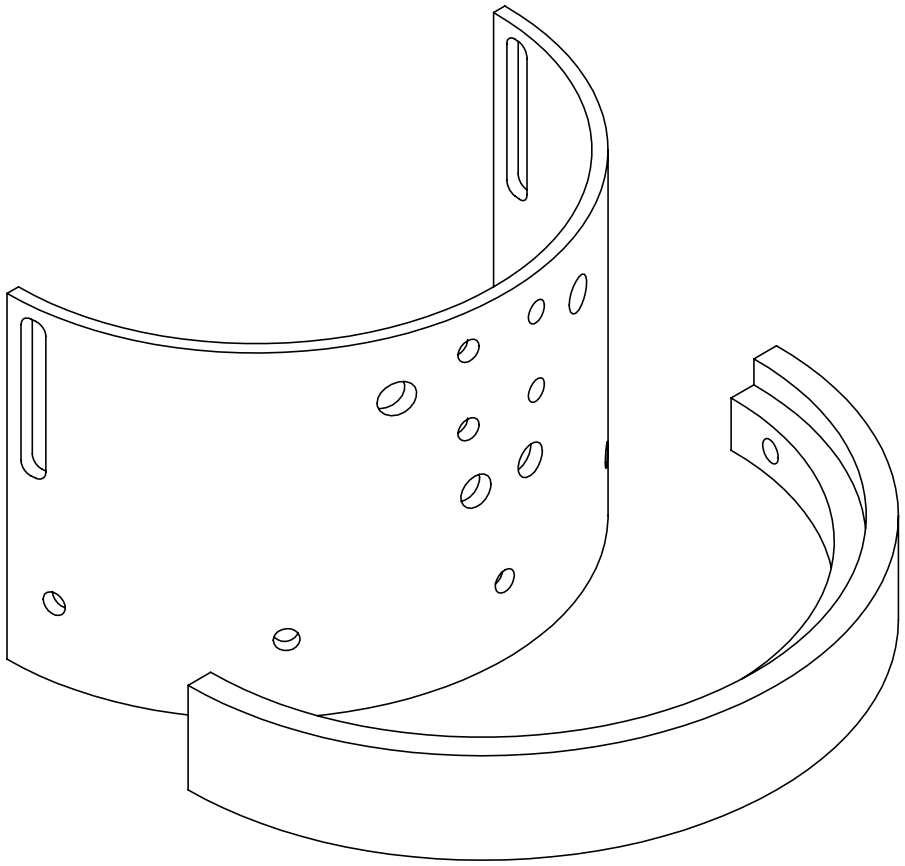

UNLESS OTHERWISE SPECIFIED: DIMENSIONS ARE IN MILLIMETERS SURFACE FINISH: TOLERANCES: LINEAR: ANGULAR:	FINISH:	DEBURR AND BREAK SHARP EDGES	DO NOT SCALE DRAWING / REVISION

	NAME	SIGNATURE	DATE
DRAWN			
CHK'D			
APPV'D			
MFG			
Q.A			

TITLE:

Thesis
17gr10201

MATERIAL:

DWG NO.

Upper Arm Part

A4

WEIGHT: 158.32g

SCALE:1:1

SHEET 27 OF 32

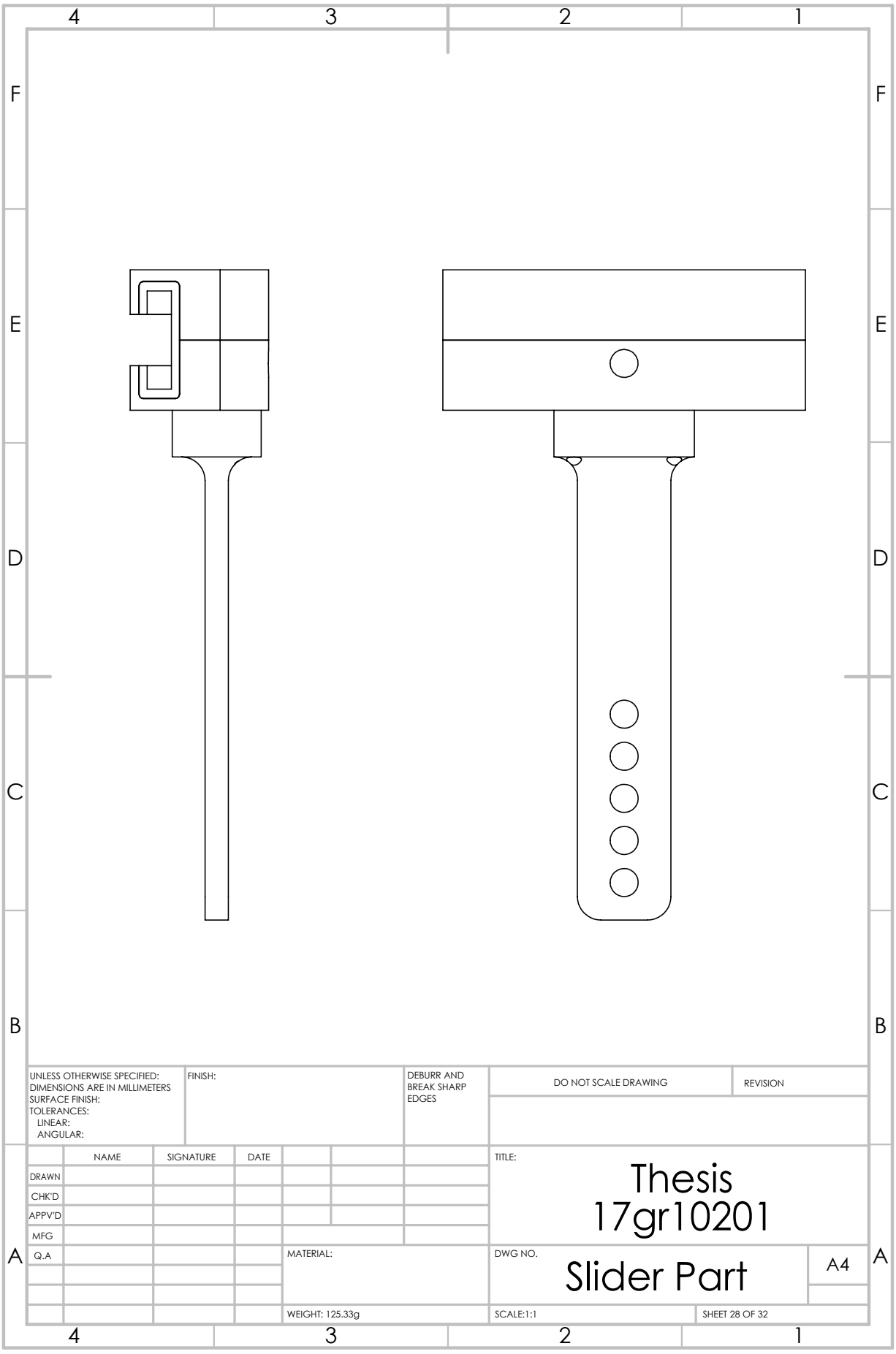
4
3
2
1
F
E
D
C
B
A
UNLESS OTHERWISE SPECIFIED:
DIMENSIONS ARE IN MILLIMETERS
SURFACE FINISH:
TOLERANCES:
LINEAR:
ANGULAR:
FINISH:
DEBURR AND BREAK SHARP EDGES
DO NOT SCALE DRAWING
REVISION
NAME
SIGNATURE
DATE
DRAWN
CHK'D
APPV'D
MFG
Q.A
MATERIAL:
WEIGHT: 125.33g
TITLE:
Thesis 17gr10201
DWG NO.
Slider Part
A4
SCALE:1:1
SHEET 28 OF 32

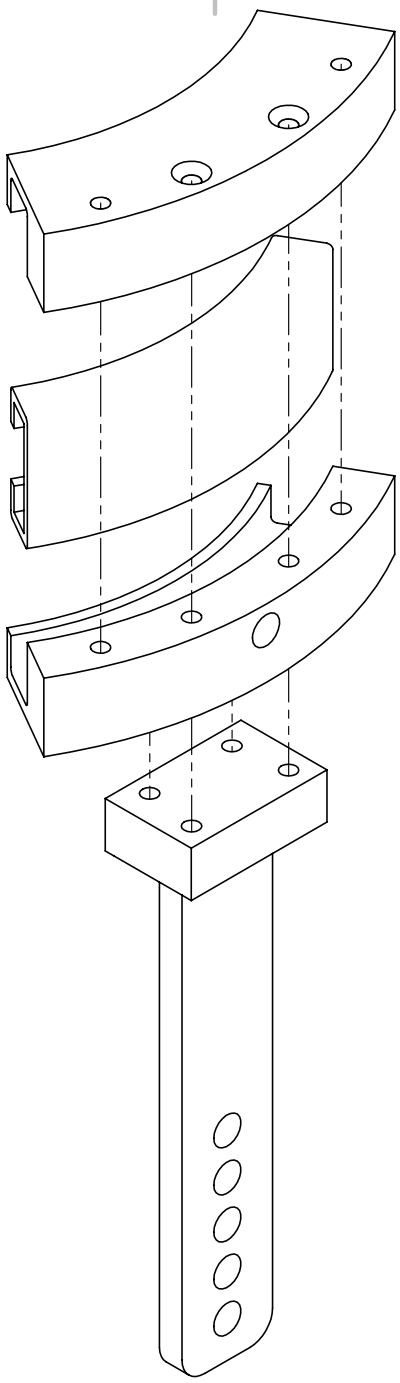

UNLESS OTHERWISE SPECIFIED: DIMENSIONS ARE IN MILLIMETERS SURFACE FINISH: TOLERANCES: LINEAR: ANGULAR:	FINISH:	DEBURR AND BREAK SHARP EDGES	DO NOT SCALE DRAWING / REVISION

	NAME	SIGNATURE	DATE
DRAWN			
CHK'D			
APPV'D			
MFG			
Q.A			

TITLE:

Thesis
17gr10201

MATERIAL:

DWG NO.

Slider Part

A4

WEIGHT: 125.33g

SCALE:1:1

SHEET 29 OF 32

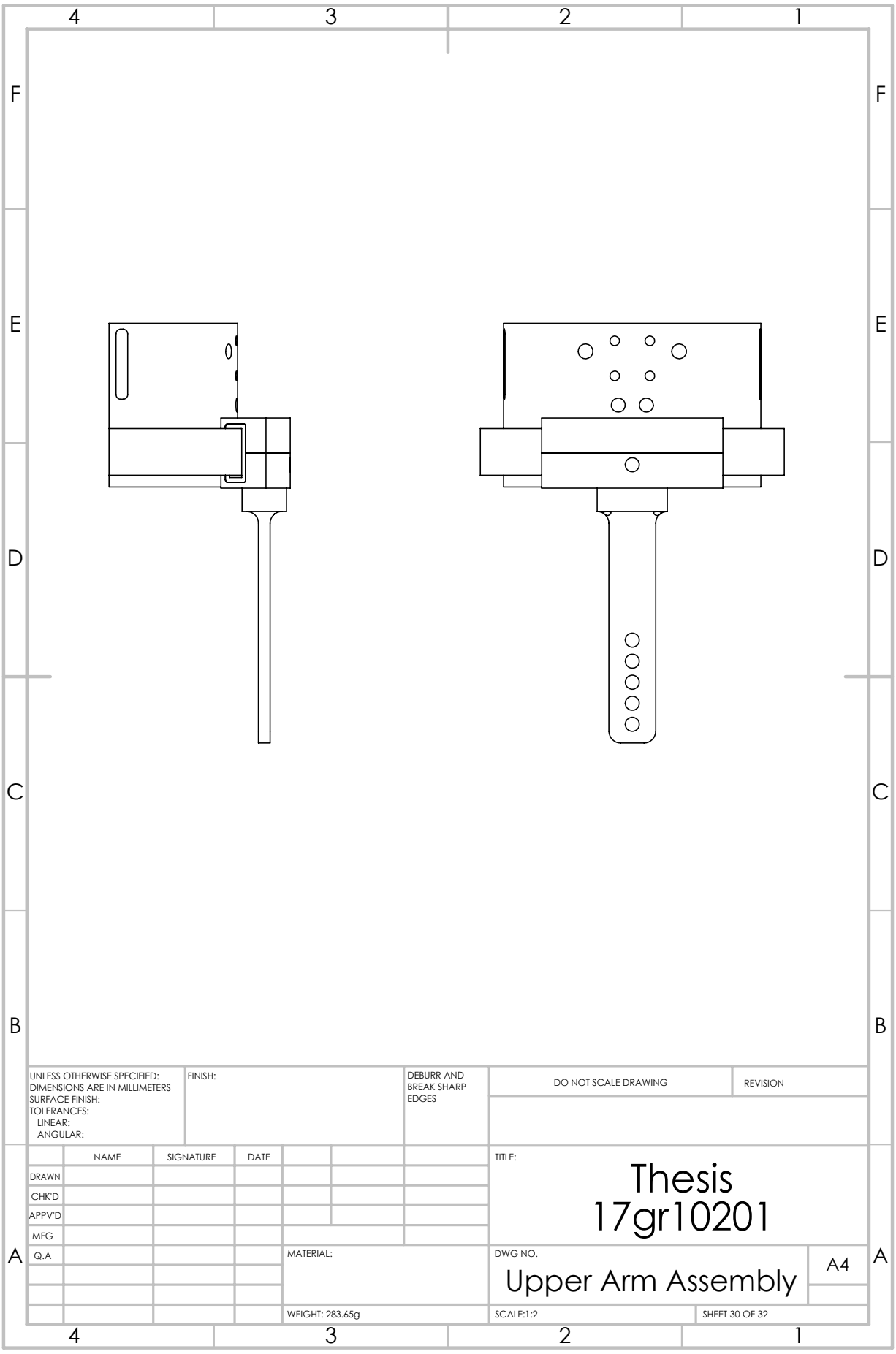
4
3
2
1
F
E
D
C
B
A
UNLESS OTHERWISE SPECIFIED:
DIMENSIONS ARE IN MILLIMETERS
SURFACE FINISH:
TOLERANCES:
LINEAR:
ANGULAR:
FINISH:
DEBURR AND BREAK SHARP EDGES
DO NOT SCALE DRAWING
REVISION
NAME
SIGNATURE
DATE
DRAWN
CHK'D
APPV'D
MFG
Q.A
MATERIAL:
WEIGHT: 283.65g
TITLE:
Thesis
17gr10201
DWG NO.
Upper Arm Assembly
A4
SCALE:1:2
SHEET 30 OF 32

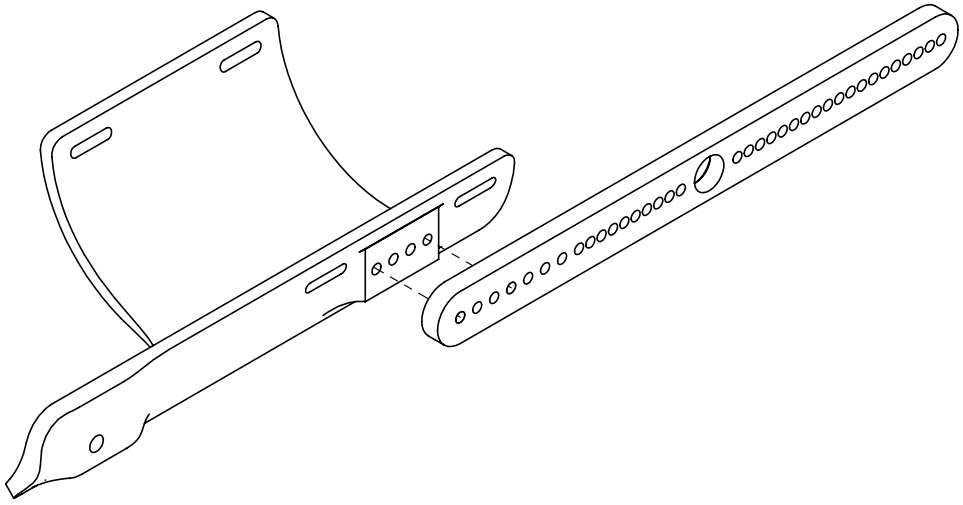

UNLESS OTHERWISE SPECIFIED: DIMENSIONS ARE IN MILLIMETERS SURFACE FINISH: TOLERANCES: LINEAR: ANGULAR:		FINISH:		DEBURR AND BREAK SHARP EDGES		DO NOT SCALE DRAWING		REVISION
	NAME	SIGNATURE	DATE				TITLE:	
DRAWN							Thesis 17gr10201	
CHK'D								
APPV'D								
MFG								
Q.A				MATERIAL:			DWG NO. Forearm Assembly	A4
				WEIGHT: 170.62g			SCALE:1:2	SHEET 31 OF 32

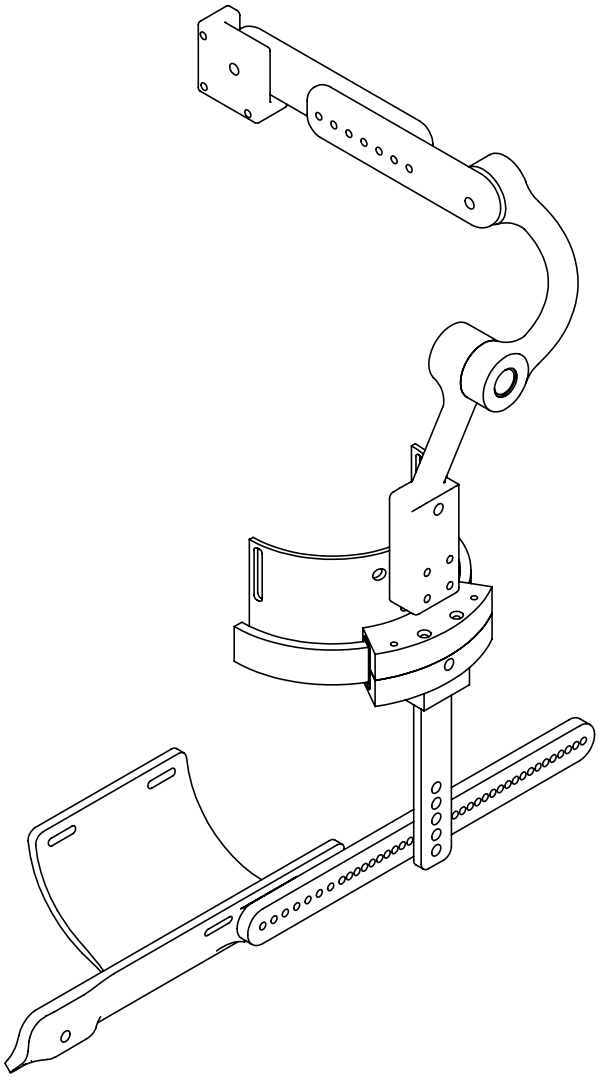

UNLESS OTHERWISE SPECIFIED: DIMENSIONS ARE IN MILLIMETERS SURFACE FINISH: TOLERANCES: LINEAR: ANGULAR:	FINISH:		DEBURR AND BREAK SHARP EDGES				DO NOT SCALE DRAWING	REVISION
	NAME	SIGNATURE	DATE				TITLE:	
DRAWN							Thesis 17gr10201	
CHK'D								
APPV'D								
MFG								
Q.A				MATERIAL:			DWG NO.	A4
							Assembly	
				WEIGHT: 936.52g			SCALE:1:3	SHEET 32 OF 32